1-1-2013

Microencapsulation of a Connexin-43 Mimetic Peptide as a Novel Wound Healing Agent in an Ocular Injury Model

Keith Brian Moore
University of South Carolina

Microencapsulation of a Connexin-43 Mimetic Peptide as a Novel Wound Healing Agent in an Ocular Injury Model

By

Keith Brian Moore

Bachelor of Science
Augusta State University, 2007

Submitted in Partial Fulfillment of the Requirements

For the Degree of Doctor of Philosophy in

Biomedical Engineering

College of Engineering and Computing

University of South Carolina

2013

Accepted by:

Jay Potts, Major Professor

Richard Goodwin, Committee Member

Robert Gourdie, Committee Member

James Blanchette, Committee Member

Lacy Ford, Vice Provost and Dean of Graduate Studies

DEDICATION

I would like to dedicate this work to three people without whom I don't think this would be possible; Kelly Moore, Carroll Moore, and David Campbell. Each gave me strength, kind words, advice, love and encouragement along the way.

ACKNOWLEDGEMENTS

I would like to acknowledge and thank Dr. Jay Potts for allowing me to work in his laboratory while obtaining my PhD. Without his mentorship and guidance this is not possible. I would also like to thank the University of South Carolina and the associated faculty and staff of the Biomedical Engineering program, especially my committee members Dr. James Blanchette, Dr. Richard Goodwin, and Dr. Robert Gourdie. The Biomedical Engineering program gave me a chance and allowed me to pursue this degree while switching disciplines from my undergraduate work in Biochemistry. For this opportunity I am most grateful.

Finally I would like to thank my lab mates Na Li and Adam Vandergriff as well as all of my fellow graduate researchers and friends at the school of medicine and the engineering departments for everything both in and out of the lab.

ABSTRACT

Corneal transplantation and related surgical procedures are areas of tissue replacement which have seen promising advances. Currently, cornea transplants are one of the most common surgical procedures, with approximately 40,000 occurring each year in the United States. Still, problems exist with a 20% rejection rate, post surgical infections, and the need for a constant supply of donors. The ability to safely and quickly heal and regenerate corneal epithelia fills an area of advancement in regenerative medicine, with implications reaching beyond the scope of vision therapies toward healing of a wide range of tissues and wounds. In vivo corneal wounds were created in rats through a surgical procedure chemically loosening and mechanically removing the epithelium from the corneal surface. Our study applies a synthetically developed peptide capable of promotion of wound healing and epithelial regeneration. The alpha-carboxy terminus 1 (αCT1) peptide is a 25 amino acid peptide from the C-terminus of connexin 43, modified to promote cellular uptake. Previous studies applying αCT1 to excisional wounds in rats produced resulting tissue having an overall reduced level of scar tissue and decreased healing time, compared to controls. Upon entering the wound site, the peptide acts as a competitive inhibitor to the ZO-1-Cx43 interaction. In doing so, the formation of gap junctions during healing is altered. Here we first characterized the development and synthesis of alginate based microcapsules, designed to deliver αCT1 in a controlled and sustained release. We hypothesized sustained release of αCT1 would enhance the peptides innate wound healing ability beyond previous results. An alginate-

poly-l-ornithine pH 4.3 microcapsule capable of delivery of 150µM of peptide over 48hrs was ultimately produced. Both directly applied αCT1 in a pluronic gel system and microencapsulated αCT1 were tested in two studies of in vivo corneal wound injuries using normal and STZ type I diabetic Sprague Dawley rats. Data derived from RT-PCR, confocal immunohistochemistry, inflammatory H&E scoring, western blotting, Elisa protein analysis, and fluorescent wound measurements indicated a significant increase in wound healing speed when αCT1 was applied at a 150µM concentration. The application of 150µM αCT1 alginate-poly-l-ornithine pH 4.3 microcapsules further increased corneal wound healing rate beyond those seen when using αCT1 alone.

TABLE OF CONTENTS

LIST OF TABLES

LIST OF FIGURES

LIST OF ABBREVIATIONS

αCT1 ..... Alpha Carboxyl Terminus 1

ARBP ..... Attachment Region Binding Protein

$CaCl_2$ ..... Calcium Chloride

Cx43 ..... Connexin 43

Esr1 ..... Estrogen Receptor 1

GLUT4 ..... Glucose Transporter 4

Krt19 ..... Keratin 19

Krt8 ..... Keratin 8

PWAS ..... Pezioelectric Wafer Active Sensors

STZ ..... Streptozotocin

TGFβ2 ..... Transforming Growth Factor β2

UV ..... Ultra Violet

ZO-1 ..... Zonnula Occludens 1

CHAPTER 1: INTRODUCTION

Cell-to-Cell Adhesion and Connexins

Connexins, also known as gap junction proteins, are a group of transmembrane proteins functioning in the creation of gap junctions. Gap junctions play multifunctional roles, acting as connecting channels between adjacent cells to transmit electrical impulses and mediate the passage of small molecules, ions, metabolites, and second messengers. Gap junctions form through the assembly of six connexin proteins across a cell membrane. The six connexins may be of the same type (homomeric) or of different types (heteromeric), with nomenclature based on molecular weight (Herve et al 2004). Initially connexins are synthesized by ribosomes bound to the endoplasmic reticulum. Once translated, the connexins are oligomerized and assembled into six unit connexons (Bennett et al 2004). Post assembly, the connexons are inserted into the plasma membrane of the cell, forming a hemichannel. Hemichannels then bond with corresponding hemichannels from adjacent cells. Once two hemichannels are bound a functional gap junction is formed. The hemichannel-hemichannel interactions may be homotypic or heterotypic (Geletu et al 2012).

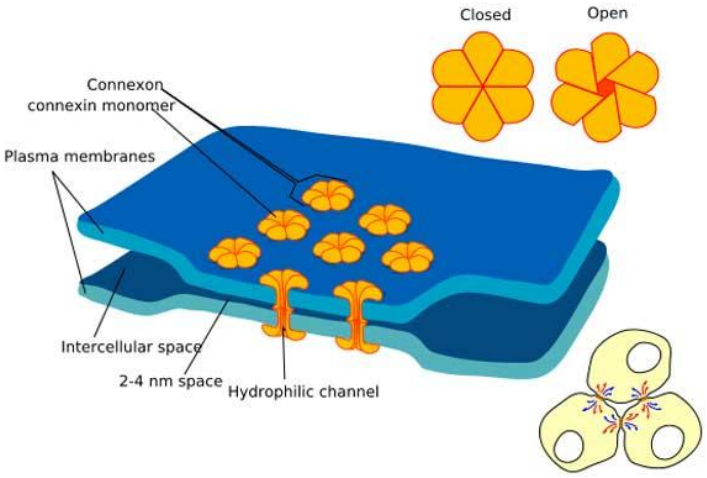

Figure 1.1 Illustration of formation of gap junction between adjacent cells. Image obtained from http://cellbiology.med.unsw.edu.au/units/science.

Each connexin consists of nine domains (two extracellular, four transmembrane, three cytoplasmic) of which all but the C-terminus and cytoplasmic loop are highly conserved between each type (Dbouk et al 2009). The variability in these two regions of the connexins allow for differences in functionality. Of interest in this research is the C-terminus region of Connexin 43. Initially gap junctions were thought to only function in simple cell to cell transport. Now, many different interactions involving varying protein to protein binding with the gap junction nexus is thought to create changes in function and regulation. Connexins have been found to interact with other cellular junction associated molecules such as cadherins (adherens junctions) and zonula occludens (tight junctions) as well (Dbouk et al 2009; Weiss 2001; Kowalczyk et al 1999). Through these interactions it is thought a complex system exists to regulate tight junctions and cell-to-cell connections.

The cytoplasmic tight junction protein ZO-1 binds at the PDZ-2 domain with the Cx43 C-terminus end at the DDLEI sequence (Duffy et al 2002). Other alpha type

connexins such as connexin 45 have also been shown to also bind to ZO-1, possibly stabilizing the Cx43-ZO-1 interaction (Laing et al 2001). The exact role of this interaction is unknown, but it is theorized that the relationship may play a key role in trafficking of molecules (Toyofuku et al 1998) for gap junction formation or as a base scaffold in gap junction formation (Duffy et al 2002). Connexins have been found to remain in an open state in response to pathology induced stress, including ischemia and hypoxia (Evans et al 2012). Furthermore, open hemichannels were shown to be associated with specific disease states such as cardiac arrhythmia and myocardial infarction. Recent work by Rhett et al 2011 indicated that the Cx43-ZO-1 interaction occurs not only at the gap junctions of the plasma membrane, but also the free connexons of the perinexus. Additional binding of connexins with tight junction associated proteins was found to occur between occludin-Cx26 and occludin-Cx32 in hepactocytes as well as claudin-Cx32 (Kojima et al 2001). Adherens junction proteins Wnt-1 and β-catenin associate with Cx43 to regulate communication, as shown in cardiac myocytes. (Ai et al 2000). A summary list of other known capable connexin 43 interacting or co-localizing proteins includes Lin-7, α-catenin, p120, N-cadherin, src, PKCα, DMPK, MAPK, P38MAPK, tubulin, F-actin, drebrin, caveolin-1, clathrin, ubiquitin, CIP 62, and NOV (Herve et al 2004).

Wound Healing and the Cornea

In this work the αCT1 peptide was evaluated for its therapeutic potential in corneal injury models using both normal and type I diabetic rats. The cornea is the nonvascular outer layer of the eye. Five layers comprise the cornea, with the outermost being the epithelium, accounting for approximately 10% of the thickness. Roughly five to six cells thick, the epithelial layer serves to block entry of materials into the eye,

absorbs oxygen, and senses pain to protect the eye from damage. The cornea epithelial layer is attached to a basement membrane. The second layer of the cornea is the Bowman's layer, which is a transparent sheet of collagen. This layer may be scarred, affecting vision. The third and thickest (90%) layer is the stroma. Made up of roughly 78% water and 16% collagen the stroma gives the cornea its flexibility and shape. Fourth is the Descemet's membrane which is a collagen membrane acting to protect against infection. The fifth layer is the single cell thick, endothelial layer. The endothelium regulates and removes leaked fluid from the stroma to prevent impaired vision, swelling, and blurring.

Typical wound healing of the skin consists of three main overlapping phases: inflammation, tissue formation, and tissue remodeling (Martin 1997). Inflammation begins immediately following wound formation, where fibroblasts and macrophages are attracted to the injured site (Gurtner et al 2008). Damaged extracellular matrix (ECM) and contaminating microorganisms are phagocytosed. During inflammation TGF-β and other ECM proteins begin to infiltrate the wound as well. Several hours after injury epithelialization begins. Clotted blood is removed as well as intercellular desmosomes, allowing cellular movement into the wound. Within 1-2 days epidermal cells proliferate and migrate into the wounded area. As reepithelization occurs, basement membrane proteins reorder and epidermal cells begin attachment. Approximately 4 days after injury new granulation tissue enters the wound. TGF-β stimulates fibroblasts to form new ECM. At this stage neovascularization also occurs, with VEGF and fibroblast growth factor inducing addition of new blood vessels to wound space. Once the ECM is reformed the fibroblasts stop producing collagen and the granulation tissue is replaced

with an acellular scar (Schultz et al 1991). After 2 weeks wound contraction and ECM reorganization occur. Fibroblasts convert to myofibroblasts and microfilaments enter the healing tissue. The wound is then pulled from the edges to contract. Remodeling continues for up to 12 months after injury. At this point, wounded tissue has approximately 70% of the strength of the previously uninjured skin (Martin 1997).

The cornea, with its avascular structure, follows a different healing process than that of the skin. A series of overlapping processes occur in a rapid fashion, beginning immediately after injury. Following the epithelial injury, a cascade of cytokines (including IL-1 and PDGF) initiate keratocyte apoptosis (Wilson et al 2001). Growth factor cytokines are then released by the lacrimal glands, which trigger keratocyte proliferation and migration from the stroma (Zeiske et al 2001). This is followed by myofibroblast proliferation and migration to the wound site. Additional cytokines, such as TGFβ are released, triggering collagen production and remodeling (Netto et al 2005). Inflammatory cells migrate to the wounded area and stromal remodeling occurs, if necessary (Ye et al 2000). As the epithelial layer completes closure the inflammatory cells undergo apoptosis and the keratocytes return to their original state (Dupps and Wilson 2006). In addition, the limbus of the corneal epithelium is a source of stem cells capable of transmigrational proliferation, but is not known to be necessary for reepithelialization after wounding (Dua et al 2010). While the outline of the healing process is known, many of the details of the process and associated factors are still under investigation.

Epithelial-Mesenchymal Transition

Epithelial-mesenchymal transition, or EMT, is a series of events where an epithelial cell is changed into a mesenchymal cell. In this work we examine the role of this pathway in response to the αCT1 peptide in corneal wound healing. EMT occurs in many biological processes, beginning in early embryonic development, where it is responsible for the formation of the mesoderm and induction of the neural crest (O'Quinn et al 2011). EMT has also been found to occur in other seminal events such as organ development, tumor cell metastasis, and fibrosis of the lungs, kidneys, heart, and liver (Chapman 2010; Guarino et al 2009; Kalluri et al 2003; Lee et al 2006). During fibrosis of major organs epithelial cells undergo EMT to become mesenchymal cells, translocating to areas of inflammation. Upon arriving, the mesenchymal cells are thought to act as fibrotic cells, depositing collagen matrix. Excess matrix deposition leads to scarring at sites of chronic inflammation and further tissue injury (Chapman 2010; Guarino et al 2009).

To understand the pervasiveness of this cellular event, the characteristics of each cell type must be understood. Epithelial cells are cuboidal, rigid cells which form sheets with strong cell-cell interactions. Typically epithelial cells form barriers for organs and tissues. Epithelial cells are immobile and tightly bound by tight junctions, adherens junctions, gap junctions, and desmosomal junctions. Mesenchymal cells on the other hand are very different. They have a non-rigid shape, loose and short lived cell-cell interactions, and are mobile.

The EMT process is a biological method of cellular rearrangement and repair of damaged tissue where immobile cells used for structural integrity and boundary formation may be mobilized to an area of need (Lim et al 2012). Once the EMT process

is complete the mesenchymal cells convert back to epithelial cells in a reverse process called MET, or mesenchymal-epithelial transition. Typically the EMT process is tightly regulated by the body, as in embryogenesis. Unregulated, EMT can lead to disease states, such as in tumorigenesis and cancer.

There are several markers to identify EMT. On the molecular level β–catenin localizes in the nucleus, while the presence of vimentin, N-cadherin, snail, slug, and twist all increase (Guarino et al 2009). Phenotypically there is a noticeable increase in cellular motility, three-dimensional invasion, and apoptosis resistance. The signaling pathway to initiate EMT has not been fully mapped, and the activation/regulation process is still being investigated. However, multiple signaling factors have been discovered. It is thought that TGFβ and Snail1 are central to EMT events (Mirza et al 2012; Vogelmann et al 2005). Metalloproteinase-3 (MMP-3) is a Snail1 activator. The presence of MMP-3 in epithelial cells activates Rac1 production, which in turn activates the production of reactive oxygen species (ROS) (Radisky 2005). The ROS then activates Snail1 production. Snail1 genes induce EMT by the regulation of cell adhesion and cellular migration. ILK (integrin-linked kinase) has been found to activate Snail1 as well. TGFβ is an important cytokine, which when bound to cell surface receptors can trigger a cascade of cellular responses to activate EMT. One central factor activated is β-catenin. When β-catenin is bound it enhances cell-cell adhesion by E-cadherin (Brembeck et al 2004; Chu et al 2004). TGFβ stimulation causes β-catenin to detach and move to the nucleus where it activates transcription of EMT genes (Chapman 2010). Cadherins are transmembrane proteins responsible for creating adherins junctions. E-cadherin typically creates stronger bonds than those of N-cadherins. During EMT E-cadherin is down

regulated while N-cadherin is up regulated post β-catenin stimulation (Chapman 2010). Activation of these transcriptional factors in the nucleus leads to a loss of strong cell-cell interactions, releasing the epithelial cell from the basement membrane and surrounding cells. The epithelial cell then rearranges the F-actin stress fibers and expresses filopodia and lamellapodia in the mesenchymal state (Lee et al 2006). Finally, transcription is activated to produce mesenchymal markers. The epithelial cell is now a phenotypic and molecular match to a mesenchymal cell.

Previous work in our lab with BMSCs has indicated that EMT may be induced ex vivo. In particular work has shown that different cell lines may be induced to undergo an EMT event in collagen gels. Rabbit lens epithelial cells seeded on dialyzed collagen gels can be primed to undergo EMT (Data not shown). Below is a summary of known EMT regulated genes and their specific roles (Table 1.1) and a pathway map showing the regulation connections of some of the genes selected in the studies outlined in chapters 3 and 4 (Figure 1.2).

Table 1.1 Summary of genes associated with the EMT pathway and their functional roles. Data from pathway analysis using a Quiagen RT^2 EMT assay and related manufacturer information.

Function	Associated Genes
Genes Up-Regulated During EMT	Ahnak, Cald1, Camk2n1, Cdh2, Col1a2, Col3a1, Col5a2, Fn1, Foxc2, Gng11, Gsc, Igfbp4, Itga5, Itgav, Mmp2 (Gelatinase A), Mmp3, Mmp9 (Gelatinase B), Msn, Serpine1 (PAI-1), Snai1, Snai2, Snai3, Sox10, Sparc, Steap1, Tcf4, Timp1, Tmeff1, Tmem132a, Twist1, Vcan, Vim, Vps13a, Wnt5a, Wnt5b.
Genes Down-Regulated During EMT	Cav2, Cdh1, Dsp, Fgfbp1, Il1rn, Krt19, Mitf, Ocln, Rgs2, Spp1 (Osteopontin), Tfpi2, Tspan13.
Differentiation & Development	Akt1, Bmp7, Col3a1, Col5a2, Ctnnb1, Dsp, Erbb3, F11r, Fgfr2, Foxc2, Fzd7, Gsc, Jag1, Krt14, Map1b, Mitf, Nodal, Notch1, Ppp3r1, Ptp4a1, Smad2, Snai1, Snai2, Sox10, Tgfβ2, Tgfb3, Tmeff1, Twist1, Vcan, Wnt11, Wnt5a, Wnt5b.
Morphogenesis	Ctnnb1, Foxc2, Jag1, Rac1, Smad2, Snai1, Sox10, Tgfβ1, Tgfβ2, Tgfb3, Twist1, Wnt11, Wnt5a.
Cell Growth & Proliferation	Akt1, Bmp7, Cav2, Ctnnb1, Egfr, Erbb3, Fgfbp1, Foxc2, Igfbp4, Ilk, Jag1, Nodal, Pdgfrb, Tgfβ1, Tgfβ2, Tgfb3, Timp1, Vcan, Zeb1.
Migration & Motility	Cald1, Cav2, Egfr, Fn1, Itgb1, Jag1, Msn, Nodal, Pdgfrb, Rac1, Stat3, Tgfβ1, Vim.
Cytoskeleton	Cav2, Krt7, Plek2, Rac1, Vim
Extracellular Matrix & Cell Adhesion	Bmp7, Cdh1, Cdh2, Col1a2, Col3a1, Col5a2, Ctgf, Ctnnb1, Dsc2, Egfr, Erbb3, F11r, Fgfr2, Fn1, Foxc2, Ilk, Itga5, Itgav, Itgb1, Mmp2 (Gelatinase A), Mmp3, Mmp9 (Gelatinase B), Ptk2, Rac1, Serpine1 (PAI-1), Spp1 (Osteopontin), Tgfb1, Tgfβ2, Timp1, Vcan.
Transcription Factors	Ctnnb1, Esr1 (ERa), Foxc2, Gsc, Mitf, Notch1, Sip1, Smad2, Snai2, Snai3, Sox10, Stat3, Tcf3, Tcf4, Twist1, Zeb1, Zeb2.

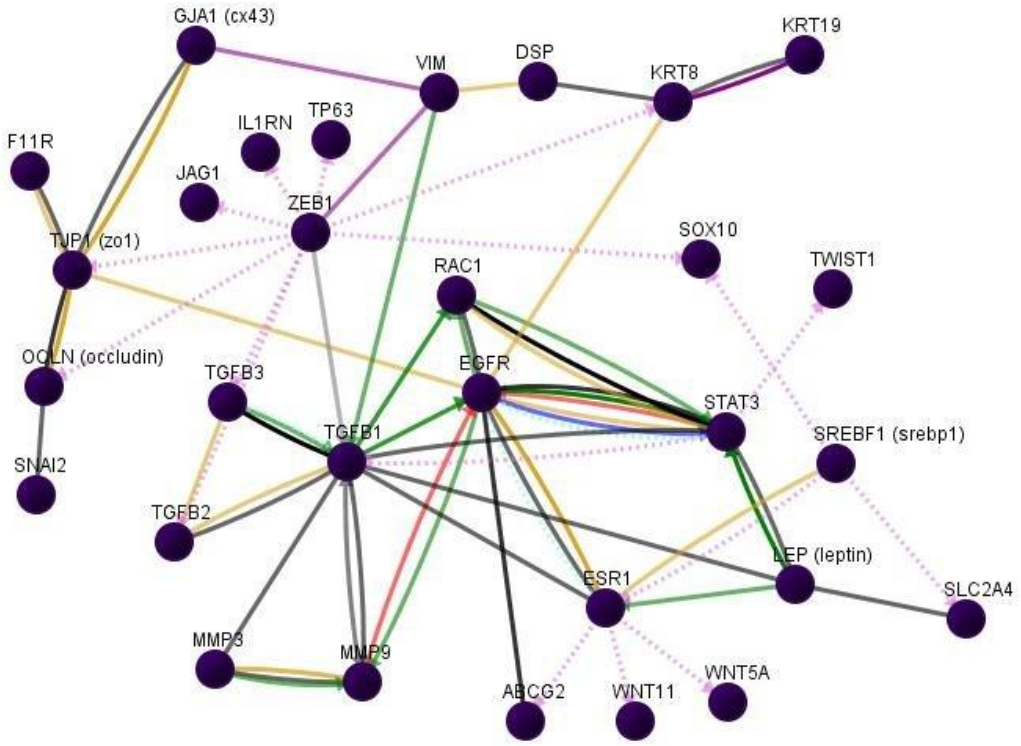

Figure 1.2 Pathway map showing the regulatory connections of sample genes from the EMT pathway. Genes shown here were selected to represent those used in chapters 3 and 4. GLUT4 is represented here by SLC2A4.

Microencapsulation and Drug Delivery Systems

For controlled release of αCT1, microcapsule delivery was investigated. Microencapsulation is a technique in which small particles are coated with a material to provide a secondary property of use. Typically the secondary property is controlled release or protection of the encapsulated material. Microencapsulation systems rely on diffusion of the encapsulated materials from the inner core to deliver the drug and have been shown to successfully deliver many different bioactive substances such as peptides, proteins, enzymes, and antibiotics. Many methods exist for encapsulation including emulsification, solvent evaporation, pan coating, electrospray encapsulation, and pulse-flow to name a few (Gaete et al 2008; Yang et al 2001). Microcapsules can vary in shape

according to synthesis procedures, with spheres, rods, cubes, and corrugated patterns reported (Enayati et al 2009). The encapsulation technique in this work is the electrospray method using sodium alginate polymer cores.

Electrohydrodynamics refers to methods of fabrication of polymeric materials using electrically charged fluids. Examples of polymer materials that may be used include sodium alginate (SA), chitosan, poly-caprolactone (PCL), poly-lactic-co-glycolic acid (PLGA), poly-ethylene oxide (PEO), poly-ethylene glycol (PEG), poly-l-lysine (PLL), poly-l-ornithine (PLO), and poly-lactic acid (PLA) (Casper et al 2005; Chew et al 2005; Xu et al 2006; Chakraborty et al. 2009; Zhang et al 2009; Takka et al 2010). Each polymer possesses its own unique properties such as biocompatibility, charge, reactivity with the drug, and viscosity in solution which affect the appropriateness of application. Within the field of electrohydrodynamics, two main categories exist: electrospinning and electrospraying. Similar in methodology, each uses one of a variety of polymers placed in a positively charged syringe attached to a high voltage generator. Using a device to control flow rate, such as a syringe pump or driver, the polymer is extruded to a grounded material. The flowing polymer, which is an electrically conductive solution, passes through the electrical potential difference. With the application of flow, gravity, and an electric polarization stress, a cone jet is formed at the needle tip (Jaworek and Krupa 1999a). Typically, without these forces, liquids will form a droplet that is geometrically controlled by the surface tension of the solution and the pull of gravity (Paine et al 2007). The cone jet is a conically shaped formation at the needle tip, to which charged particles of liquid exist at the apex of the cone. Once a minimally stable level of both flow and electrostatic voltage are present (dependent on the materials) the charged particles

separate from the apex and break apart into reproducible droplets (Jaworek and Krupa 1999b). These droplets are then collected using a grounded device or solution, as nano or microcapsules. With electrospinning, the grounded device is typically a solid collector of various shape or size. Electrospraying can involve extrusion into a grounded solution or onto a grounded surface. Both electrospinning and electrospraying are gaining interest as methods of delivery of drugs and other activators of biological processes because they can be easily altered, thus changing release rates and pharmacokinetics. Other methods of drug delivery may require additional processing steps involving heat, pressure, shear stress, or reactive secondary chemicals which can degrade or decrease the functionality of the drug (Enayati et al 2011). Thus, the electrospray method is ideal in its lack of these negative procedures.

Alginate is a polymer commonly used in microencapsulation for its biocompatibility and is used here as a base microencapsulating material. Extracted from the cell walls of brown seaweeds, alginate is popular due to ease of obtainability and production at a low cost (Orive et al 2006; Zhang et al 2009, 2010). Sodium alginate is a straight-chain, hydrophilic, polyuronic acid composed of 1→4 linked β-D-mannuronic acid and α-L-guluronic acid residues (Lee and Mooney 2012). The alginate, in addition to mannuronic acid, is also composed of guluronic acid. When crosslinked to cations, such as calcium, a hydrogel is formed (Arghya et al 2010; Zhang et al 2008). Figure 1.3 below shows the chemical structure of sodium alginate, used in our microcapsule synthesis.

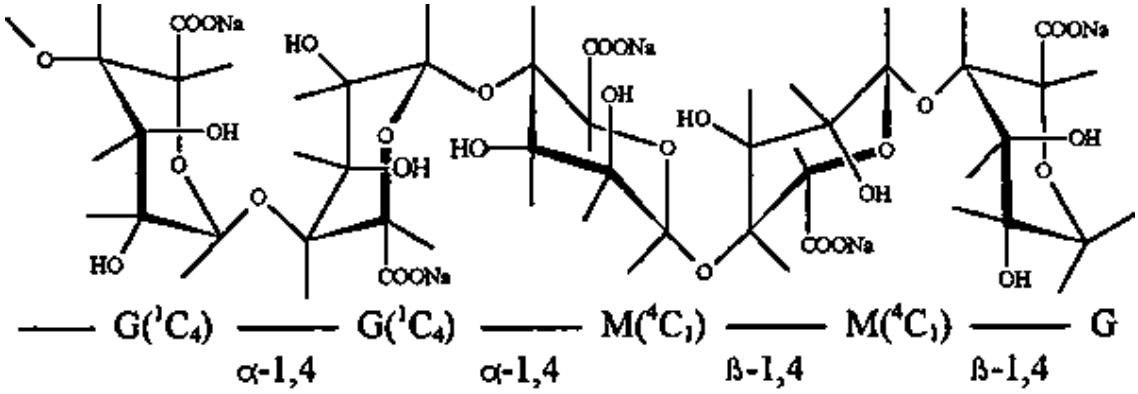

Figure 1.3 Chemical structure of sodium alginate polysaccharide with both guluronic (G) and mannuronic acids (M) shown. Image produced by the Food and Agriculture Administration of the United Nations.

CHAPTER 2: SYNTHESIS AND CHARACTERIZATION OF A DRUG DELIVERY SYSTEM FOR THE αCT1 PEPTIDE

2.1 Abstract

A need exists to prolong the release of rapidly metabolized peptides of a low molecular weight, while delivering this peptide without environmental interference. Previous studies have used Bovine Serum Albumin as a model peptide to study release characteristics from alginate microcapsules. BSA is 66kDa in size, while the peptide of interest here, connexin-43 carboxyl-terminus mimetic peptide (αCT1), is 3.4kDa; a large difference in terms of release. Such a change in size results in a much different set of release parameters. The overall goal is a sustained release over a 24+ hr period, which would allow prolonged application of the peptide to a wound site in order to investigate therapeutic effects. As a result, diffusion methods using sodium alginate microcapsules, with additional poly-l-lysine (PLL) and poly-l-ornithine (PLO) coating, have been explored. We first aimed to establish and characterize our size distribution parameters through a set of parametric tests. Variations in polymer coating, change in pH, and loading ratio have previously been shown to effect release using model compounds. Here we test specific changes in these parameters to show effects on the release of αCT1. Additionally, the microcapsules were attached to several biomaterials and surgical implants by ultraviolet crosslinking to study effectiveness of attachment and delivery. Analysis and measurements using phase contrast microscopy, atomic force microscopy (AFM), and scanning electron microscopy (SEM) were used to characterize changes in microcapsule morphology.

2.2 Introduction

Drug delivery systems (DDS) may be created in the nano and micro scale. Depending on the disease state and desired target to which the drug is to be delivered, a number of factors must be evaluated. Each DDS has inherent properties that make it ideal for certain applications. For example, in vivo interactions with the DDS may be altered based on the size, geometry, material properties (hydrophobicity, hydrophilicity, charge, etc.), biocompatibility, degradation rate, density, transport characteristics, and clearance rate of the delivery material (Chew et al 2006; Pham et al 2006; Rutledge et al 2007; Chakraborty et al 2009).

Within the electrospraying method, multiple techniques exist for encapsulating drugs. One method comprises synthesis of microcapsules and placement in drug containing solutions, allowing adsorption of the drug onto the microcapsule surface (Chakraborty et al 2009). A second method involves simultaneous spraying of an encapsulating polymer of one charge with a drug containing polymer of the opposite charge, thus creating a multilayered sphere (Langer et al 1969; Enayati et al 2011). Drugs may also be dissolved and mixed with polymers prior to capsule formation, creating capsules in one of two ways. First the mixed drug/polymer has a volatile solvent added to the solution, which is removed by evaporation between extrusion and collection. Once removed the nano/microcapsule is solidified and stabilized (Wu et al 2009). Second, the mixed drug/polymer may be extruded into an ionic solution, which acts to chemically bind and stabilize the created capsules (Xu et al 2006, 2007; Zhang et al 2010a). This method of electrospray microencapsulation is employed in this research, using calcium chloride. Another method is coaxial electrospraying. This process uses a

syringe within a syringe to extrude a drug containing core within a polymer shell layer (Hwang et al 2008).

Alginate is a polymer commonly used in microencapsulation for its biocompatibility. Extracted from the cell walls of brown seaweeds, alginate is popular due to its lack of toxicity, ease of obtainability, and low cost production (Orive et al 2006; Zhang et al 2009, 2010). Structurally alginate is, "A straight-chain, hydrophilic, colloidal, polyuronic acid composed primarily of anhydro-β-D-mannuronic acid residues with 1→4 linkage." (Mbanaso & Roscoe 1982; Draget et al 1989). The alginate, in addition to mannuronic acid, is composed of guluronic acid. When sodium alginate is crosslinked to cations, such as calcium, a hydrogel is formed (Arghya et al 2010; Zhang et al 2010b). Low w/v mixtures (1.5-3%) of sodium alginate have been shown to have sufficient strength and compatibility in vitro when used with living cells (Lin et al 2008; Zhang et al 2010b). Many polymers, previously listed in chapter 1, have been explored for use in microencapsulation, with the hope of finding an ideal solution that provides biocompatibility, the ability to form stable capsule membranes, and ease in control of the release properties. Promising results have been shown in both synthesis and biological experiments using PLL and PLO (Rosinski et al 2005; Calafiore et al 1999). Here we explore the use of these polymers in low concentrations as coatings for the sodium alginate based microcapsules.

In this work the connexin-43 carboxyl-terminus peptide (αCT1) has been microencapsulated in sodium alginate to create a controlled drug delivery system. The αCT1 peptide is a biotinylated 25 amino acid sequence from the C-terminus of connexin 43 originally synthesized in the laboratory of Dr. Robert Gourdie (Ghatnekar et al 2009).

Connexins play a key role as mediators in both cell growth and cell death, function in the immune response, hematopoiesis, and development of progenitor cells (Oviedo-Orta et al 2004; Vinkin et al 2011). An antennapedia section exists to aid in cellular uptake of the peptide without inducing genetic activity. For analysis, a biotin tail has also been incorporated into the peptide. A control peptide has also been created with the inactive 16 amino acid antennapedia portion conserved and the active sequence reversed. Previous research conducted using αCT1 has shown significant effects on reduction in the formation of skin scars, wound healing, and gap junction remodeling upon ventricular injury (O'Quinn et al 2011). An exact model of the peptide action has yet to be fully elucidated, but research has shown possible interaction with gap junction remodeling and connexin 43 interaction with zonnula occludin-1 (ZO-1) as points of interest (Rhett et al 2008, 2011). Subsequent research has shown an effect of αCT1 on the interaction between connexin 43 gap junctions and ZO-1 (Hunter et al 2005; Ghatnekar et al 2009,). Rapid metabolism of the peptide (~2 hours) has prevented previous studies of the long term effects in these injury models.

2.3 Materials and Methods

Electrospray Method of Microencapsulation

Sodium alginate (Sigma-Aldrich catalog#A0682) was mixed under sterile conditions at a concentration of 2% w/v, and purified by filtration at 0.2µm. Small aliquots (280µl) of filtered alginate were loaded into a 3cc syringe and attached to a syringe driver. A volume of 30ml of 0.15M calcium chloride ($CaCl_2$) (Sigma-Aldrich) was placed in a 50ml beaker below the syringe pump as an ionic gelling bath, leaving a needle to bath working distance of 7mm. A high voltage generator was attached to the

needle tip (30cc blunt tip, Amazon Supply) with a ground placed in the $CaCl_2$ solution. A constant voltage was next set on the high voltage generator to pass a field of current through the needle tip attached to the syringe. The syringe pump was started to push the filtered alginate solution through the needle tip and into the $CaCl_2$ gelling bath. As the extruded alginate was pushed by the syringe pump it passed through the positively charged needle into the negatively charged $CaCl_2$ gelling bath, creating spherical microcapsules. To test changes in microcapsule diameter, the voltage generator was set at voltages of 2.5, 3.0, 3.5, 4.0, 4.5, 5.0, and 6.0kV in individual tests, while flow rate (60mm/hr) and pH (7.4) were held constant during synthesis. These experiments were repeated with (1.5kV) and without (0kV) the presence of an initial voltage being applied to the needle by the voltage generator prior to the start of the syringe pump. This was done to see if any changes in microcapsule size resulted from the change. Microcapsules were synthesized with and without the voltage set prior to starting the syringe pump, but voltage remained constant throughout the extrusion process once started. Subsequent experiments to determine changes in microcapsule diameter were done using changes in flow rate (15mm/hr, 30mm/hr, 45mm/hr, and 60mm/hr) while voltage (4.0kV) and the presence of a starting voltage (1.5kV) were held constant.

Alginate-poly-l-lysine (A-PLL) and alginate-poly-l-ornithine (A-PLO) microcapsules were produced by a 1 step method as a means to circumvent rapid diffusion and loss of peptide in initial time points that occur by multi-step methods of synthesis. The initial method of 2% alginate preparation and instrument setup was repeated as described above. Polymer solutions of either poly-l-lysine (Alfa Aesar L-lysine monohydrate 98%) or poly-l-ornithine (Alfa Aesar L-ornithine hydrochloride

99%) were mixed at a 0.5% w/v in 0.15M $CaCl_2$. A 0.5% w/v concentration for both polymers was selected based on preliminary results allowing dissolution of the material and ease in buffering to desired pH values. The pH was buffered accordingly using 0.1M HEPES, 0.1M hydrochloric acid (HCL), or 0.1M sodium hydroxide (NaOH). Polymer solutions were made at pH values either acidic (4.3) or biologically stable (7.4) for use during release studies. Synthesized 2% alginate microcapsules were extruded into a polymer/0.15M $CaCl_2$ bath and allowed to gel 12 minutes. Microcapsules were removed from the gelling bath post-synthesis and rinsed in sterile deionized water, followed by examination of morphology by SEM and AFM.

Microencapsulation and Release Profile of αCT1 Peptide

Release profiles of αCT1 were studied over 48 hrs from alginate microcapsules extruded into $CaCl_2$ solutions with pH values of 4.3, 7.4, or 9.3. In addition release profiles from poly-l-lysine and poly-l-ornithine coated capsules were studied using the same set of solution pH values. Lowering the pH to a value opposite in scale to the isoelectric point (pI) value (theoretical 11.47) of αCT1 is thought to help slow the release rate by charge repulsion between the peptide and the external gelling solution. The literature suggests potential methods of controlling release through changes in many parameters such as pH, polymeric coatings, changes in peptide concentration, addition of secondary ions or chemicals, and drying of capsules post synthesis (Gray et al 1988, Dashevsky 1998, Gombotz et al 1998, Vandenberg et al 2001, Tama et al 2011). This data is not representative of the αCT1 peptide size and high isoelectric point (11.47 vs. BSA 4.7). The most similar cited release data to αCT1 is insulin (5.8 kDa). In our studies we have elected to study release in alginate alone, alginate with polymer coating, and a

combination of both with variation in pH of the gelling solutions to characterize changes in αCT1 release.

For these experiments, extrusion parameters were kept constant at 6.0kV, 0kV initial voltage, and a flow rate of 60mm/hr in all tests. Previous published studies found a total αCT1 peptide concentration between 100-200μM created a therapeutic range (Ghatnekar et al 2009). Therefore initial peptide concentration was kept constant at 200μM. Alginate concentration was also kept constant at 2%, while the polymer/$CaCl_2$ bath was synthesized at 0.5%polymer/0.15M $CaCl_2$ as previously listed. Initially, microcapsules were created using these parameters to show the effect of change from neutral pH solutions (7.2) to acidic (4.3) using 2% alginate without polymer coating. Tests were performed to show the effect of addition of both 0.5% A-PLL and A-PLO microcapsules to acidic pH solutions (pH 4.3). An additional set of release profiles, conducted on microcapsules synthesized at 6.0kV, 60mm/hr, pH 7.4, were performed to examine the effects of loading concentration, comparing the 200μM concentration (used here in the pH and polymer coating tests) with a doubled 400μM amount. Post synthesis, microcapsules were rinsed in deionized water to remove excess gelling solution. The capsules were then re-covered in 0.5mL deionized water, with time points taken over 48 hours. Early time points of 1, 2, 4, 6, and 8hrs were taken to account for early burst release of peptide from the microcapsules, with successive measurements taken at 24 and 48hrs respectively. Analysis of peptide concentration was performed using a Micro BCA protein assay kit (Thermo Scientific) with αCT1 replacing BSA for our standard curve. Additional standard curves using BSA were run against the αCT1 to establish any variations in linearity and changes in concentrations between the different molecular

weight protein and peptide used in the standards. All tests were run on a BioTek Synergy 2 spectrophotometer and performed in triplicate. Statistics were compiled using the GraphPad Prism program with analysis using the student's t-test program.

Ultraviolet Crosslinking Attachment to Biomaterials

An efficient and fast method of attachment of microcapsules to implanted materials was sought by ultraviolet (UV) crosslinking. Microcapsules were attached to silicone, collagen, and PWAS sensor biomaterials exhibiting different material properties to determine the rate of attachment and overall area of coverage on the material surface. Flat 2.5% collagen cut into $1cm^2$ strips was coated by pipetting 30µl of empty 200µm alginate microcapsules onto the surface. This volume of capsules was chosen to achieve complete initial coverage of the collagen surface. The microcapsules were allowed to settle on the collagen surface and then UV crosslinked at one of four UV powers (6300, 8000, 9000, 9999 µJ x100) using a Stratagene UV Stratalinker 1800. Previous work using collagen tube samples indicated a UV power of 6300 µJ x100 was the minimum value necessary for crosslinking. Therefore this value was used as a baseline starting point with three other representative values up to 9999 (maximum instrument value) as test points. Increasing UV power was expected to create a hardening of the materials and therefore stronger bonding of the microcapsules to the biomaterials. After UV crosslinking, the samples were then rinsed in deionized water to remove unattached capsules after one of two determined stop points: 0.5 or 24hrs. These time points were selected to give an almost immediate short term point and long term point to compare the effects of drying on total attachment. Similar attachment tests were performed on piezioelectric wafer active sensors (PWAS) and small ($1cm^2$) silicone discs to evaluate

coverage ability of UV crosslinking with the microcapsules on multiple implantable biomaterials for future in vivo experiments. Electromechanical impedance is measured by the PWAS sensor as a means of evaluating in vivo reactions to implants (Giurgiutiu et al, 2004, Bender et al, 2006). On both the PWAS sensors and silicone discs, a coat of 100µl of 0.7% methylcellulose was applied to the surface for attachment prior to microcapsule placement. Both of the later materials received 80µl of ~200µm empty microcapsules using the identical UV powers and time parameters tested on the collagen strips. The difference in volumes of microcapsules applied to the silicone and PWAS sensors (80µl vs. 30µl) compared to the collagen is based on differences in the sample biomaterial sizes and the maintenance of complete surface coverage with microcapsules before UV crosslinking. These volumes were found to provide saturation of the materials surface with microcapsules prior to UV crosslinking. Analysis and images were obtained using a Zeiss Lumar V12 fluorescent microscope with Axiovision Release 4.9.2 software and a Zeiss Axiovert 135 phase contrast microscope with Axiovision Release 4.5 software. Statistical analysis was performed using the GraphPad Prism program analyzing an unpaired student's t-test to determine significance.

SEM Of UV Crosslinked Microcapsules

Microcapsules were created at a diameter of 200µm with an encapsulated αCT1 peptide concentration of 100µM using 2% sodium alginate as described above. SEM was performed to characterize surface morphology and UV crosslinking effects on these capsules. Microcapsules were prepared for SEM in two ways. The first method involved preparation of microcapsules by UV crosslinking at 9000µJ x 100 twice to 0.7% methylcellulose coated glass coverslips. This was done to match our protocol for surface

attachment to biomaterials previously listed in the UV crosslinking section. A 24hr incubation period at 4°C was allowed, followed by air drying under laminar flow for 2hrs. The microcapsules were then critical point dried (Tousimis Samdri-PVT-3B) and gold sputter coated (Cressington 108 Auto/SE) for 3 minutes.

The second method of preparation, performed to better view surface morphology without UV crosslinking, was carried out based on a modified protocol using the osmium-tannic acid-osmium method (OTO) (Murphy 1980). Loose microcapsules were initially placed in a 0.1M Na Cacodylate, 3mM $CaCl_2$, pH 7.2 buffer followed by a buffered fix of 2% paraformaldehyde, 2% glutaraldehyde, and 0.1% ruthenium red. The microcapsules were next rinsed in 0.9% saline and placed in a secondary buffered fix consisting of 1% osmium tetroxide and 0.1% ruthenium red. Next the samples were rinsed in 0.9% saline and placed in a series of alternating buffered fixatives containing either 1% tannic acid in 1% glutaraldehyde or 1% osmium tetroxide. Rinses in these buffered fixatives were repeated 8 times at 20 minutes each with rinsing in 0.9% saline in between steps. The microcapsules were finally rinsed with 0.9% saline to remove any buffer, dehydrated in a series of ethanol baths, critical point dried, and gold sputter coated. SEM images were taken using a JEOL JSM-6300 SEM at 10kV.

AFM of UV Crosslinked Microcapsules

Analysis of microcapsule attachment to the implant materials and material structure was performed using AFM. Glass coverslips were coated with 0.7% methylcellulose followed by representative samples (4.5kV or 6.0kV total voltage, 0kV initial voltage, and 60mm/hr flow rate) of 2% alginate microcapsules. The microcapsules were UV crosslinked at 9000uJ x100 twice and incubated at 4°C for 24hrs prior to AFM

analysis. The samples were run on an Asylum MFP-3D Series AFM instrument (Asylum Research), measuring relative adhesive forces and microcapsule stiffness according to previously a published protocol (Norris et al 2008). Prior to analysis, the coverslips were attached to a glass microscope slide and equilibrated in the isolation chamber on the AFM stage for 5 minutes. The laser was adjusted on the silicon nitride coated cantilever with a diving-board tip at 0.01N/m constant force (Asylum Research) to achieve maximum signal through alignment of the laser. Once aligned, the tip was brought into contact with the microcapsules using the AFM software, (Asylum IGORPro). Once in contact, an image of the scan area was taken which allowed a view of the sample and its features. The initial scan taken was a 20µm x 20µm area and subsequent smaller scans were performed down to a 2µm x 2µm area. From the chosen 2µm square area, we randomly selected 3-4 regions of interest to sample, selecting both peaks and valleys. These tips have a radius of curvature of less than 20nm. To obtain stiffness, the AFM was used in the "indentation mode". This data is converted through the program into either force-distance curves or indentation-distance curves. The force distance curve was taken at this point by allowing the tip to approach the surface and retract, in quick pulses; this then relayed the static deflection of the tip on the surface. An average of 6 independent spots had a force distance curve performed on them. These were then averaged and normalized against the glass slide surface from which the force distance curve was generated. The result was a plot with two averaged curves, one for the approach and one for the retraction demonstrating pico-Newton forces along the nanometer scale of approach and retraction. In order to corroborate that the data was reliable, the curves generated were analyzed for similar slopes on both the approach and retraction.

2.4 Results

2.4.1 Parametric Microcapsule Analysis

Electrospray microencapsulation was performed as a comparative set of tests to establish the parameters necessary to produce a specific diameter of microcapsule. In this proof of concept design, microcapsules were synthesized in a specific working range of voltages while examining the changes in microcapsule diameter with and without the addition of a starting voltage. Further comparisons were made using the same working range of voltages, while examining the effect on diameter with changing flow rate. A range of voltages between 2.5kV-6.0kV, a starting voltage of either 0kV or 1.5kV, and a series of flow rates (15mm/hr, 30mm/hr, 45mm/hr, and 60mm/hr) are used here as parameters.

Figure 2.1.1 shows the results of the parametric design. Figure 2.1A provides a graphical representation of the average microcapsule diameters in the 2.5-6.0kV working range under the two initial voltage conditions of 0kV or 1.5kV with the attached table below showing exact measurements with standard error. Flow rate was kept constant at 60mm/hr for all samples in figure 2.1. Each point corresponds to the average microcapsule diameter of 25 representative capsules. A direct relationship between the total voltage and microcapsule diameter size was observed with a constant flow rate. Using a starting voltage of 0Kv and total voltage of 2.5Kv produced microcapsules with a diameter of 1383.1±12.5µm. When we changed our initial voltage to 1.5Kv we again saw a direct dependency between the total voltage and the microcapsule diameter. Similar to the results shown using a 0Kv starting voltage, a 2.5Kv total voltage produced microcapsules with diameters of 1259.8±7.9µm, which shrunk to 173.0±1.7µm when the

total voltage was increased to 6.0Kv. When individual total voltages were compared between the 0kV or 1.5kV starting voltages, no significant differences were seen ($p<0.05$). Both starting voltages had microcapsules that were larger and smaller at identical total voltage (figure 2.1A table). Summarizing results, an overall decrease in diameter was seen when the initial voltage was changed from 0kV to 1.5kV at total working voltage points of 2.5kV (8.91% decrease), 3.5kV (25.92%), 4.0kV (3.29%), and 4.5kV (14.38%). (Figure 2.1) Similarly, an increase in microcapsule diameter between 0kV and 1.5kV initial voltage was seen at 3.0kV (2.7% increase), 5.0kV (15.04%), and 6.0kV (8.19%). The lack of a consistent pattern of increase or decrease in microcapsule size and the results of the statistical analysis ($p>0.05$) indicated changes in starting voltage between 0kV and 1.5kV are not a significant parameter in changing microcapsule diameter. Overall our results confirm the presence of size variability in using the electrospray method.

Examples of images of our synthesized microcapsules are seen in Figures 2.1 B, C, and D. Figure 2.1B shows microcapsules extruded at 4.0kV, with a starting voltage of 0kV and a continuous flow rate of 60mm/hr. Similarly, Figures 2.1C and 2.1D show microcapsules synthesized at 4.5kV and 6.0kV with a 0kV starting voltage and 60mm/hr flow rate, respectively.

Previous reports suggest that changes in flow rate are a determining factor in microcapsule diameter during synthesis (Chakraborty et al 2009, Zhang et al 2009). We set out to determine whether changing the flow rate would have an effect on the variability of microcapsule size. Holding total voltage (4.0kV) and starting voltage (1.5kV) constant, we tested flow rates of 15mm/hr, 30mm/hr, 45mm/hr and 60mm/hr.

Microcapsules made at each of these flow rates showed an average change in diameter of <20µm when the overall voltage, initial voltage, and alginate concentration were held constant. (results not shown) Using a one way ANOVA test with Gaussian approximation a $p>0.05$ was seen, indicating no significant changes in microcapsule diameters when flow rate was changed. Taken together these data suggest that total voltage, rather than flow rate drove microcapsule diameter. As a result, the remaining experiments in this paper used a constant flow rate of 60mm/hr in the microcapsule synthesis experiments. Finally, these data indicate that a voltage of at least 3.0kV is necessary to overcome the surface tension of the alginate as it is extruded at this needle's working distance, with values above 3.5kV and less than 6.5kV required to produce microcapsules with ideal morphology and diameter size consistency.

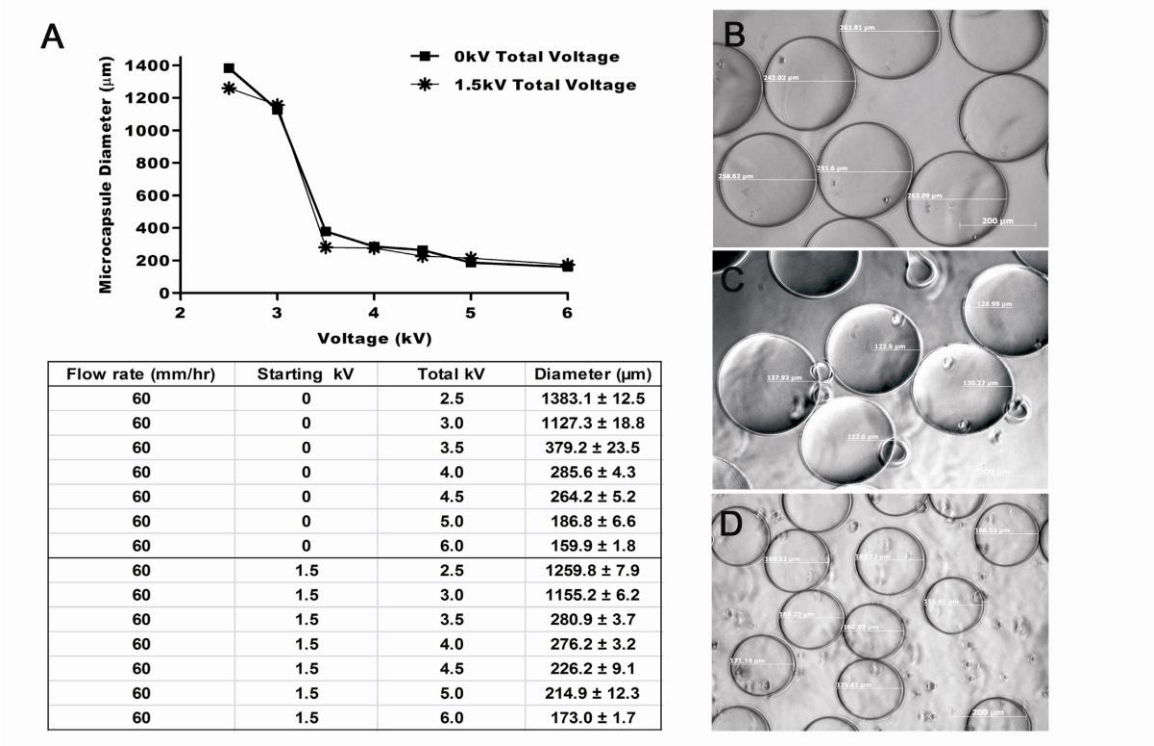

Flow rate (mm/hr)	Starting kV	Total kV	Diameter (µm)
60	0	2.5	1383.1 ± 12.5
60	0	3.0	1127.3 ± 18.8
60	0	3.5	379.2 ± 23.5
60	0	4.0	285.6 ± 4.3
60	0	4.5	264.2 ± 5.2
60	0	5.0	186.8 ± 6.6
60	0	6.0	159.9 ± 1.8
60	1.5	2.5	1259.8 ± 7.9
60	1.5	3.0	1155.2 ± 6.2
60	1.5	3.5	280.9 ± 3.7
60	1.5	4.0	276.2 ± 3.2
60	1.5	4.5	226.2 ± 9.1
60	1.5	5.0	214.9 ± 12.3
60	1.5	6.0	173.0 ± 1.7

Figure 2.1 Results of the parametric study of sodium alginate microcapsules. **(A**) 2% sodium alginate microcapsules were made with seven different voltages between 2.5kV-6.0kV using a constant starting voltage of 1.5kV. These results are shown in the graph indicated by stars, with average diameters listed for each parameter in the table below the graph. The study was repeated with the same total voltages and a constant voltage of 0kV. These results are represented by squares, with average capsule diameters in the table below. (**B**) Phase contrast image of microcapsules created at 4.0kV, 0kV starting voltage, and 60mm/hr. (**C)** Phase contrast image of microcapsules created at 4.5kV, 0kV starting voltage, and 60mm/hr. (**D)** Phase contrast image of microcapsules created at 6.0kV, 0kV starting voltage, and 60mm/hr.

2.4.2 Loading and Release of αCT1 From Alginate and Polymer Coated Microcapsules

To characterize our microcapsules as a potential drug delivery vehicle, a series of release profile experiments were conducted. Of interest was the controlled release of αCT1 for extended use in future regenerative medicine studies. Our desired outcome was to obtain a continuous release over a 24+ hr period. In conducting these release experiments, we examined the effect of pH of the gelling bath solution first with sodium alginate microcapsules, followed by the effects of both pH of the gelling bath with addition of either PLL or PLO polymer coating to the alginate capsules. Additional tests were performed varying the ratio of αCT1 to sodium alginate prior to application. These results are presented in Appendix A.1.

Initially, loading efficiency experiments were conducted on four samples using 6.0kV total voltage, 0kV starting voltage, 60mm/hr flow rate, an αCT1 concentration of 200µM, and a 2% alginate solution. Measurements using a micro BCA protein assay indicated a loading efficiency of 72.53 ± 1.59%. Two identically synthesized sets of microcapsules, one at a concentration of 200µM and one at 400µM, were analyzed for release. The results, shown in figure 2.2, indicated a rapid initial burst of αCT1 prior to the initial 1hr time point when loading with 400µM. As such, only 11.22µM was measured over the initial 4hrs vs 27.73µM when loading with 200µM. Using the same controlled parameters, we next synthesized 2% alginate capsules at a 200µM peptide concentration and measured the release over 48hrs with the pH of the calcium chloride gelling bath at either 4.3 or 7.2. Figure 2.3A shows the 48hr release profile of 2% alginate microcapsules extruded into an acidic 4.3 calcium chloride bath while 2.3B

shows capsules extruded into a neutral 7.2 pH bath, and 2.3C extruded into a basic 9.3 pH bath. The insets on each graph show the first five hours of release for better appreciation of the rapid release of the peptide. Average results for each time point are presented in the table in Figure 2.3. Previous reports have suggested that an acidic pH acts to reduce the pore size of the microcapsules and therefore slows peptide release (Dashevsky 1998, Vandenberg et al 2001). When microcapsules were extruded into an acidic environment, an overall lower initial release of peptide in the first hour (21.93µM vs 11.67µM) was observed (Figure 2.3 table). However, the acidic environment allowed for an extended release over the first four hours. In comparison, a larger total amount of peptide is released over the 48hr period at a neutral pH vs. acidic pH, but by only 5.7µM. The lowest total release over the first four hours was seen in the basic 9.3 pH environment. The biological impact of this difference in peptide is unknown at this time and must be examined in order to determine significance. Based on these results, addition of an acidic environment at synthesis slows release of the αCT1 peptide and thus extends the profile timeline.

We next tested whether a change in pH of the alginate solution (pH 4.3 vs pH 7.2) prior to synthesis with a neutral buffered gelling bath (pH 7.2) would produce changes to initial burst or extended release kinetics over a 48hr period. No significant changes ($p>0.05$ comparing identical time points between pH 4.3 and 7.2) to either the initial release of the peptide or extended release were observed (Data not shown).

We then set out to determine if coating the alginate microcapsules could enhance peptide release. The results in figure 2.4 show a comparison of release over 48hrs in three microcapsule types at a pH of 4.3 using the same parameters and peptide concentration as

described above. In each case the alginate solution was mixed at a 2% concentration while the additional polymer coating solution was made at 0.5% w/v. Figure 2.4A presents release data over 48hrs from 2% alginate capsules without additional polymer coating at a pH of 4.3. Figure 2.4B shows the A-PLL (poly-l-lysine) polymer coated microcapsules release data over 48hrs at a pH of 4.3. Figure 2.4C similarly shows the release data of A-PLO (poly-l-ornithine) polymer coated capsules at a pH of 4.3. The Figure 2.4 table shows the concentration values of peptide release at each time point for each of the three capsule types. Total peptide released from the A-PLL capsules was 44.68 ± 2.99µM vs. 113.99 ± 42.85µM for the A-PLO capsules at a pH of 4.3. This represents a 155.13% increase in released peptide through the change in polymer type at equal polymeric concentrations. In addition, the total peptide concentration released was 284.58% (84.35µM difference) greater from the A-PLO coated capsules compared to the uncoated 2% alginate capsules at the same pH. The peptide release seen in the A-PLO capsules had higher standard error values in hours 1-4 in these tests, which was greater than values found in the other two capsule types in figure 2.4. Calculating the maximum high range of the A-PLL capsules in comparison to the low range of the A-PLO capsules resulted in a 49.23% (23.47µM) change in total peptide release between the two capsule types. However, statistical analysis of hours 1-4 on the A-PLO vs A-PLL and A-PLO vs 2% alginate without polymer at an acidic pH resulted in significance in both cases ($p < 0.05$).

When taken together, these data lead us to conclude the addition of polymer coating in this one step method significantly increases the total amount of peptide we are able to effectively release and deliver over a 48hr period. More specifically we saw

another significant increase in peptide release in using a PLO coating at a 0.5% w/v concentration. By combining the changes in both pH and polymer coating, a more attractive controlled design of microcapsules can be achieved with αCT1.

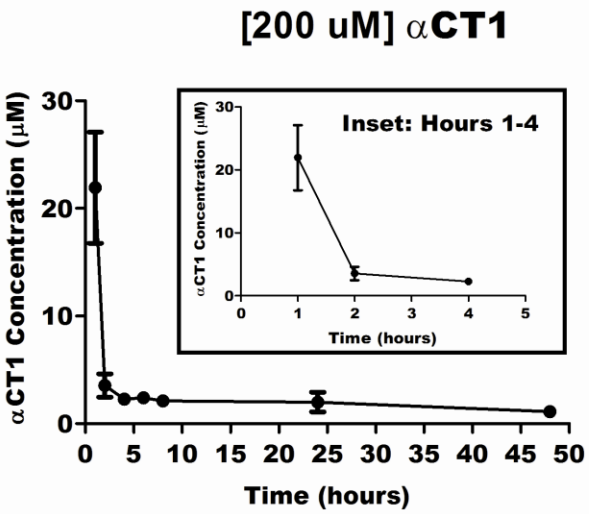

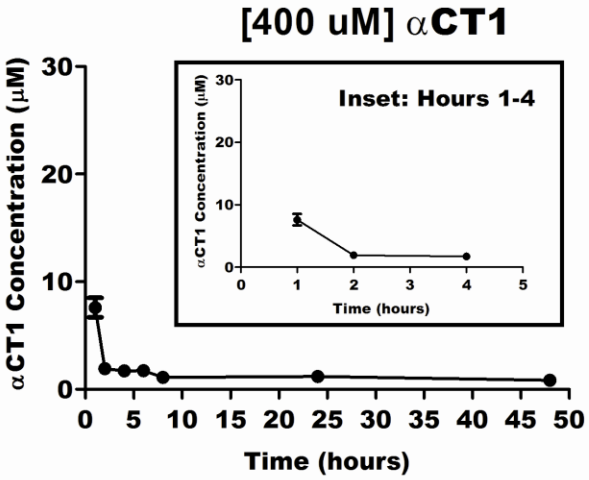

Average Peptide Concentration (uM) + Standard Error		
Time (Hours)	2% Alginate Capsules [200 uM] αCT1	2% Alginate Capsules [400 uM] αCT1
1	21.93 ± 5.15	7.6 ± 0.92
2	3.53 ± 1.07	1.91 ± 0.50
4	2.27 ± 0.13	1.71 ± 0.39
6	2.39 ± 0.06	1.73 ± 0.40
8	2.12 ± 0.21	1.12 ± 0.02
24	1.99 ± 0.92	1.17 ± 0.03
48	1.11 ± 0.12	0.83 ± 0.16

Figure 2.2 Release profiles examining change in release with differing initial loading of αCT1 over 48hrs. Profiles of both 200μM (top) and 400μM (bottom) loaded microcapsules synthesized with no starting voltage, 6.0kV total voltage, and 60mm/hr flow rate are shown. Individual values are listed in the table below.

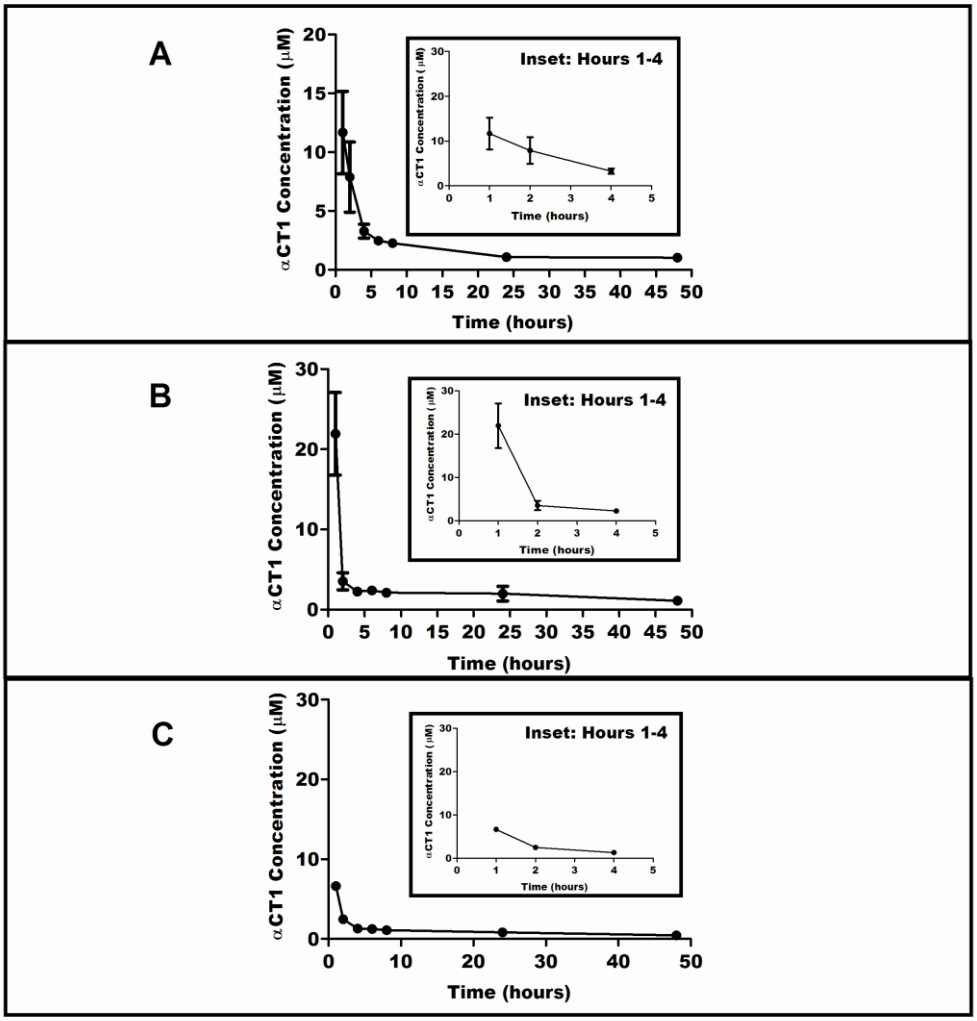

Average Peptide Concentration (uM) + Standard Error			
Time (Hours)	2% Alginate at pH 4	2% Alginate at pH 7	2% Alginate at pH 9
1	11.67 ± 3.51	21.93 ± 5.15	6.63 ± 0.15
2	7.88 ± 2.98	3.53 ± 1.07	2.48 ± 0.18
4	3.27 ± 0.59	2.27 ± 0.13	1.31 ± 0.12
6	2.47 ± 0.05	2.39 ± 0.06	1.26 ± 0.07
8	2.26 ± 0.06	2.12 ± 0.21	1.12 ± 0.01
24	1.07 ± 0.02	1.99 ± 0.92	0.85 ± 0.16
48	1.02 ± 0.09	1.11 ± 0.12	0.45 ± 0.15

Figure 2.3 Release profile comparison of 2% alginate microcapsules synthesized and gelled in a 0.15M $CaCl_2$ bath at a pH of 7 vs. identical capsules synthesized at a pH of 4.3 and 9.3. All microcapsules were made with an αCT1 concentration of 200μM, no starting voltage, a flow rate of 60 mm/hr, and a total voltage of 6.0kV. (**A**) 2% alginate microcapsule release profile with synthesis in a gelling bath at a pH of 7. (**B**) 2% alginate microcapsule release profile with synthesis in a gelling bath at a pH of 4.3. (**C**) 2% alginate microcapsule release profile with synthesis in a gelling bath at a pH of 9.3. Below is a table of average measured αCT1 concentrations over 48 hrs at each time point. Measurements are the result of three separate tests and evaluation using a Micro BCA protein assay with substituted αCT1 peptide standards at 562nm.

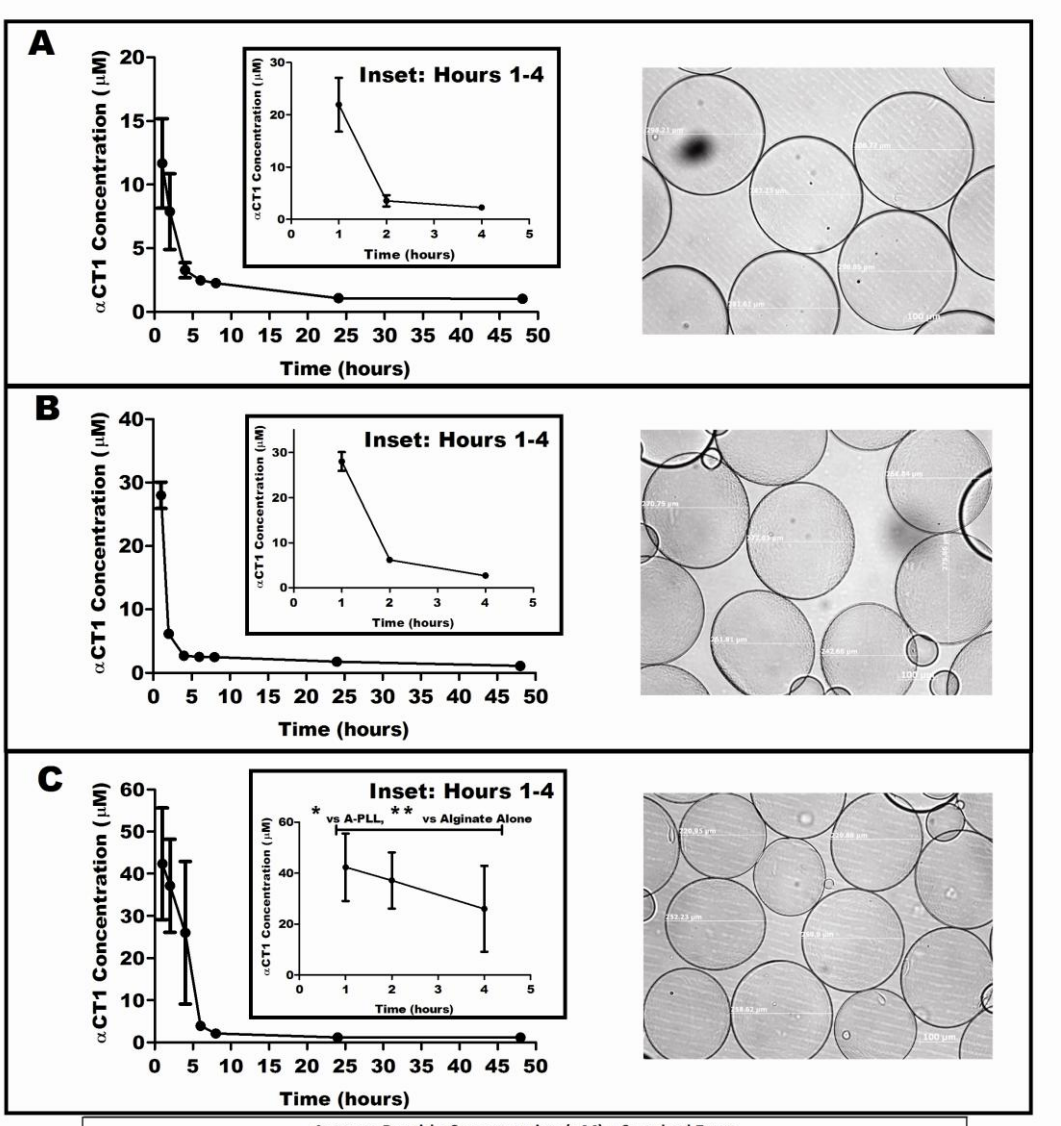

Average Peptide Concentration (uM) + Standard Error			
Time (Hours)	Alginate Only at pH 4	Alginate-Poly-L-Lysine at pH 4	Alginate-Poly-L-Ornithine at pH 4
1	11.67 ± 3.51	27.98 ± 2.07	42.38 ± 13.26
2	7.88 ± 2.98	6.16 ± 0.22	37.16 ± 11.01
4	3.27 ± 0.59	2.68 ± 0.09	26.03 ± 16.90
6	2.47 ± 0.05	2.53 ± 0.09	3.94 ± 1.15
8	2.26 ± 0.06	2.49 ± 0.04	2.12 ± 0.43
24	1.07 ± 0.02	1.76 ± 0.38	1.17 ± 0.03
48	1.02 ± 0.09	1.08 ± 0.10	1.19 ± 0.07

Figure 2.4 Release profiles comparing 2% alginate microcapsules synthesized in a 0.15M CaCl2 gelling bath at a pH of 4.3 against both A-PLL and A-PLO microcapsules synthesized at an identical pH of 4.3. Additional images of 2% alginate, A-PLL, and A-PLO microcapsules synthesized at a pH of 4.3, total voltage of 3.5kV, and flow rate of 60 mm/hr are shown beside each corresponding graph. Below A, B, and C is a table listing exact values of peptide measured at each time point with standard error. (**A**) 2% alginate microcapsule release profile with synthesis in a gelling bath at a pH of 4.3. (**B**) A-PLL microcapsule release profile. (**C**) A-PLO microcapsule release profile.

2.4.3 UV Attachment of Alginate Microcapsules to Biomaterials

We sought to use UV crosslinking of our microcapsules as a means of attachment to specific implantable biomaterials of interest. Here we show attachment to three different biomaterials; 2.5% collagen, silicone discs, and PWAS sensors. UV crosslinking provides a means of stabilization of the alginate/polymer materials while also acting as a non-interfering and biocompatible method.

Four differing UV powers (6300, 8000, 9000, and 9999µJ x100) were chosen for use. In addition, we also varied the time after UV crosslinking the capsules were on the substrates prior to testing to determine if any significance existed. Two time points were chosen; one of a short duration (0.5hrs) and a second longer duration (24hrs) to examine the effect of drying time on attachment. Microcapsules were synthesized at a 2% alginate concentration and diameter of 200µm, followed by coating on the biomaterial surface. Samples were then crosslinked at the set powers following placement of the microcapsules to the biomaterial. Incubation post crosslinking at both the short and long time points was carried out at 4°C before rinsing with deionized water three times to remove unattached capsules. Attached capsules were imaged and the total area covered by microcapsules was marked and measured. Figure 2.5A shows a representative sample of 2.5% collagen coated with 2% alginate microcapsules post UV crosslinking at 9999µJ x 100. Similarly, figure 2.5B shows an image of a PWAS sensor coated and UV crosslinked at 9000µJ x 100. Figure 2.5C shows an image of a silicone disc coated in microcapsules post UV crosslinking at 8000µJ x 100.

The results shown in the corresponding graphs indicate the percent area covered by microcapsules on each material surface (Figure 2.5D (2.5% collagen), 2.5E (PWAS

sensor), and 2.5F (silicone disc)). Results in each graph indicate average area of coverage based on four separate trials. Analysis of the data show the longer (24hr) incubation time drastically increased the area of microcapsule attachment on all three materials. The results also showed that the greatest total surface coverage for both the collagen (40.17% ± 19.10) and PWAS sensors (39.03% ± 6.72) was achieved when UV crosslinking was done at a power of 9000µJ x 100. In contrast, the silicone attachment indicated the highest area of microcapsule attachment occurred with a UV power of 9999µJ x100 (22% ± 9.72), with the results of 8000 (17% ± 7.03) and 9000µJ x100 (21% ± 2.23) producing similar results at 24hrs. In all instances using the UV crosslinking method, we observed that a total surface area of coverage was never greater than 45% following rinsing. To maintain microcapsule morphology and prevention of any possible changes in peptide release from the microcapsules, a small amount of supernatant was left on the capsules to insure integrity. This volume was minimal but necessary for integrity to be preserved. The amount of supernatant used was estimated to be enough to slightly cover the capsules. In total, for future applications, UV crosslinking was shown to provide a viable method of attachment and delivery of microcapsules with maintained morphology, but limitations in total coverage of surface area of the materials was observed.

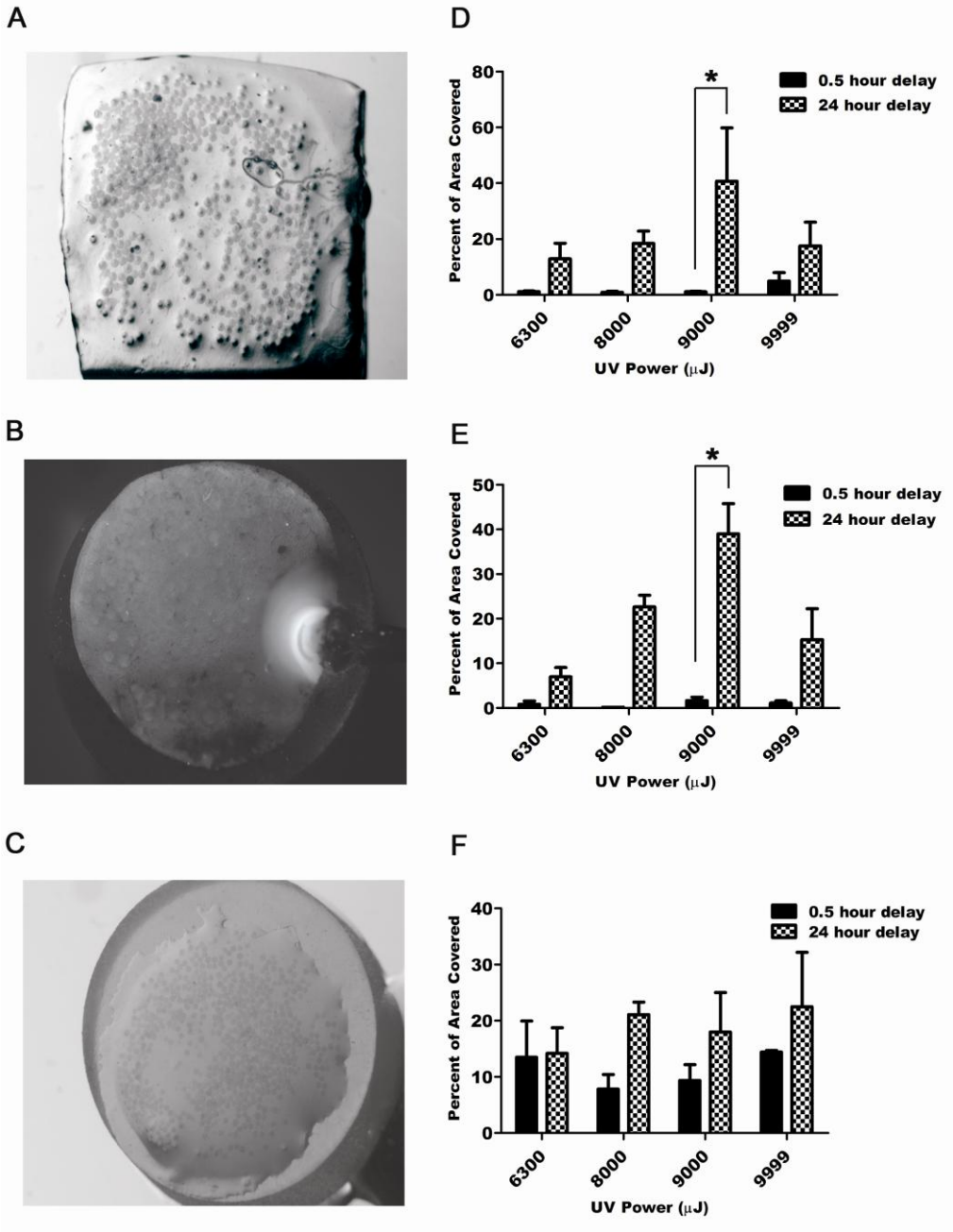

Figure 2.5 UV crosslinking of microcapsules to biomaterials (**A**) Post rinse microcapsules shown attached to 2.5% collagen after 24hrs incubation and UV crosslinking at 9999µJ x100. (**B**) Post rinse microcapsules shown attached to a PWAS sensor after 24hrs incubation and UV crosslinking at 9000µJ x100. (**C**) Post rinse microcapsules shown attached to silicone after 24hrs incubation and UV crosslinking at 8000µJ x100. (**D**) Graph illustrating average microcapsule attachment to 2.5% collagen at 4 UV powers and either a 0.5hr or 24hr incubation. (**E**) Average microcapsule attachment to PWAS sensors at 4 UV powers and either a 0.5hr or 24hr incubation. (**F**) Average microcapsule attachment to 1cm^2 silicone disks at 4 UV powers and either a 0.5hr or 24hr incubation.

2.4.4 The Affect of UV Crosslinking on Microcapsule Integrity and Morphology

To investigate the possible effects of UV crosslinking on microcapsule morphology, samples of microcapsules were analyzed by SEM imaging. Maintenance of spherical morphology and pore structure is critical to achieve proper release of peptide from the microcapsules in the same manner shown in our release studies. Samples of 200µm 2% alginate microcapsules were placed on glass coverslips coated with 0.7% methylcellulose, UV crosslinked at 9000µJ x100 twice, then incubated for 24hrs at 4°C. A UV power of 9000µJ was selected based on the perceived effectiveness shown at this power in the UV crosslinking attachment data previously shown. Post incubation the microcapsules were dried and processed for SEM. Figures 2.6A (200X), 2.6B (2,500X), 2.6C (700X) and 2.6D (700X) show representative examples of these microcapsules at the indicated magnifications. Upon examination of these capsules, we observed little negative effect on morphology due to UV crosslinking damage. Figure 2.6A shows possible clumping and lateral bonding of the microcapsules to one another, which may have an effect on the overall surface area available. This could lead to variations in the release rate of the microcapsules. Overall the microcapsules maintained a spherical morphology upon processing and UV crosslinking. In addition, no surface damage was observed when examined at higher power (Fig 2.6B). These data further support the idea that UV crosslinking is a viable option as a means of microcapsule attachment.

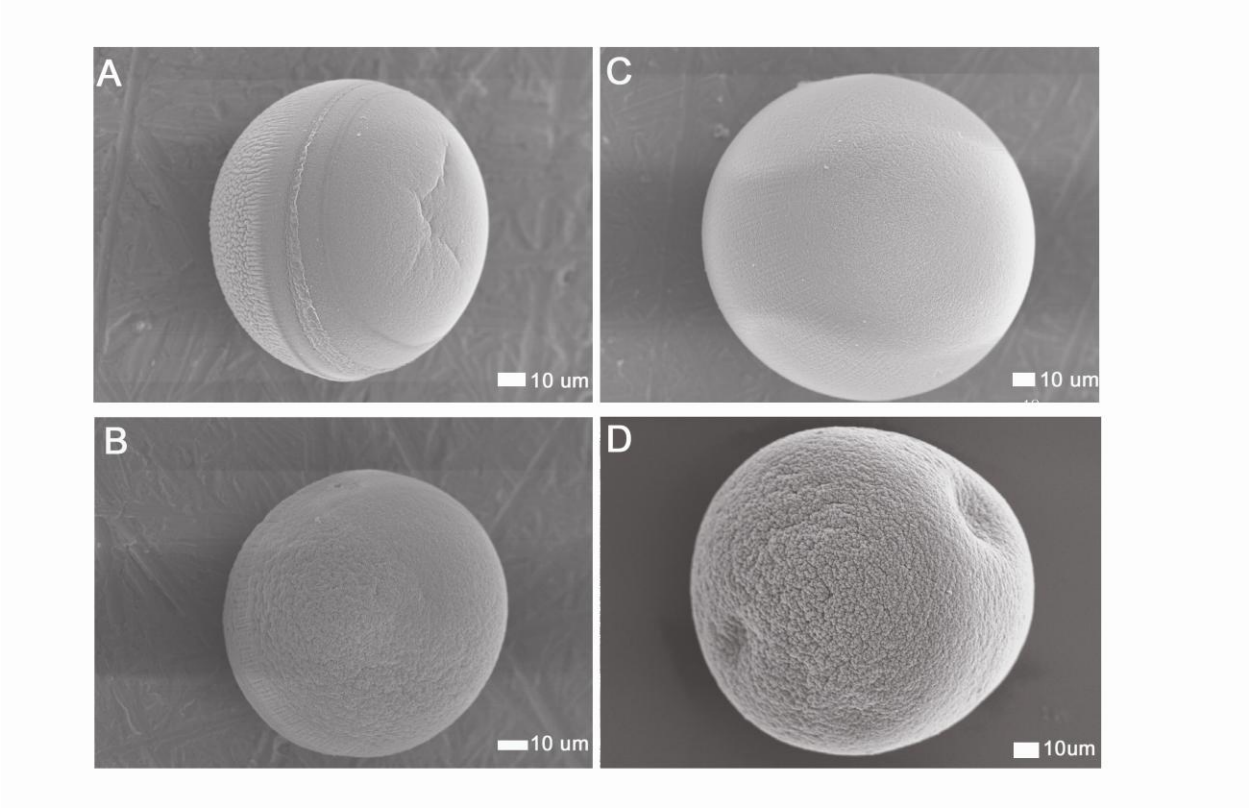

Figure 2.6 SEM images of αCT1 containing microcapsules synthesized at voltages of 4.5kV and 6.0kV using 2% sodium alginate. (**A**) Sample image of a microcapsule synthesized at 4.5kV without UV crosslinking and a 550X magnification. (**B**) 550X magnification, 10kV image of 6.0kV synthesized microcapsule with UV crosslinking at 9000µJ twice. (**C**) 550X magnification, 10kVmicrocapsule synthesized at 4.5kV with UV crosslinking at 9000µJ twice. (**D**) 700X magnification, 10kVmicrocapsule synthesized at 6.0kV without UV crosslinking.

2.4.5 Assessment of the Microcapsule Mechanical Properties Using AFM

Finally, we sought to determine if there were differences in the mechanical properties of the microcapsules at the various conditions used to extrude the microcapsules and upon UV crosslinking. To that end, AFM was used to characterize the mechanical properties (e.g. stiffness) of the UV crosslinked microcapsules. AFM can measure the stiffness and rigidity of the microcapsule while also examining the morphology in a similar manner as we did with SEM.

Two representative sizes of 2% alginate microcapsules were selected for examination; 260µm (4.5kV total voltage, 0kV starting voltage, and 60mm/hr flow rate) and 160µm (6.0kV total voltage, 0kV starting voltage, and 60mm/hr flow rate). Each sample was first placed on 0.7% methylcellulose coated glass coverslips then UV crosslinked at 9000µJ x 100 as described above in the SEM procedure. Glass coverslips were used in place of the biomaterials previously listed to compensate for rigidity and size needs on the AFM. Figure 2.7 shows the results of the AFM testing of our microcapsules. Figure 2.7B (4.5kV) and 2.7D (6.0kV) represent the results of AFM scanning of microcapsules without UV crosslinking. Figures 2.7A (4.5kV) and 2.7C (6.0kV) contain the results of scanning on UV crosslinked microcapsules. Figure 2.7A, 2.7B, 2.7C, and 2.7D each contain the results of the scans in the form of a heat map (left) and a force map (right). Consistency scans were performed on each capsule type prior to analysis to check for consistency in microcapsule morphology and curvature (not shown). When a comparison of the force maps for both A and C is done, a dramatic variation in material property is observed. The samples scanned prior to UV crosslinking showed little variation in adhesion forces with median forces at 54.26pN for 6.0kV and 90.27pN

for 4.5kV extraction. However, the samples scanned after UV crosslinking indicated an order of magnitude change in overall adhesion and a 10 fold change in adhesion forces between the microcapsule samples (median values of 100nN for 6.0kV vs. 7.7 nN for 4.5kV). The UV crosslinking does increase the stiffness of the microcapsules, as expected, however, the AFM data suggests the UV crosslinked microcapsule structures experienced a change in stiffness that may be attributed to other factors than strictly UV power. Possibilities include microcapsule size and density of dispersion on the material surface. The AFM data also allows us to characterize the microcapsule shape post UV crosslinking, in comparison with the SEM images, as maintaining good spherical morphology.

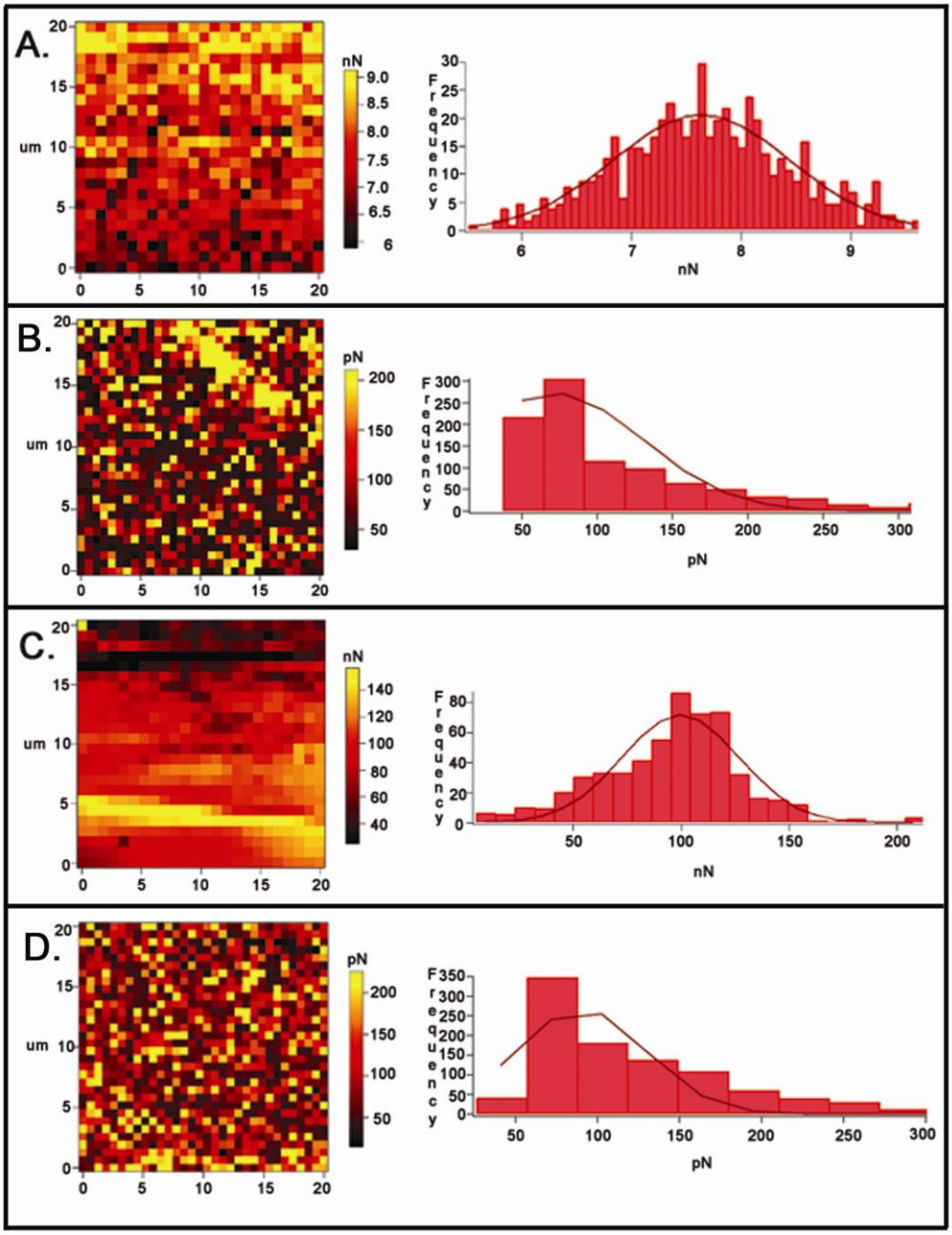

Figure 2.7 AFM characterizing two microcapsule samples; 4.5kV total voltage and 6.0kV total voltage, which were either UV crosslinked to glass coverslips prior to analysis at 9000µJ x100 or left untreated and analyzed. Data is obtained from 20µm x 20µm scan areas on the coverslips where microcapsules were identified with the area then narrowed to 2µm^2 areas. Three areas of interest with peaks and valleys were then scanned on each sample. An average of 6 independent spots had a force distance curve performed on them. (**A**) 4.5kV microcapsules with UV crosslinking resulting heat map (left) and force map (right). (**B**) Data obtained for non-UV crosslinked 4.5kV extruded microcapsules. (**C**) 6.0kV extruded microcapsules with UV crosslinking. (**D**) 6.0kV non-UV crosslinked microcapsules.

2.5 Discussion

The creation of consistent, reliable and controlled microcapsules is a desire in the drug delivery field and was examined in this study. The data presented here describes the parameters necessary to produce such microcapsules with controlled size and morphology. Our data support numerous studies that have documented the inherent variability present in using the electrospray method of microencapsulation. In addition we set out to determine the effect of using a small, low molecular weight peptide on the release profiles of standard and modified sodium alginate microcapsules. The first parameter we examined was the addition or removal of an initial electric field established slightly below the working range of synthesis during encapsulation. Voltage applications for electrohydrodynamic techniques, such as the electrospray method, are subject to decreasing microcapsule diameter with increasing voltage strength, up to a certain point. A voltage below 1.2kV/cm creates reduced microcapsule diameters; however voltages above this value fail to increase microcapsule diameter (Katti et al. 2004). In our studies we determined that using voltages higher than 6.0kV on our instrument resulted in little change in microcapsule diameter. Therefore, microcapsules synthesized at voltages higher than those previously listed were omitted (data not shown).

Establishing a release profile for low molecular weight peptides has proven difficult when working with microcapsules due to the reliance on simple diffusion from the spheres. As a result, many groups have sought to create methods to control this release by altering extrusion parameters or inclusion of additional materials meant to interfere with the pathway of diffusion. Our study has shown changes created by

encapsulation of a small, low molecular weight peptide in contrast to other larger proteins such as BSA.

In addition to differences in molecular weight, the photoelectric points of the encapsulated peptide appear to have effects on diffusion from the microcapsule. A peptide or protein with a low pI, such as that seen in BSA (4.7), diffuses faster in a neutral environment. In contrast, the αCT1 peptide has a much higher (theoretical 11.47) pI value and thus lowering the pH below this number is thought to help decrease release rate. Based on our results, when comparing a neutral pH environment with an acidic pH environment, there was a reduced level of peptide diffusion. By altering the pH the peptide was shown to have a lower initial burst and more evenly dispersed release over the first four hours. Over the first four hours the average difference in total peptide released differed by <5 μM at each time point. When compared to typical initial burst measurements the total peptide released in the first four hours shows sustained diffusion using these parameters. Other attempts to obtain modified diffusion have been made by the addition of polymer coating of microcapsules. We chose to coat microcapsules using both PLL and PLO. Again, we saw extended release in early (1-4hrs) time points similar to values shown using an acidic environment, but with increased peptide release over a longer duration of time (8hrs vs 4hrs). Thus it appears that choosing a proper pH environment and polymer coating can be used to improve release duration of low molecular weight peptides.

In an attempt to attach and deliver microcapsules on biomaterials for implantation, we examined the use of UV crosslinking on the integrity of the extruded microcapsules. UV attachment was performed on three biological materials; polymerized

collagen, silicone wafers, and PWAS sensors. Two incubation periods were used for attachment of the microcapsules to the biomaterials, 0.5hrs and 24hrs at 4°C. In each case an incubation time of 24hrs prior to rinsing produced the greatest coverage area of microcapsules. In addition multiple UV powers were used to attach the microcapsules to the biomaterials, ranging from 6300, 8000, 9000, and 9999µJ X100. Attachment of the microcapsules to the hydrophobic silicone disks showed the lowest total coverage area percentage of the three materials at 24hrs and 9000µJ, (17% vs ~40%) which was found to be the parameters of highest attachment in both collagen and PWAS sensors. Attachment to the silicone disks also had the most variability between the UV powers and different incubation times. On the other hand, UV crosslinked microcapsules on both 2.5% collagen and PWAS sensors produced total coated areas of 39-40%. This level of coverage was achieved without addition of any outside adhesive agents or potentially interfering materials, which could elicit an inflammatory response or prove to be non-biocompatible. We feel that UV crosslinking may provide promise as an efficient microcapsule attachment method. Further testing must be performed before UV crosslinking can be considered a significant advantage.

To begin this testing we sought to determine the effects of UV crosslinking on the biomechanical properties of the alginate microcapsules. Both SEM and AFM analysis of our UV crosslinked microcapsules was performed. No significant changes in overall morphology or microcapsule size were noted upon imaging of the UV crosslinked structures. SEM images show consistency in round morphology with little structural damage after crosslinking. AFM analysis showed that changing synthesis parameters (i.e. voltage) created a change in microcapsule stiffness after UV crosslinking. Previous

studies using simulated models have evaluated AFM and finite element modeling values to assess the membrane elastic-plastic properties of microcapsules similarly (Wan, et al 2002; Mercade-Prieto et al 2011). Our preliminary AFM analysis demonstrated a 10 fold change in overall stiffness between 4.5kV and 6.0kV synthesized capsules. Further AFM analysis of the microcapsules created at these voltages must be conducted to determine the significance of the change. Moreover further AFM analysis including polymer coated microcapsules must be completed.

Finally, previous experiments using excisional skin wounds have been conducted using the topical application of the αCT1 peptide in vivo (Rhett et al 2008; Ghatnekar et al 2009). In addition, several papers have been published using both nano and micro scale polymeric DDS systems synthesized using electrohydrodynamic methods for use with wound healing models with promising results (Zhao et al 2005; Rho et al 2006; Choi et al 2008). Our data suggests that by appropriate modification and attachment, a controlled delivery may be obtained using these sodium alginate microcapsules for use with in vivo models.

2.6 Conclusions

Sodium alginate microcapsules provide a promising means of controlled delivery of biomaterials and drugs, including the αCT1 peptide. Our study provides a characterization of this DDS, both in synthesis and pharmacokinetics capabilities. Furthermore, we have provided a new attachment method of delivery for coating of biomaterials with microcapsules for multiple in vivo circumstances. Multiple microscopy techniques show that use of this method provides potential positive effects to the microcapsule functionality.

CHAPTER 3: APPLICATION OF THE αCT1 PEPTIDE BOTH DIRECTLY AND THROUGH CONTROLLED RELEASE IN A RAT CORNEAL INJURY MODEL

3.1 Abstract

The ability to safely and quickly close wounds and lacerations is an area of need in regenerative medicine, with implications toward healing a wide range of tissues and wounds. Using an in vivo corneal injury model, our study applied the αCT1 peptide, capable of promotion of wound healing and epithelial regeneration. The αCT1 peptide is a 25 amino acid peptide from the C-terminus of connexin 43 (Cx43), modified to promote cellular uptake. Previous studies applying αCT1 to excisional skin wounds in porcine models produced tissues having an overall reduced level of scar tissue and decreased healing time. Rapid metabolism of αCT1 in previous work led to the investigation of extended release on wound healing rate used in this study. Here we delivered αCT1 both directly, in a concentrated pluronic solution, and in a sustained system, using polymeric alginate-poly-l-ornithine (A-PLO) microcapsules, previously characterized in chapter 2. Cell toxicity analysis showed minimal cell-loss with microcapsule treatment. Measurement of wound healing using histology and fluorescence microscopy indicated significant reduction in healing time of αCT1 microcapsule treated rat corneas compared with controls (49.92% decrease in wound area) at 24hrs. RT-PCR analysis showed an initial up regulation followed by down regulation of the gene keratin-19 (Krt19). Zonnula occludin-1 (ZO-1) showed an opposite down regulation followed by an up regulation whereas Cx43 showed a biphasic response. Inflammatory indexes

demonstrated a reduction in the inflammation of corneas treated with αCT1 microcapsules when compared with pluronic gel vehicle. These results suggest αCT1, when applied in a sustained release system, acts as a beneficial wound healing treatment.

3.2 Introduction

The cornea is the nonvascular outermost layer of the eye. Roughly five to six cells thick, the corneal epithelium accounts for 10% of the corneal thickness and blocks entry of materials into the eye, absorbs oxygen, and senses pain as a protective response. The cornea acts as the entry point of light into the eye, and therefore, must remain unaltered to maintain proper vision and allow for the correct formation of an image on the retina. Issues such as trauma, opaque discoloration, and keratoconus (thinning) create the need for corneal replacement surgery, or keratoplasty, using donor tissue. The ability to heal native corneal tissue would alleviate side effects such as infection and keratoplasty as well as the need for donor tissue (Aomatsu et al, 2012; Fukuda et al, 2012; Grupcheva et al, 2012; Karamichos et al 2011; Lu et al, 2012; Shi et al, 2012; Shimmura et al, 2005; Trinkaus-Randall et al 1998; Yao et al, 2012). As previously detailed, corneal wound healing involves several complex overlapping processes involving keratocyte proliferation and migration, myofibroblast recruitment, inflammation induction and response, and epithelial regeneration. The steps of this process are known, but details of the signaling pathways are still unclear. In our research the Epithelial Mesenchymal transition (EMT) pathway was investigated to determine the relationship to corneal wound healing and the resulting reaction to αCT1 treatment, specifically here focusing on krt19. Preliminary data suggested a strong up regulation of krt19 in response to αCT1 in vitro. EMT is a biological method of cellular rearrangement and repair of damaged tissue

where immobile cells used for structural integrity and boundary formation may be mobilized to an area of need (Lee et al 2006). Once the EMT process is complete the mesenchymal cells convert back to epithelial cells in mesenchymal-epithelial transition. Typically the EMT process is tightly regulated by the body, as in embryogenesis (Radisky 2005). The EMT process is not as well understood in the eye, with different opinions on the relationship with corneal wound healing.

The αCT1 peptide is a biotinylated 25 amino acid sequence, comprised of a 16 amino acid antennapedia domain, connected to a 9 amino acid (RPRPDDLEI) sequence from the C-terminus of Cx43 (Rhett et al 2009, 2011). The cytoplasmic tight junction protein zonula occluden 1 (ZO-1) binds at its PDZ-2 domain with the DDLEI sequence of the Cx43 C-terminus end (Duffy et al, 2002). Previously Barker et al (2002) found that intact ventricular myocardium exhibited a low level of ZO-1-Cx43 interaction. This interaction may be disrupted, leading to changes in protein-protein interactions which affect formation of gap junctions. Connexins play a key role as mediators of both cell growth and death and function in immune response, hematopoiesis, and development of progenitor cells (Herve et al, 2004, Oviedo-Orta et al, 2004; Vinin et al, 2011). Binding of the C-terminus of Cx43 to ZO-1 is believed to affect cellular communication and gap junction remodeling in wound healing (Soder et al, 2009). αCT1 competitively inhibits this binding (Hunter et al, 2005; Soder et al, 2009), increases the rate of wound healing, and when applied to in vivo models reduced scar tissue formation in multiple wound healing models including cardiovascular injury, biomedical device implantation, and excisional skin wound models (Ghatnekar et al, 2009; O'Quinn et al, 2011; Soder et al, 2009). Barker et al also developed a control peptide with the active C-terminus 9 amino

acid sequence reversed while the inactive 16 amino acid antennapedia portion was left unchanged. While these results are promising αCT1 showed a rapid metabolism rate. As a result we synthesized microcapsules capable of extending release of αCT1 over 48 hrs to determine to therapeutic potential.

Microcapsule synthesis is accomplished using multiple methods, of which the electrospray method is used in this study. Electrospray microencapsulation uses a voltage differential between a positively charged syringe attached to a high voltage generator and a grounded material, such as a crosslinking gelling bath. A device to control flow rate, such as a syringe pump, passes a polymeric material through the voltage field, which overcomes the surface tension force to produce droplets of a specific size (Chakraborty et al, 2009; Enayati et al, 2011). Sodium alginate is a widely used polymer based on its biocompatibility, semi-permeability, and low cost production (Hilborn et al, 2007; Orive et al, 2006; Tama et al, 2011; Wright et al, 2012; Zhang and He, 2009). In this study sodium alginate microcapsules serve as the base microencapsulation material with a single layer of 0.5% poly-l-ornithine coating added.

3.3 Materials and Methods

Surgical Creation of Corneal Wounds and Post-Surgical Treatment

Male Sprague-Dawley rats (Harlan Laboratories) weighing 240-260 grams were used in this study. All experiments were carried out in compliance with the Guide for the Care and Use of Laboratory Animals by the National Academy of Sciences and University of South Carolina Animal Resources Facility guidelines. Before and after surgery animals were housed two per cage with food and water given ad libitum. Prior to surgery, rats were placed under using an anesthesia mixture of 60mg/kg Ketamine,

7.5mg/kg Xylazine, and 1mg/kg Acepromazine. Two drops of a topical anesthetic, Alcaine (Alcon Canada, Mississauga, Canada) were applied to each eye. Excess Alcaine was removed with a sterile ophthalmic sponge (Merocel, Beaver-Visitec International). A 5mm trephine was placed on the surface of the cornea and two drops of 20% isopropyl alcohol were placed on the cornea surface for exactly 30 seconds. Exposure to the alcohol solution created a loosened 5mm area of corneal epithelium where the trephine was placed. Under a dissecting microscope, the 5mm area of damaged corneal epithelium was removed by gentle scraping, leaving the exposed stromal layer. Once the epithelium was removed the cornea was rinsed with 1% saline and wiped with an ophthalmic sponge to remove any remaining loose epithelium.

Post surgery, rats were placed into one of five time point groups spanning a one month period; 1 day, 3 days, 10 days, 21 days or 30 days. These five time points were repeated for four separate treatments with a total of 100 rats used in the study (25 per treatment/5 per time point). At each time point a total of 10 eyes were used with identical treatment in both eyes of each rat to eliminate eye to eye cross contamination. Treatment groups were comprised of two controls (pluronic gel alone and reverse sequence peptide) and two treatments with αCT1 peptide (direct application and diffusion from encapsulated αCT1 A-PLO microcapsules). In order to ensure sustained delivery of peptide into the cornea, a pluronic gel carrier (Pluronic F-127, Sigma) was used at a concentration of 25% w/v. The pluronic solution remains liquid at 4°C, but gels once in contact with the warm eye. Control group rats received treatments of either 10µl 25% pluronic gel or 10µl of 150µM reverse peptide/25% pluronic gel. Application of αCT1 consisted of either 10µl 150µM αCT1/25% pluronic gel per eye or 150µM αCT1

Microcapsules/10µl 25% pluronic gel per eye with A-PLO microcapsules. Each treatment was applied immediately after surgery (0 hrs), at 24 hrs, and at 72 hrs. All rats were ethically sacrificed at the designated endpoints.

Synthesis of αCT1 Loaded A-PLO Microcapsules

Microcapsules were synthesized according to the protocol previously detailed in chapter 2. Sterile sodium alginate (Sigma-Aldrich catalog#A0682, high maluronic acid content, low viscosity) poly-l-ornithine (Alfa Aesar L-ornithine hydrochloride 99%) microcapsules were synthesized and release of αCT1 was measured. All microcapsules were synthesized with a 2% alginate/0.5% PLO concentration and gelled in 0.15M calcium chloride ($CaCl_2$) (Sigma-Aldrich) solution for 12 minutes. The synthesis parameters were constant at a needle to working bath distance of 7mm, a voltage of 6.0kV, and a flow rate of 60mm/hr. Microcapsule solutions were buffered to pH 4.3 using 0.1M HEPES and 0.1M hydrochloric acid (HCL). A-PLO microcapsules were loaded with αCT1 at an initial concentration of 200µM.

Cytotoxicity Testing of Microcapsules

Cytotoxicity of materials used for A-PLO microcapsule synthesis was tested using an XTT based In Vitro Toxicology Assay Kit (Sigma Aldrich) on rabbit lens epithelial cells (RLECs) according to manufacturer's instructions. A cellular optimization assay was performed using a range of RLECs from $1x10^6$–$1x10^3$ cells per well to determine the linear range of XTT reaction in these cells. Based on the results of these tests, 60,000 cells per well were seeded onto a 96-well plate in media containing DMEM/1%FBS, 50ug/mL Gentamycin, 0.5% Penicillin, and 0.1% Amphocyterin B for 24 hrs. The cells were then treated with a mixture of media with 2% $CaCl_2$, 150µM A-PLO microcapsules

pH 4.2, 150µM A-PLO microcapsules pH 7.2, 150µM αCT1, or 150µM 2% alginate microcapsules pH 7.2, followed with incubation for 24 hrs. Cells treated with media alone served as a positive control, while cells treated with 2% Triton-X 100 (Sigma Aldrich) served as a negative control. After 24 hrs the cells were rinsed in media, and XTT was added to each well at a 0.33 mg/mL concentration diluted in cell culture medium with 8.3 µmol/L phenozene methyl sulfate (Sigma Aldrich). The cells were then incubated for 24 hrs and absorbance was read at 450nm using a BioTek Synergy 2 spectrophotometer. Results are the average of six repeats from separate cell isolations and are reported as a percentage of the positive control following background subtraction of media only wells. Standard error and mean were analyzed and plotted using GraphPad Prism 5 software.

Fluorescent Wound Imaging for the Evaluation of Wound Closure Rate

To assess wound closure rates, 2µl drops of Fluress (fluorescein sodium and benoxinate hydrochloride, Akorn Incorporated) GFP labeled fluorescent dye were placed on the wounded cornea and allowed to cover the eye surface. Excess dye was removed using a sterile ophthalmic sponge, leaving a thin coat attached to the corneal surface. Fluress coats the cornea and penetrates the injury site, but is rinsed from the intact cornea. This allows fluorescence visualization of differences in the topography in areas of tissue damage. Images were taken of the wound at 0 hrs (immediately post surgery), 1 day, 3 days, 10 days, 21 days, and 30 days, using a Zeiss Lumar V12 fluorescence microscope with a 20X objective and 1.5X lens magnification. All images were taken immediately prior to application of treatments. Each wound site area was measured using Axiovision Release 4.8.2 software. The percent decrease in wound area was calculated

for each trial and treatment by comparing differences in wound area between initial and final measurements taken at each time point. Graphing and statistical analysis for significance was performed using GraphPad Prism 5 software.

Histology and Inflammation Score

At previously described post surgery time points, whole eyes were completely removed from the ocular cavity and immediately dissected to remove the cornea. A central strip was cut from the surgically wounded section of the cornea and snap frozen using liquid nitrogen. Frozen strips were held at -80°C for 3 hours and cryosectioned using a Zeiss Microm HM 505N Cryostat. Cornea sections were then air dried and H&E stained using a Leica AutoStainer XL. Images were taken at 10x and 40x magnifications using a Nikon SMZ 1500 light microscope. Slides were then blind scored for inflammation using a 0-10 scale based on a previously published protocol modified for corneal tissue (Singh et al, 2003). Each sample was analyzed for cell infiltration, irregularities in cell shape, breakage of epithelial cells, and presence of vacuoles. A score of 0-2 indicated no cellular infiltrates/intact epithelial layer, 2-4 few infiltrates/breakage in the epithelial layer, 4-6 many infiltrates/non-intact epithelium, and 6-10 represents highly inflamed tissue. As reference controls, corneas receiving no treatment were taken immediately post-surgery, sectioned, and also scored with the treated samples. Statistical analysis was performed using a two-tailed student's t-test with $p<0.05$ set as significant.

RT-PCR of Epithelial-Mesenchymal Transformation Pathway Genes

Corneas were sectioned at 1, 3, and 21 day time points for each of the pluronic gel, control peptide, αCT1, and αCT1 A-PLO microcapsule treatments. Entire corneas were cut into sections, with individual ¼ sections placed in 1mL of Trizol Plus RNA

purification reagent (Invitrogen), and processed according to manufacturer's protocol. Extracted RNA was tested for quality and quantity using an Agilent 2100 bioanalyzer and Agilent RNA 6000 nano kit (Agilent Technologies, Inc). Two random samples of RNA per treatment type were selected for each of the three (1, 3, 21 days) time points making sure no two RNA samples were selected from the same rat source in the same treatment group. These samples were then converted to cDNA at a concentration of 250nM using a BioRad iScript cDNA kit (Bio-Rad Laboratories) according to manufacturer's instructions. Gene specific primers for Krt19, ZO-1, and Cx43 of the EMT pathway were designed using BLAST web based software and synthesized commercially by IDT technologies (Table 3.1). The gene attachment region binding protein (ARBP) was used as a calibrator reference. Primers were tested for efficiency using RNA from day 3 pluronic gel treated rats and optimized using PCR gel analysis (data not shown).

Real-time PCR was run with each gene according to a previously published protocol (Valarmathi et al, 2009) using a MyiQ single color real time PCR detection system (Bio-Rad Laboratories) with SsoAdvanced SYBR Green supermix, 3pmol/rxn primers and 1µl cDNA. All data were analyzed using the Relative Expression Software Tool (REST XL), with pluronic gel treated samples serving as the baseline control. Statistical analysis was performed using both the REST XL and GraphPad Prism data analysis software.

Table 3.1 RT-PCR Primer Sequences

Gene	Forward Primer	Reverse Primer	BP
ARBP	5'-CGACCTGGAAGTCCAACTAC-3'	5'-ATCTGCTGCATCTGCTTG-3'	109
Cx43	5'-TCAGCCTCCAAGGAGTTCCACCAAC-3'	5'-GCACTGACAGCCACACCTTCCC-3'	159
Krt19	5'-AGCATGAAAGCTGCCCTGGAA-3'	5'-ATACTGCTGATCACACCCTGGA-3'	92
ZO-1	5'-CCATCTTTGGACCGATTGCTG-3'	5'TAATGCCCGAGCTCCGATG-3'	123

Immunofluorescence Staining and Confocal Microscopy

Whole eyes were removed and fixed in 2% paraformaldehyde at 4°C for 24 hrs. Corneas were dissected from the eye to remove the cornea, with each cornea cut into four equal ¼ sections. Immunofluorescence preparation was performed and staining was carried out on single ¼ sections, including portions of the injury site, as previously described (Valarmathi et al, 2009). Primary antibody dilutions used for immunofluorescence staining are listed in Table 3.2. Staining was performed for 1 hr at RT in the dark with the exception of DAPI (30 minutes) and anti-Cx43 (2 hours). Alexa Fluor 488 (Molecular Probes, Invitrogen) secondary antibodies were added in dilutions of 1:100 in blocking buffer for 1 hour at RT in the dark. Images were obtained with a Zeiss LSM 510 Meta CSLM microscope. Negative controls using only secondary antibodies were also performed.

Table 3.2 Primary antibodies used in confocal microscopy immunohistochemistry

Primary Antibodies	Dilutions	Manufacturer	Purpose of Interest
Phalloidin (Alexa Fluor 546)	1:100	Invitrogen	F-actin marker of cytoskeleton
DAPI (4',6-diamidino-2-phenyl-indole)	1:1000	Invitrogen	Nuclei marker
Phospho-Histone H3 (Ser28)	1:200	Cell Signaling	Cell migration
Anti-Connexin 43, C-terminus	1:200	Millipore	Migrating cells in EMT
Anti-Cytokeratin-19	1:50	Novus-Biologicals	Migrating cells in EMT
TNF-α	1:100	Phar Mingen	Inflammatory cytokine
Anti-mI-TAC (CXCL11)	1:100	R&D Systems	Chemokine/activated T cells

3.4 Results

3.4.1 Microcapsule Release and Biocompatibility Analysis

This study compared wound healing of a directly applied dose of 150μM αCT1 vs. controlled αCT1 release through A-PLO pH 4.3 microcapsules at the same concentration. Previous studies using αCT1 showed the peptide was metabolized within 2hrs of application in vivo (Rhett et al 2011), leading to development of a method for sustained release. For proof of concept, FITC labeled αCT1 is shown microencapsulated in 180μm microcapsules in fig. 3.1A. Our previously results in chapter 2, summarized in fig. 3.1B, show A-PLO pH 4.3 microcapsules synthesized at an initial concentration of 200μM released an average of 113.99 ± 42.85μM αCT1 over a 48hr period. In these tests, the small size of αCT1 led to a rapid burst release of 80% of the αCT1 in the first two hours from 2% alginate microcapsules. Polymer coating of the 2% alginate with 0.5% poly-l-

ornithine, combined with a reduction in pH from an initially tested 7.4 to an acidic 4.3, led to a delay in release over 48hrs, rather than an initial burst. All microcapsules in these results were synthesized at a 6.0kV voltage/60mm/hr flow rate, which was used in these in vivo studies.

To ensure microcapsule biocompatibility, we performed an XTT cytotoxicity assay using RLECs treated with A-PLO microcapsules at both neutral and acidic pH values, uncoated 2% alginate microcapsules pH 7.2, and 150μM αCT1. In addition, a 2% solution of media/0.15M $CaCl_2$ used in the microcapsule synthesis gelling bath was tested. The graph in fig. 3.1C shows the cell optimization of XTT used to determine the ideal RLEC count, (determined to be 60,000 cells per well) based on the linear region. Treatment with the microcapsules from this study (A-PLO pH 4.2) and two additional microcapsule types (alginate alone and A-PLO pH 7.2) with variations in both pH and material type provided an examination of the in vitro cellular reaction of each of the synthesizing materials/solutions. Percent survival values shown in fig. 3.1D were as follows; 2% $CaCl_2$ showed a 80.90 ± 5.42% survival, A-PLO pH 4.2 a 92.05 ± 3.25% survival, A-PLO pH 7.2 a 99.19 ± 0.99% survival, 150μM αCT1 a 91.75 ± 4.74% survival, and 2% alginate microcapsules pH 7.2 a 96.46 ± 1.97% survival. Buffering the pH in A-PLO microcapsules from a neutral pH of 7.2 to an acidic pH of 4.2 showed a negative effect on cell survival, with a reduction of 7.14%. Comparatively, uncoated 2% alginate microcapsules showed a 4.41% higher survival rate at a neutral pH 7.2 than the A-PLO pH 4.2 capsules. The lowest survival percent was shown when a 2% $CaCl_2$ solution was tested.

A

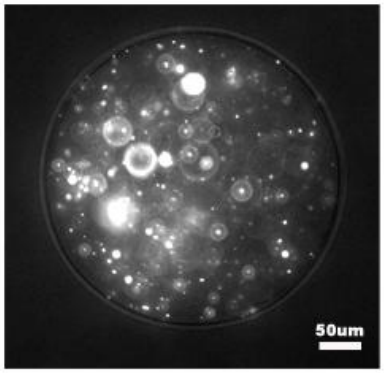

B

Peptide Release From A-PLO Microcapsules	
Hours	*ACT1 Concentration (μM)*
1	42.38 ± 13.26
2	37.16 ± 11.01
4	26.03 ± 16.90
6	3.94 ± 1.15
8	2.12 ± 0.43
24	1.17 ± 0.03
48	1.19 ± 0.07

C

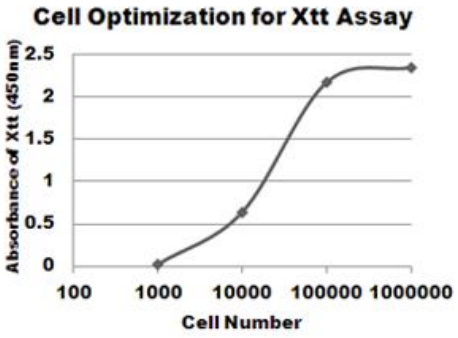

D

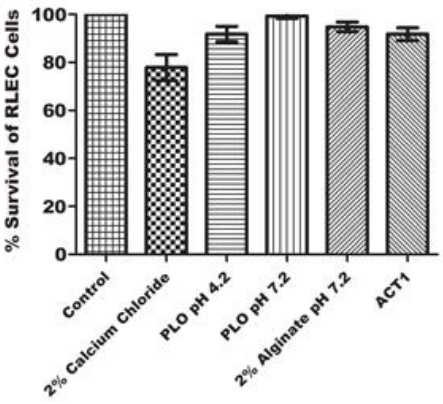

Figure 3.1 Summary of in vitro release and reactivity of alginate-polymer microcapsules. (**A**) 20X phase contrast image of microencapsulated FITC labeled αCT1 peptide. (**B**) Release profile of A-PLO microcapsules pH 4.3. Data represents four independent trials. (**C**) Cellular optimization graph using rabbit lens epithelial cells treated with XTT/PMS over 24hrs. The linear region indicates optimal cells tested. (**D**) XTT cytotoxicity test results of polymeric microcapsules and calcium chloride on 60,000 rabbit lens epithelial cells. Results are the average of six trials.

3.4.2 Analysis of Corneal Wound Closure

Having determined the optimal microcapsule profile and determined the biocompatibility of the encapsulating materials, we next sought to test them in an in vivo wound model. Cornea measurements of wound closure rates for all four treatments at each of the time points (post surgery, 1, 3, 10, 21, 30 days) were evaluated through imaging of GFP labeled Fluress ophthalmic dye on the wounded corneas. Using a Zeiss Lumar V12 stereomicroscope and Axiovision software we captured and measured the area of the wound at each time. For each treatment 25 randomly selected eyes were measured. Our results indicated at the 10, 21, and 30 day time points the wounds had reached complete closure in all tests (day 10 shown in fig. 3.2, while day 21 and day 30 not shown). Samples of these wound closure images are shown in figure 3.2 for day 0 (post surgery), day 1, and day 3, while the averaged results are listed in table 3.3. The results in table 3 indicate the percent change in wound area of the final day 1 or day 3 measurements subtracted from the initial day 0 measurements, as indicated in the table. Each of the treatments were analyzed using the Grubb's test for outliers with significance set to $p<0.05$ to remove any non-significant data points.

Examining the results in table 3.3, the largest change in wound closure rate occurred in the first 24hrs after surgery. The treatment group receiving direct application of αCT1 showed an average increase in wound closure of 31.92% vs. pluronic controls, while those receiving αCT1 A-PLO microcapsule treatments showed a 49.92% increase in wound closure compared to pluronic controls. From the 24-72hrs time points, αCT1 treated corneas saw an additional 17.40% increase in wound closure. The αCT1 A-PLO microcapsule treated corneas dropped below the rate of the direct αCT1 values at this 24-

72hr time period, but still increased wound closure 10.16% faster than pluronic treatment. Based on the release profile of the A-PLO microcapsules, we found ~93% of encapsulated αCT1 was released within the first four hours, as shown in fig. 3.1B. This is an improvement on the rapidly metabolized direct application of αCT1 shown through previous in vivo studies, as previously referenced, and believe it accounts for the changes in wound closure rates for the A-PLO treatments. Additional graphical representation of the percent difference in wound closure from table 3.3 is provided in Appendix A.2, with results indicating significant differences at 1 day for reverse, αCT1, and αCT1 microcapsule treatments as well as 3 day αCT1 microcapsule treatment compared to pluronic treatments.

To further corroborate our wound closure data, samples of cornea taken at the 3 day time point were cryo-sectioned and histologically stained with H&E. These images indicate the epithelial layer was completely removed during surgery, exposing the stroma. We were able to visualize the cell number of the epithelial layer by examining the stained nuclei. Images taken at 40x magnification shown in figures 3.3B, D, F, and H show that the epithelial layer has reached ~4-5 cells thick by the 3 day time point in regions of the cornea that have completely healed. Normal full thickness cornea has an epithelial layer of 5-6 cells. Comparing the four treatment groups there are no visible changes in the epithelial layer from treatment to treatment; i.e. increased layer thickness caused by increased corneal wound healing resulting from addition of αCT1 and A-PLO treatments. Sample images of untreated cornea wounds taken immediately post surgery are shown along the wound edge (Fig. 3.3I refer to all figures and in order (10x)) and within the wound margin (Fig. 3.3J (40x)). We conclude corneal healing approached both

complete wound closure and full thickness reepithelialization at 3 days post surgery. Complete wound closure and full thickness reepithelialization were seen by 10 days post surgery (not shown).

To assess changes in the level of inflammation following treatment of the cornea we performed a blind inflammatory scale assessment. Both αCT1 treated and A-PLO αCT1 microcapsule treated were blind scored on a 0-10 inflammation scale against pluronic treated and untreated post surgical samples. Five randomly chosen slides of day 3 corneas were imaged from each of the four treatment groups and given a score based on the previously listed criteria. Figure 3.3K indicates the average values of each score with SEM. Untreated post surgical control samples had an average score of 0.5, while pluronic treated averaged 8.18, indicating a high level of inflammation. The αCT1 treated (4.17) and A-PLO αCT1 microcapsule (4.73) samples each showed moderate inflammation at 3 days. Statistical analysis indicated these values to be significantly less than pluronic controls in both cases.

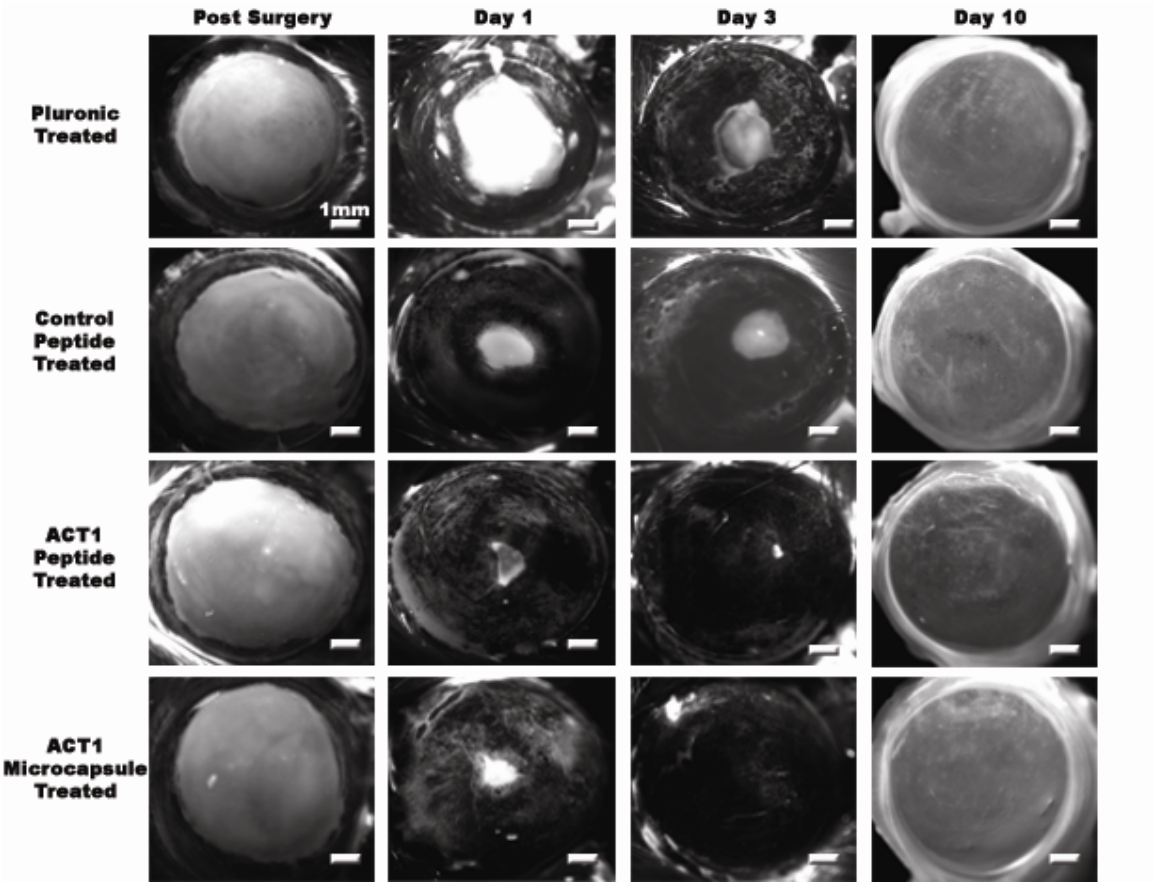

Figure 3.2 Progressive wound healing over 10 days in a rat corneal injury model. Fluress ophthalmic dye staining of corneal defects immediately after surgery. Repeated at 1 day, 3 days, and 10 days. Additional staining completed on days 21 and 30 (not shown). Treatments from top to bottom on each eye: 25% pluronic gel, 150µM control peptide, 150µM αCT1, and 150µM A-PLO microencapsulated αCT1.

Table 3.3 Summary of wound closure rates measured using Fluorescein ophthalmic dye. Each data point represents 25 randomly selected eyes from each treatment. Grubb's test for outliers used to remove points found non-significant ($p>0.05$).

	Pluronic Treated	**Control Peptide Treated**	**αCT1 Treated**	**αCT1 Microcapsule Treated**
% change 0-24hrs	38.86 ± 27.12	52.32 ± 29.59	70.78 ± 22.43	88.78 ± 12.69
% change 24-72hrs	76.70 ± 19.60	89.59 ± 8.15	94.1 ± 10.08	86.86 ± 19.72
% change 0-72hrs	84.60 ± 15.19	94.93 ± 5.60	97.16 ± 4.93	99.15 ± 1.39

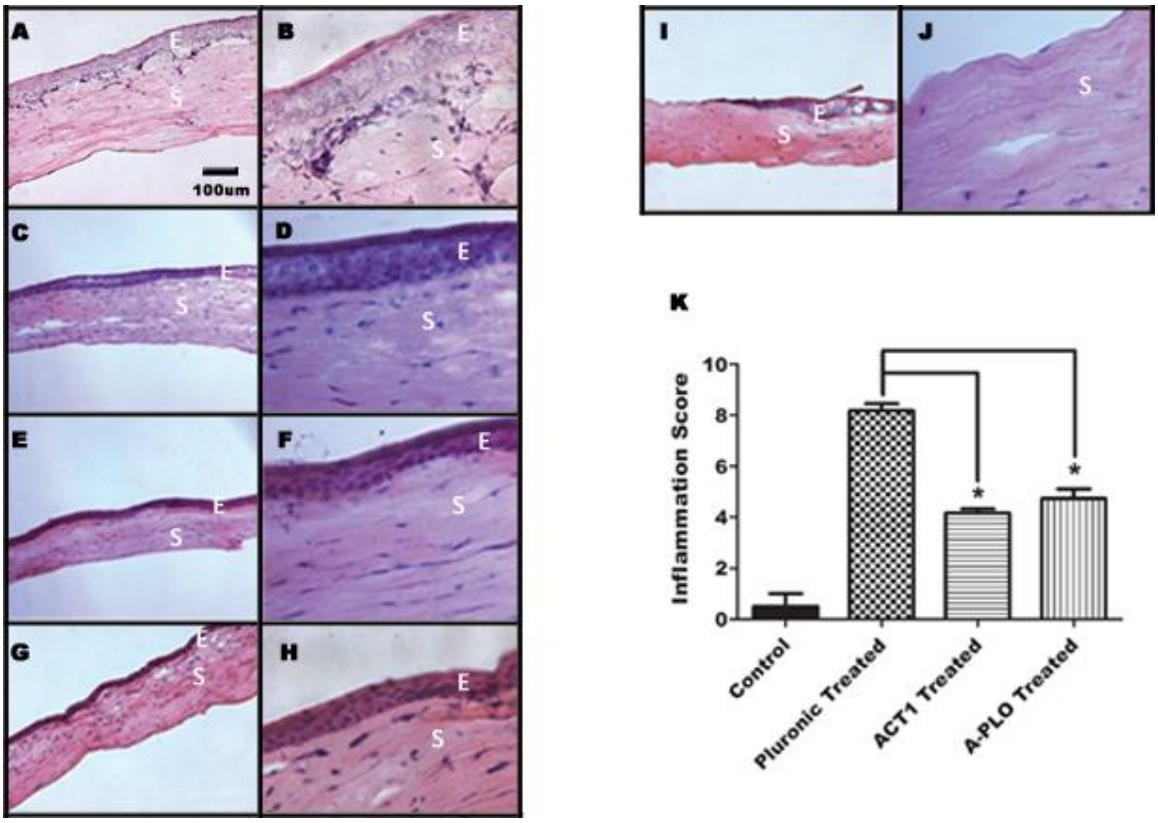

Figure 3.3 Histological cryo-sectioning and staining of day 3 corneas using hematoxylin and eosin. Each row contains a representative cornea sample for each treatment at 10x magnification (left) and 40x magnification (right). (**A, B**) 25% Pluronic gel treated, (**C, D**) 150µM control peptide treated (**E, F**) 150µM αCT1 treated (**G, H**) 150µM A-PLO microencapsulated αCT1 treated. Images **I** and **J** show a 10x (left) and 40x (right) time 0 untreated cornea for comparison. The images are labeled with *E*, to mark the epithelial layer, and *S* for the stromal layer. (**K**) Summary of inflammatory scoring for time 0 untreated control samples, pluronic, αCT1, and A-PLO αCT1 microcapsule treatments at day 3.

3.4.3 Examination of Wound Healing Response by RT-PCR and Immunohistochemistry

The biochemical response of the wounds to the treatment groups was analyzed by focusing on genes from the epithelial to mesenchymal transformation (EMT) pathway and those specific for the Cx43-ZO-1 interaction. Reepithelialization of the cornea involves gap junction and tight junction remodeling, thought to be affected by the presence of αCT1. Therefore, we hypothesized as corneal cells undergo remodeling and healing there would be a measureable change in EMT genes.

Genes for Cx43, Krt19, and ZO-1 were analyzed by RT-PCR at 1 day, 3 day, and 21 day samples from all treatment groups. These time points were selected to analyze the immediate impact of the treatments (1 day), the impact at near wound closure (3 days), and the long term impact (21 days). The results are summarized in fig. 3.4 using pluronic treated samples at each time point as baseline controls. On day 1, all treatments caused a down regulation of Cx43, with both αCT1 (-1.80) and A-PLO (-1.61) capsules less than the control treatment (-2.05). Cx43 is known to be down regulated immediately after a wound response, consistent with our data at 1 day. By day 3 all three treatment groups were up regulated in the Cx43 group (control: 1.12, αCT1: 1.60, and A-PLO: 1.50) with αCT1 treatment statistically significant ($p<0.05$). The 21 day treatment group showed biphasic results between the control group and the two αCT1 treatments (control up 2.16 fold, αCT1 down 1.16 fold, and A-PLO down 1.31 fold). The results of ZO-1 at day 1 and 3 were consistent with the data for Cx43 in all treatment groups with down regulation at day 1 (control down 1.98 fold, αCT1 down 1.18 fold, and A-PLO down 1.44 fold) and up regulation at day 3 (control up 1.27 fold, αCT1 up 1.21 fold, and A-PLO up 1.24 fold).

Our third examined gene, Krt19, is a stemness related marker thought to be down regulated during the EMT process, through roles in cell migration (Kong et al, 2010; Zhou et al, 2008). Aomatsu et al (2012) were able to confirm down regulation of Krt19 using Snail and Slug overexpression in human corneal epithelial cells (Aomatsu et al, 2012; Ma et al, 2010). Here we show an immediate up regulation of Krt19 at day 1 in all treatments, with significance in both αCT1 (up 3.49 fold) and A-PLO treatment (up 2.57 fold) groups. By day 3 and continuing to day 21, Krt19 is consistently down regulated with significance shown at day 3 A-PLO treatment (down 3.66 fold).

Confocal microscopy using Krt19 (Fig. 3.5 A and B) and Cx43 (Fig. 3.5 C and D) was performed to validate the RT-PCR results. Figure 3.5 shows sample images of day 1 and day 3 A-PLO treated corneal wounds. Arrows mark the reepithelializing wound margins in each image. Day 1 staining with Krt19 was expressed along the progressing wound edge as seen in fig. 3.5A. Later time points with day 3 and day 21 (not shown) Krt19 staining showed little to no presence in all images. Cx43 antibody staining also produced staining similar to the results seen in the RT-PCR data. Minimal Cx43 staining is shown in fig. 3.5C at day 1, while abundant within and around the wound margins at day 3, as viewed in fig. 3.5D. This data further confirms our results for day 1 and day 3 Cx43 and Krt19, shown in fig. 3.4.

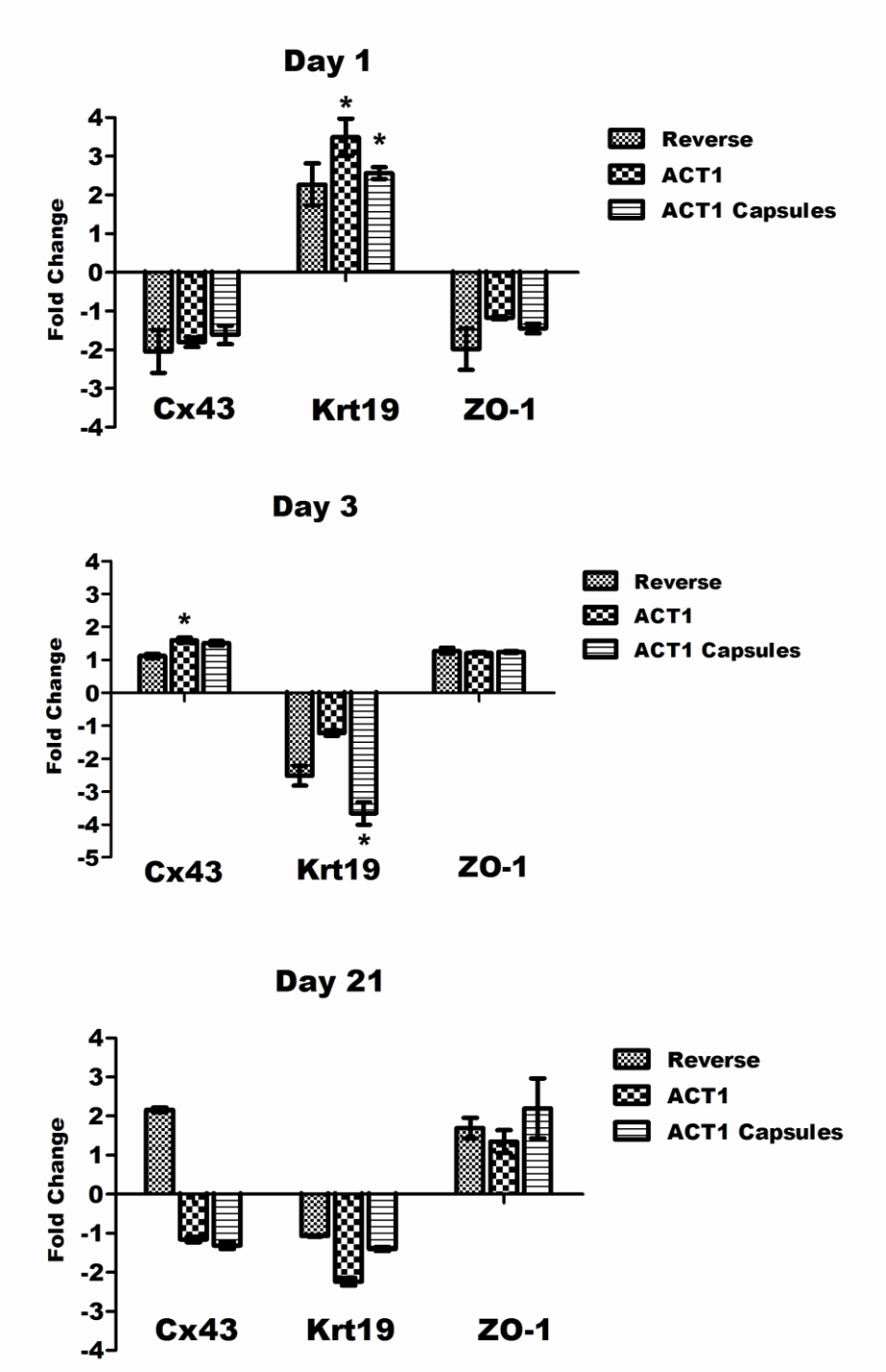

Figure 3.4 RT-PCR analysis of corneas for gene expression of Cx43, Krt19, and ZO-1. Each time point is represented in the corresponding graphs for day 1 (top), day 3 (middle) and day 21 (bottom). Pluronic treated corneas serve as the baseline control, with the data presented for the up and down regulation of control peptide treated, αCT1 treated, and αCT1 A-PLO microcapsule treated samples.

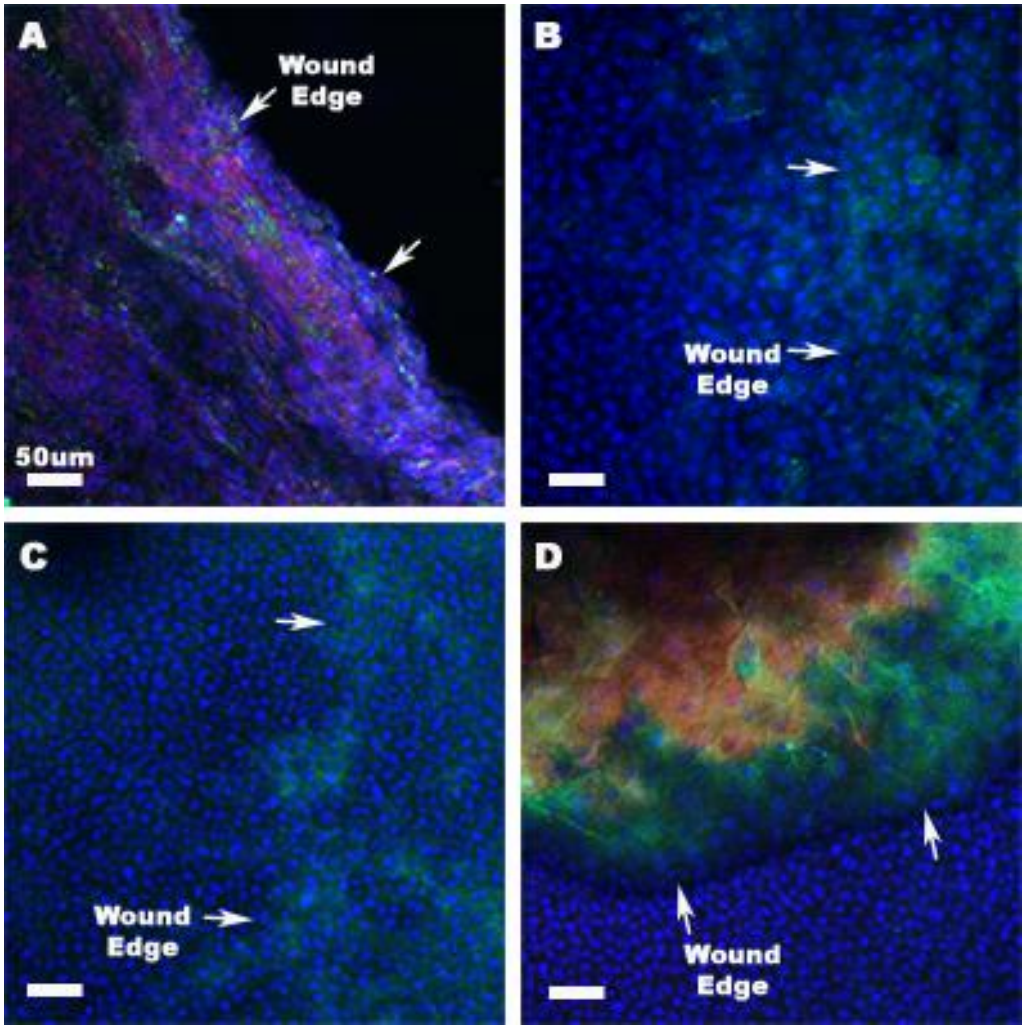

Figure 3.5 Confocal microscopy of 1 day and 3 day cornea samples receiving treatment with αCT1 A-PLO microcapsules. All images are at a 20x magnification. (**A**) 1 day cornea: Blue-DAPI, Green-Keratin 19, Red-Phalloidin (**B**) 3 day cornea: Blue-DAPI, Green-Keratin 19, Red-Phalloidin (**C**) 1 day cornea: Blue-DAPI, Green-Connexin 43, Red-Phalloidin (**D**) 3 day cornea: Blue-DAPI, Green-Connexin 43, Red-Phalloidin

3.4.4 Corneal Response to A-PLO Microcapsules

Treatment with αCT1 A-PLO microcapsules increased the rate of wound closure, but initially created a minor inflammatory response during healing in a small number of treated rats. Examples of the regions of affected tissue are shown in the upper and lower left images of fig. 3.6. The resulting tissue was first seen in day 3 corneas with minimal to no presence at day 30. Samples of corneal tissue exhibiting this affected tissue were stained for the inflammatory markers TNF-α and ITAC (CXCL11). CXCR3 (chemokine C-X-C motif receptor 3) is a receptor expressed during inflammatory responses and associated with activated T cells as well as NK cells (Ondeykal et al, 2005). ITAC is an associated chemokine, active in the regulation of CXCR3 and up regulated during immune response. TNF-α, along with IL-6 and IL-1, is a well known pro-inflammatory cytokine and marker of immune response. Smooth muscle actin staining served as a cytoskeletal structural marker. The pro-inflammatory markers shown in fig. 3.6A (TNF-α) and fig. 3.6B (ITAC) were both expressed in tested corneas at 3 days with reduced presence by 30 days (not shown). Comparing the results shown here with the cytoxicity data from fig. 3.1D we saw a different response in vivo and in vitro to A-PLO microcapsules pH 4.2. Additional rats were tested with either 10µL drops of 0.15M $CaCl_2$ or 10µL aliquots of triple DI water rinsed A-PLO pH4.2 microcapsules. Only rats receiving the $CaCl_2$ treatment continued to exhibit the inflammatory response. We feel that the natural progression of the corneal injury coupled with residual $CaCl_2$ applied to the wound with the A-PLO microcapsules during treatment produced the inflammatory response. Subsequent corneal injury studies performed in the laboratory did not produce

any inflammatory reaction with microcapsule treatment when extensively rinsed with deionized water prior to application in the eye.

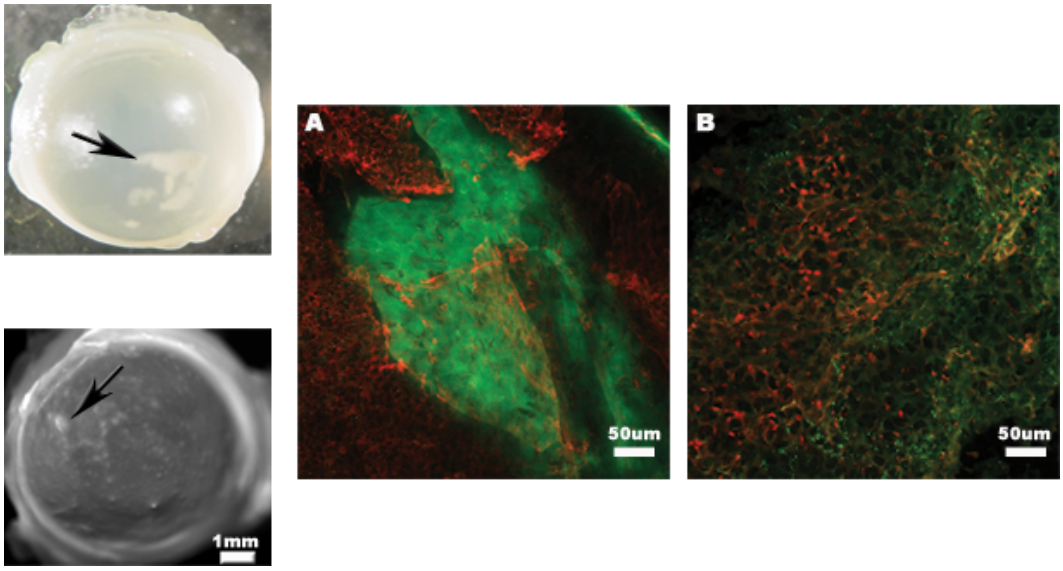

Figure 3.6 The inflammatory response of the rat cornea to the αCT1 A-PLO microcapsule treatment in limited rats. Images are shown in both the upper left and lower left of the figure showing two representative portions of the affected tissue of the cornea at 30 days. (**A**) Confocal image at a 20x magnification of the affected tissue in a 3 day microcapsule treated cornea. Green-TNF-α, Red-smooth muscle actin. (**B**) 20x magnification of the affected tissue in a 3 day microcapsule treated cornea. Green-ITAC, Red-smooth muscle actin.

3.5 Discussion

Examining the cytotoxicity of the A-PLO microcapsule synthesis related materials we found a high level of biocompatibility in vitro. Percent survival values using RLECs indicated a >92% survival with all materials (A-PLO pH 4.2, A-PLO pH 7.2, 2% alginate microcapsules pH 7.2, 150μM αCT1) except 2% $CaCl_2$ which showed a 80.90 ± 5.42% survival. Buffering the pH in A-PLO microcapsules from a neutral pH of 7.2 to an acidic pH of 4.2 showed a small negative effect on cell survival, with a reduction of 7.14%. Comparatively, uncoated 2% alginate microcapsules showed a 4.41% higher survival rate at a neutral pH 7.2 than the A-PLO pH 4.2 capsules. The lowest survival percent was shown when a 2% $CaCl_2$ solution was tested. Based on this result, extensive washing of the $CaCl_2$ gelling solution from the microcapsules post synthesis is necessary when applying the microcapsules in vivo. As a result of >90% survival in all XTT trials, the A-PLO microcapsules were considered to be biocompatible for the corneal studies. The relatively small reduction in cell survival created by lowering the pH from 7.2 to 4.2 allowed for a high overall survival rate, while reducing the microcapsule pore size and extending αCT1 release.

The results of the wound closure analysis indicated controlled release of αCT1 over the first four hours enhanced the wound healing rate of the microcapsule treated corneas 18% over direct αCT1 treatment. Direct αCT1 treated corneas received a onetime peptide application to the wound of 150μM, while microcapsule treated corneas received αCT1 release in the same dose for the full 24 hrs. At the 1 day point the rats in all treatment groups received a second treatment. It is thought that the first 24-36 hrs are the period when αCT1 is most functional in affecting gap junction formation in the healing

wounds. As a result αCT1 treated corneas receiving a direct dosage of 150μM of the peptide show a greater wound closure rate than A-PLO treated corneas receiving an extended amount of αCT1 over this 24-72 hr time (i.e. directly applied αCT1 is actually more prevalent in the wound very early based on the slower release of the peptide from the microcapsules over 48hrs). Additionally, a large standard error resulted when evaluating the 24-72 hr period, which is thought to further account for differences in the direct αCT1 and A-PLO treatment final values. Looking at the total wound closure over the first 3 days (0-72hrs) the αCT1 A-PLO microcapsule treatment showed the fastest overall wound closure speed, reaching nearly complete closure of 99.15% (14.55% faster than pluronic treatment) on average. This was followed by a 97.16% (12.56% faster than pluronic treatment) closure rate of αCT1. As a result, we hypothesize that αCT1 treatment by A-PLO microencapsulation leads to a faster wound closure rate for corneal wound injuries over the complete time period. While direct αCT1 treatment in the 24-72 hr period is faster, the values indicated over the total 3 day time period showed a nearly complete closure (99.15%) when using A-PLO microcapsule treatment (Table 3.3).

To examine inflammatory response of the cornea to treatment, αCT1 treated and A-PLO αCT1 microcapsule treated cyrosectioned samples were blind scored on a 0-10 inflammation scale against pluronic treated and untreated post surgical samples A significant decrease in inflammation was found when compared to pluronic treated control samples. Inflammatory scoring was performed to ensure the αCT1 treatment groups were providing no additional inflammatory response exceeding those found in the control groups. On the contrary we saw less inflammation at the 3 day mark with these treatments. The addition of αCT1 increased the wound healing rate and therefore by the

3 day time point moved beyond the inflammatory stage of healing faster than pluronic treated samples. Coupled with the XTT cytotoxicity data, we found little negative compatibility issues when treating with αCT1 and A-PLO microcapsules in vivo.

Barker et al (2002) found in cardiac myocytes that Cx43 and ZO-1 were present in low amounts in normal tissue but were expressed and co-localized upon tissue disruption. Here we show, through our RT-PCR data, a similar down regulation in corneal wound healing of ZO-1 consistent with typical Cx43 action. Between this 24 and 72 hr time point as the wound is healing, Cx43 and ZO-1 are up regulated as cell-cell adhesion and gap junction formation is recurring. By day 21 there was a departure from this consistency. The control group was shown to be up regulated in both Cx43 and ZO-1, while both αCT1 and A-PLO treatments showed Cx43 (down regulated) and ZO-1 (up regulated) no longer consistently co-expressed. While not statistically significant, this departure is of note.

The immediate up regulation in the RT-PCR data of Krt19 at day 1 is provocative, as the wound closure data shown in figures 3.2 and 3.3 indicated rapid re-epithelialization. Down regulation of the gene at 3 and 21 days follows the known EMT patterns, as the wound is continuing closure and completion of healing of the multi-layered corneal epithelium. This data suggests immediately after wounding a transmigration stage of re-epithelialization is occurring rather than an EMT proliferation of cells from the limbal region. Based on the levels of up regulation, Krt19, as well as other cytokeratins, play a role in the re-epithelialization of corneal wounds. The treatment of corneal wounds with αCT1 is hypothesized to have resulted in an up regulation of migration of epithelial cells.

Finally we examined to minor response to A-PLO microcapsules in vivo looking at confocal immunohistochemistry of ITAC and TNFα. It is believed that a natural progression of the corneal injury coupled with residual $CaCl_2$ from the gelling bath applied to the wound with the microcapsules during treatment produced the inflammatory response in a small number of rats. This data is consistent with the results of the XTT cytotoxicity experiment previously listed. The results of subsequent corneal injury studies performed in the laboratory did not produce any inflammatory reaction with microcapsule treatment when the microcapsules were extensively rinsed with deionized water prior to application in the eye.

3.6 Conclusions

Treatment of corneal wound injuries with αCT1 peptide increased wound closure speed. The addition of a polymeric αCT1 A-PLO microcapsule system further increased the wound healing speed over αCT1 alone. Use of poly-l-ornithine as a polymeric drug delivery system was shown to be biocompatible, while the $CaCl_2$ gelling solution was found to be cytotoxic in vivo. Future use of this cationic crosslinking solution will require extensive washing with deionized water to ensure complete removal. Examination of Cx43 and ZO-1 in the corneal wound healing process showed results similar to previously published cardiac myocyte data, suggesting Cx43 and ZO-1 are coupled through down regulation immediately after injury or gap junction disruption, and are linked in up regulation during the healing process. Krt19 was shown to be significantly expressed 24hrs after wounding with αCT1 and αCT1 A-PLO treatment. This EMT related protein may play a role in both migration of epithelial cells immediately after wounding and down regulation during a later EMT stage of cellular

proliferation by day 3 post injury. Treatment with αCT1 may play a role in the early effects of migrational stages of corneal healing, as well as EMT pathway genes.

CHAPTER 4: APPLICATION OF THE αCT1 PEPTIDE BOTH DIRECTLY AND THROUGH CONTROLLED RELEASE IN A TYPE I DIABETIC CORNEAL INJURY MODEL

4.1 Abstract

The αCT1 peptide is a synthetically produced mimetic modified from the DDLEI C-terminus sequence of connexin 43. Previous research using various wound healing models have found promising therapeutic effects when applying the drug, resulting in increased wound healing rates and reduced scarring. Previous data suggested a rapid metabolism rate in vitro, creating an interest in long term release. Using a streptozotocin (STZ) type I diabetic rat model with a surgically induced corneal injury, we delivered αCT1 both directly, in a pluronic gel solution, and in a sustained system, using polymeric alginate-poly-l-ornithine (A-PLO) microcapsules, previously characterized in chapter 2. Fluorescent staining of wound area over a 5 day period indicated a significant increase in wound closure rates for both αCT1 and αCT1 microcapsule treated groups, with αCT1 microcapsule groups showing the most rapid wound closure overall. Analysis of inflammatory reaction to the treatment groups indicated significantly lower levels of both ITAC and TNFα markers using confocal quantification and Elisa assays. Additional analysis examining genes selected from the EMT pathway using RT-PCR and Western blotting suggested αCT1 modification of TGFβ2, Krt8, Esr1, and Glut4 over a 14 day period. Combined, this data indicates a possible suppression of the inflammatory response by αCT1, leading to increased wound healing rates.

4.2 Introduction

Type I diabetes, also known as diabetes mellitus, is a common disease characterized by hyperglycemia resulting from a deficiency in insulin production. In this diabetic state, β-cells in the pancreas produce little to no insulin. For the STZ model of type I diabetes, mild to severe diabetic states are induced in a dose dependent manner by targeting the β-cells ability to function normally (Arora et al 2009; Soetikno et al 2011). Several secondary health problems are commonly associated with diabetes, including risk of stroke, impaired vision, diabetic retinopathy, glaucoma, diabetic ulcers, and decreased wound healing efficiency (Pradhan et al 2007, Rao et al 2010; Sweetnam et al 2012). Of interest here is impaired wound healing ability. Research has shown decreased leukocyte and macrophage function, difficulties in ECM deposition, and slowed re-epithelialization (Lee Y.H. et al 2012) occurring in diabetic wound healing. The αCT1 peptide is a novel wound healing agent we believe could be effective in treating diabetic wounds.

In vivo, the cytoplasmic tight junction protein zonnula occludin-1 (ZO-1) binds at its PDZ-2 domain with the C-terminus of Cx43 (Duffy et al 2002; Rhett et al 2012). Previous results studying the Cx43-ZO-1 interaction in the heart found that intact ventricular myocardium exhibited a low level of ZO-1-Cx43 interaction (Barker et al 2002). Wound formation leads to disruption in these interactions, which in turn creates changes in protein-protein interactions, affecting formation of gap junctions. To investigate this effect αCT1, a 25 amino acid sequence comprised of a 16 amino acid antennapedia domain connected to a 9 amino acid (RPRPDDLEI) sequence from the C-terminus of Cx43, was synthesized (Rhett et al 2008, 2011). The antennapedia sequence is inactive in genetic activity and aids in cellular uptake. Connexins play a key role as

mediators of both cell growth and death and function in immune response, hematopoiesis, and development of progenitor cells (Herve et al 2004; Oviedo-Orta et al 2004; Vinkin et al 2011). Binding of the C-terminus of Cx43 to ZO-1 is believed to affect cellular communication and gap junction remodeling in wound healing (Soder et al 2009). αCT1 acts as a competitive inhibitor of this binding (Hunter et al, 2005; Soder et al 2009), increases the rate of wound healing, and reduces scar tissue formation in multiple wound healing models (Ghatnekar et al, 2009; O'Quinn et al 2011; Soder et al 2009). A control peptide, with the active C-terminus sequence reversed, was created with the inactive 16 amino acid antennapedia portion unchanged.

Epithelial Mesenchymal transition (EMT) is a biological method of cellular rearrangement and repair of damaged tissue where immobile cells used for structural integrity and boundary formation may be mobilized to an area of need (Lee et al 2006). Once the EMT process is complete the mesenchymal cells convert back to epithelial cells in the process called MET, or mesenchymal-epithelial transition. Typically the EMT process is tightly regulated by the body, as in embryogenesis (Radisky 2005). The EMT process is not as well understood in the eye, with differing opinions on the relationship with wound healing. However, both Kawakita et al 2012 and Aomatsu et al 2012 were able to show the prevalence of EMT in the eye using cornea epithelial cells in relation to TGFβ and Slug signaling in recent studies. Similar results summarizing the occurrence of endothelial mesenchymal transitions in the cornea have been published as well (Lee J. et al 2012), leading to the belief that EMT is in fact occurring in the cornea during healing.

In this study we hypothesized that a controlled dose treatment with αCT1 microencapsulated in A-PLO would produce a significant increase in wound healing

when applied to a diabetic corneal injury model. Previous studies have not completely shown the method of peptide action. Here we examine genes from the EMT pathway, selected for their relationship to potential points of peptide influence, such as proliferation, motility, inflammatory regulation, and morphogenesis. In vitro experiments probing control and αCT1 treated bone marrow stromal cell monolayers also indicated potential genes of interest; keratin 8, keratin 19, and TGFβ2. Additionally, we evaluated the roles of EMT associated genes related to insulin sensitivity by examining glucose transporter 4 (GLUT4) and estrogen sensitive receptor 1 (Esr1).

4.3 Materials and Methods

Induction of Type I Diabetes, Corneal Surgery, and Wound Treatment

Induction of type I diabetes was performed by single dose I.P injections of STZ (Sigma Aldrich) at 65mg/kg in Sodium Citrate buffer pH 4.5 (Sigma Aldrich), given to male Sprague-Dawley rats (Harlan Laboratories) weighing 240-260 grams. After delivery, rats were given a 24hr equilibration period prior to STZ to injection. After injection, a one week period was allowed for complete diabetic illness to take effect. At the end of the one week period rats were fasted overnight (18hrs) then tested for blood glucose levels from the tail vein using a ReliOn Confirm blood glucose meter and ReliOn ultra-thin lancets. Rats with blood glucose levels exceeding 225mg/dL were considered diabetic and used in this study.

Surgeries were carried out according to the same protocol previously described in chapter 3. All experiments were performed in compliance with the Guide for the Care and Use of Laboratory Animals by the National Academy of Sciences and University of South Carolina Animal Resources Facility guidelines. Post surgery, rats were placed into

one of four time point groups spanning a two week period; 1 day, 3 days, 5 days, or 14 days. These four time points were repeated for four separate treatments, with a total of 80 rats used in the study (25 per treatment/5 per time point). At each time point a total of 10 eyes were used with identical treatment in both eyes of each rat to eliminate eye to eye cross contamination. Each treatment group contained two controls (pluronic gel alone; control peptide) and two treatments with αCT1 peptide (direct application in pluronic gel; αCT1 A-PLO microcapsules). To ensure sustained delivery of peptide into the corneal wound, a pluronic gel carrier (Pluronic F-127, Sigma Aldrich) was used at a concentration of 25% w/v. Control group rats received treatments of either 10µl 25% pluronic gel or 10µl of 150µM control peptide/25% pluronic gel. Application of αCT1 was again delivered at either 10µl 150µM αCT1/25% pluronic gel per eye or 150µM αCT1 Microcapsules/10µl 25% pluronic gel per eye with A-PLO microcapsules. Each treatment was applied immediately after surgery (0 hrs), at 24 hrs, and at 72 hrs. All rats were ethically sacrificed at the designated endpoints.

Synthesis of αCT1 Loaded A-PLO Microcapsules

Microcapsules were synthesized to match those used in chapter 3, according to the protocol previously detailed in chapter 2. Sterile sodium alginate (Sigma-Aldrich catalog#A0682, high maluronic acid content, low viscosity) poly-l-ornithine (Alfa Aesar L-ornithine hydrochloride 99%) microcapsules were synthesized and release of αCT1 was measured. All microcapsules were synthesized with a 2% alginate/0.5% PLO concentration and gelled in 0.15M calcium chloride ($CaCl_2$) (Sigma-Aldrich) solution for 12 minutes. The synthesis parameters were constant at a needle to working bath distance of 7mm, a voltage of 6.0kV, and a flow rate of 60mm/hr. Microcapsule solutions were

buffered to pH 4.3 using 0.1M HEPES and 0.1M hydrochloric acid (HCL). A-PLO microcapsules were loaded with αCT1 at an initial concentration of 200μM to match all microcapsules tested in chapter 3. A summary of the release profile of the A-PLO microcapsules used here can be referred to in figure 3.1.1B.

Wound Measurements and Analysis

Assessment of wound area was carried out according to the same protocol described in chapter 3. In review, 2μl drops of Fluress (fluorescein sodium and benoxinate hydrochloride, Akorn Incorporated) GFP labeled fluorescent dye were placed on the wounded cornea and allowed to cover the eye surface. Excess dye was removed, leaving a thin coat attached to the corneal surface. Images were taken of the wound at 0 hrs (immediately post surgery), 1 day, 3 days, 5 days, and 14 days, using a Zeiss Lumar V12 fluorescence microscope with a 20X objective and 1.5X lens magnification. All images were taken prior to application of treatments. The area of each wound site was measured using Axiovision Release 4.8.2 software. The percent decrease in wound area was calculated for each trial and treatment by comparing differences in wound area between initial and final measurements taken at each time point. Graphing and statistical analysis for significance was performed using GraphPad Prism 5 software analyzing the percent difference vs pluronic treated control groups and Kaplan-Meier survival analysis.

Confocal Quantification of Inflammation Using ITAC and TNFα

Cornea samples from all four treatments were fixed overnight at 4°C in 2% paraformaldehyde. Fixed samples were then stained for immunohistochemistry using antibodies for ITAC and TNFα according to a previously published protocol (Valarmathi et al, 2009). Staining was carried out 1hr at RT for both ITAC and TNFα on samples

from all four treatments at time points of 1 day, 3 days, and 5 days. Nuclear staining with DAPI diluted 1:2000 was also performed for 30 minutes. Alexa Fluor 488 (TNFα) or 546 (ITAC) (Molecular Probes, Invitrogen) secondary antibodies were then added at 1:100 dilutions in blocking buffer 1hr. Images were obtained with a Zeiss LSM 510 Meta CSLM microscope of two separate regions within the wound margin where inflammation fluorescence was visualized for both ITAC and TNFα. Pluronic gel treated samples from the 1 day time point were used to initially set the upper threshold settings for each inflammatory marker. The reuse setting of the microscope was then applied to all subsequent images, allowing for identical microscope conditions at each treatment and time point. Additionally, all samples were stained and imaged under identical conditions and at the same time to eliminate variation in processing and photo bleaching over time. Negative controls were created using samples stained with only secondary antibodies.

Table 4.1 Summary of antibodies used for confocal inflammatory quantification.

Primary Antibodies	**Dilutions**	**Manufacturer**	**Purpose of Interest**
DAPI (4',6-diamidino-2-phenyl-indole)	1:2000	Invitrogen	Nuclei marker
TNF-α	1:100	Phar Mingen	Inflammatory Cytokine
Anti-mI-TAC (CXCL11)	1:100	R&D Systems	Chemokine/activated T cells

Images were next analyzed using the ImageJ 1.45s software package (National Institutes of Health, Bethesda, Md). Measurements were set to analyze mean intensity with limits to threshold and the threshold adjusted to create a binary image of the stained areas of inflammation. Binary images were then processed using the smooth function to solidify the edges. Each measurement was performed in triplicate and recorded. The

measurements were converted to percent of total coverage using the formula 100-((x-255)*100), with x representing the measured value and 255 the maximum threshold limit. Values were graphed using the GraphPad Prism 5 software and statistical analysis using two way ANOVA comparing against pluronic treated samples with significance set at $p<0.05$.

Elisa of Corneal Protein Using the Inflammatory Marker TNFα

To validate the confocal inflammatory quantification data, Elisa (enzyme linked immunosorbant assay) was performed using the TNFα cytokine marker. Wounded cornea samples were dissected from all four treatment groups at 1, 3, and 5 days. Samples were homogenized and placed in a solution of T-PER tissue protein extraction reagent (Thermo Scientific) and Halt protease inhibitor (Thermo Scientific). The solutions were centrifuged at 10,000 g for 5 minutes. The resulting protein supernatant was analyzed for total concentration using a Coomassie assay (Thermo Scientific) according to manufacturer's instructions on a BioTek Synergy 2 spectrophotometer. Elisa was then conducted in triplicate on protein samples using a rat TNFα ReadySET-Go! (eBioscience) kit according to manufacturer's instructions. The resulting relative protein concentrations were graphed using the GraphPad Prism 5 software and statistical analysis performed using two way ANOVA comparing against pluronic treated samples with significance set at $p<0.05$.

RT-PCR of EMT Markers

RT-PCR was performed in the same manner as described in chapter 3. Corneas were sectioned at 1, 3, and 14 day time points for each of the pluronic gel, control peptide, αCT1, and αCT1 A-PLO microcapsule treatments. Entire corneas were cut into

sections, with individual ¼ sections placed in 1mL of Trizol Plus RNA purification reagent (Invitrogen), and processed according to the manufacturer's protocol. Extracted RNA concentration was measured using an Agilent 2100 bioanalyzer and Agilent RNA 6000 nano kit (Agilent Technologies, Inc). Two samples of RNA per treatment type were selected for each of the three (1, 3, 14 days) time points, ensuring no RNA samples were selected from the same rat source in the same treatment group. These samples were then converted to cDNA at 250nM using a BioRad iScript cDNA kit (Bio-Rad Laboratories) according to manufacturer's instructions. Gene specific primers for Keratin 19, Keratin 8, and TGFβ2 of the EMT pathway and the insulin sensitive genes Esr1 and GLUT4, related to the EMT pathway were designed using BLAST web based software and synthesized by IDT technologies (Table 4.1). The gene attachment region binding protein (ARBP) was used as a calibrator reference. Primers were tested for efficiency using RNA from day 3 pluronic gel treated diabetic rats and optimized by PCR gel analysis (data not shown).

Real-time PCR was run with each gene according to a previously published protocol (Valarmathi et al, 2009) using a BioRad CFX Connect single color real time PCR detection system (Bio-Rad Laboratories) with SsoAdvanced SYBR Green supermix, 1µl cDNA, and 3pmol/rxn primers. All data was analyzed using the Relative Expression Software Tool (REST XL), with pluronic gel treated samples serving as the baseline control. Statistical analysis was performed by both the REST XL Pair Wise Fixed Reallocation Randomization Test and GraphPad Prism data analysis software using $p<0.05$ as statistically significant.

Table 4.2 Summary of primers used in RT-PCR analysis.

Gene	Forward Primer	Reverse Primer	Product Length (bp)
ARBP	5'-CGACCTGGAAGTCCAACTAC-3'	5'-ATCTGCTGCATCTGCTTG-3'	109
Krt19	5'-AGCATGAAAGCTGCCCTGGAA-3'	5'-ATACTGCTGATCACACCCTGGA-3'	92
GLUT4	5′-CTCTCAGGCATCAATGCTGTT-3′	5′-GAGACCAACGTGAAGACGGTA-3′	122
Esr1	5′-AGTGAAGCCTCAATGATGGG-3′	5′-CAAAGATCTCCACCATGCCT-3′	281
Krt8	5′-CTTCTCCCTAGTCACCCACT-3′	5′-TTCCATGTTCGGTCTGCTTC-3′	110
TGFβ2	5′-GCCAATGTAGTAGAGGATGGCTC-3′	5′-AAACTAACCACTTTCTTGCGTG-3′	108

Western Blotting of EMT Markers

Wounded cornea samples were dissected from all four treatment groups at 1, 3, and 14 days. Samples were homogenized and placed in a solution of T-PER tissue protein extraction reagent (Thermo Scientific) and Halt protease inhibitor (Thermo Scientific). The solutions were centrifuged at 10,000 g for 5 minutes. Resulting protein supernatant was analyzed for total concentration using a Coomassie assay (Thermo Scientific) according to manufacturer's instructions on a BioTek Synergy 2 spectrophotometer.

Solutions of 20ug/lane of protein mixed 1:1 with Laemmeli buffer/β-mercaptoethanol were denatured at 70°C, then loaded onto BioRad Criterion 4-15% TGX 12+2 gels. A volume of 20µL of BioRad Precision Plus was also loaded on each gel as a standard. SDS-Page was then performed at 200V for ~40 minutes in Tris/Glycine/SDS buffer (Biorad). Gels were next wet transferred by western blotting onto supported nitrocellulose membranes (BioRad) at 100V for 45 minutes in transfer buffer (Tris/Glycine buffer (BioRad) with methanol pH 8.0). Blotted membranes were blocked for 1hr in a solution of 5% non-fat dry milk (BioRad) and PBS-Tween (Sigma), rinsed three times in PBS-Tween, and stained overnight at 4°C with primary antibodies (Table

4.3). Antibodies were selected to match genes tested for RT-PCR; Krt19, Krt8, TGFβ2, Esr1, and GLUT4. The Erk1 antibody was used as a reference control. Blots were then rinsed three times in PBS-Tween and stained 1hr with secondary HRP labeled antibodies (Invitrogen). Blots were exposed 1 minute to Hyglo chemiluminescent HRP detection reagent (Denville Scientific Inc.) and images captured using a BioRad ChemiDoc XRS+ system with QuantityOne software. Bands were measured for density with equal volume boxes applied to each blot to standardize total area. Each time point was performed in duplicate for every antibody. To compare the results from blot to blot, measurements were converted to values representing fold change analyzed against pluronic treated samples for 1 day, 3 day, and 14 day times. Results were then graphed using GraphPad Prism software with statistical analysis using two way ANOVA and $p<0.05$ statistically significant.

Table 4.3 Summary of antibodies used for western blotting.

Primary Antibodies	Dilutions	Manufacturer
Krt19	1:500	Novus Biologicals
Krt8	1:10000	Novus Biologicals
TGFβ2	1:500	Santa Cruz Biotechnology
Esr1	1:500	Santa Cruz Biotechnology
GLUT4	1:500	Santa Cruz Biotechnology
Erk1	1:1000	BD Biosciences

4.4 Results

4.4.1 Analysis of Diabetic Corneal Wound Closure

Examination of wound closure rate was conducted through fluorescent staining with an ophthalmic dye and subsequent measurements of the changing area of the corneal wounds. A total of 25 eyes with measurements spanning the time points at 0 hrs, 1 day, 3

days, and 5 days were selected from each treatment group to determine the average change in wound area over time. Additional measurements were also taken at 14 days but were excluded after near 100% closure was seen in all eyes by day 5. Figure 4.1 provides a visual summary of the wound closure rate while table 4.4 lists the average values for each treatment over the 5 day (120hr) period as percent change in wound area ± SEM. From this data we were able to conclude αCT1 treatment led to a faster wound closure rate than control treatments, while microencapsulated αCT1 treatment showed even greater wound closure speed. Statistical analysis of this data was conducted through two way ANOVA analysis of the differences in average wound closure vs pluronic treatment ($p<0.05$). Figure 4.2A represents this data graphically with Figure 4.2C containing the specific numerical results. Significant differences in wound closure were found in both αCT1 and microencapsulated αCT1 treatments at 1 day (20.83% and 24.67% respectively) and 3 days (12.73% and 15.90% respectively). In comparison no time points were found significant for control peptide treatments. To further analyze the significance of the differences in both αCT1 and microencapsulated αCT1 treated wound closure we conducted a Kaplan-Meier survival analysis replacing percent closure with survival. The results of this study are presented in Figure 4.2B and numerically in Figure 4.2D. The curve pattern was conserved between the Kaplan-Meier and the percent difference data. From figure 4.2D we saw by the 5 day period a complete closure of the wounds in all eyes for the αCT1 microcapsule treated rats. The αCT1 treated wounds were at 90.41% closure, while control peptide treated were 36.55% closed. Additionally, a Mantel-Cox analysis comparing the curves in figure 4.2B found both αCT1 and

microencapsulated αCT1 treated curves to be significantly different compared to control peptide treated.

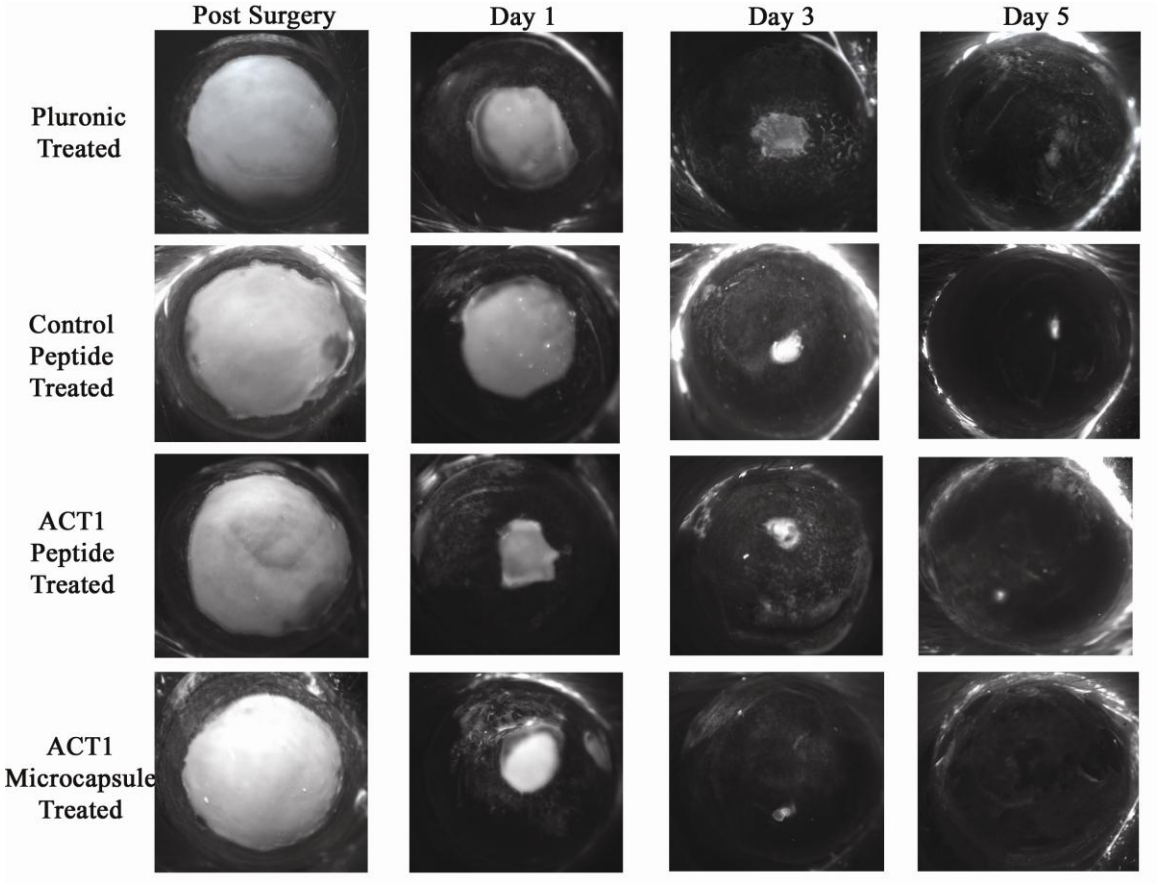

Figure 4.1 Progressive wound healing over 5 days in a diabetic rat corneal injury model. Fluress ophthalmic dye staining of corneal defects immediately after surgery. Repeated at 1 day, 3 days, and 5 days. Treatments from top to bottom on each eye: 25% pluronic gel, 150µM control peptide, 150µM αCT1, and 150µM A-PLO microencapsulated αCT1.

Table 4.4 Summary of diabetic wound closure rates measured using Fluorescein ophthalmic dye. Each data point represents 25 randomly selected eyes from each treatment. Grubb's test for outliers used to remove points found non-significant ($p>0.05$).

	Pluronic Treated	**Control Peptide Treated**	**αCT1 Treated**	**αCT1 Microcapsule Treated**
% change 0-24hrs	44.69 ± 21.34	45.22 ± 22.80	65.52 ± 20.15	69.36 ± 14.02
% change 24-72hrs	73.71 ± 26.60	80.97 ± 18.79	87.12 ± 18.70	97.67 ± 4.27
% change 0-72hrs	83.04 ± 21.43	87.01 ± 16.09	95.77 ± 5.44	98.94 ± 2.10
% change 0-120hrs	90.27 ± 13.50	98.37 ± 1.42	99.44 ± 1.84	100 ± 0.00

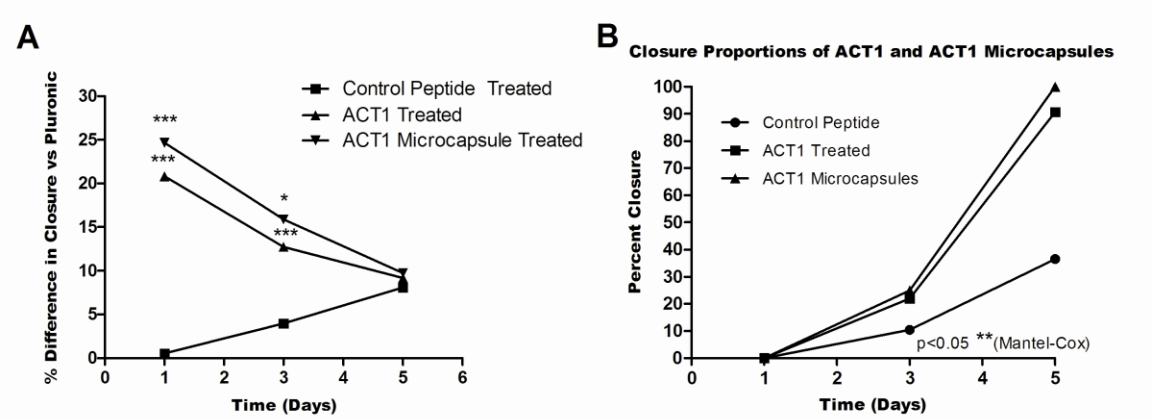

C

% difference vs pluronic	Control Peptide Treated	ACT1 Treated	ACT1 Microcapsule Treated
% change from 0-24hrs	0.53	20.83	24.67
% change from 0-72hrs	3.97	12.73	15.90
% change from 0-120hrs	8.10	9.17	9.73

D

Kaplan-Meier	Control Peptide Treated	ACT1 Treated	ACT1 Microcapsule Treated
Day 1	0.00	0.00	0.00
Day 3	10.42	22.00	25.00
Day 5	36.55	90.41	100.00

Figure 4.2 Diabetic corneal wound closure analysis of the (**A**) average percent differences in wound closure vs pluronic controls and (**B**) Kaplan-Meier survival analysis modified for percent closure over a 5 day period. Summaries of individual values for A are found in table (**C**) and values for B are found in table (**D**).

4.4.2 Investigation of Inflammation Using Confocal Quantification and Elisa

We next set out to examine the effects of each treatment on inflammation over the first five days of wound closure. Two markers of inflammation, ITAC (CXCL11) and TNFα, were selected to stain representative cornea samples at 1, 3, and 5 days. Using ImageJ software, mean intensity values were measured and converted to percent coverage of the entire image. A total of 12 measurements per inflammation marker were analyzed with average values shown in Figure 4.3.

The results of ITAC examination at day 1 indicated ~30-40% total coverage for all treatments except control peptide (56.23 ± 4.07%). By day 3 this trend continued with ~30-40% coverage seen in all treatment groups. By 5 days, as complete wound closure was approached, only pluronic treated corneas still showed values in the 30-40% range (32.96 ± 9.49%), with control peptide dropping to 14.05 ± 4.72%. Both αCT1 and microencapsulated αCT1 treated corneas showed significant reduction compared to pluronic treated with values of 4.23 ± 1.22% and 11.39 ± 1.16% respectively. Data from the confocal TNFα quantification showed values that were different overall, but shared a similar trend over the same three time points. At 1 day both αCT1 (43.29 ± 3.53%) and microencapsulated αCT1 (22.49 ± 5.02%) treated corneas showed values lower than those seen in both controls, with both significantly different compared to pluronic treated. The pattern of expression with TNFα was the same as ITAC at 3 days, with a spike in αCT1 (74.91 ± 2.16%) producing the highest levels. This was followed by pluronic treated (27.24 ± 6.40%), control treated (52.12 ± 5.11%), and finally microencapsulated αCT1 treated (13.89 ± 1.12%) at the lowest expression. By day 5, pluronic and control peptide treated corneas continued to show the highest values; also seen in the day 5 ITAC

results. Additionally, αCT1 and microencapsulated αCT1 treated samples again showed significantly lower expression vs pluronic at 5 days, matching the results from 5 day ITAC as well.

To corroborate the confocal quantification data, Elisa analysis using antibodies for TNFα was performed, with results shown in Figure 4.4. The day 1 Elisa results followed the same pattern as those seen in confocal quantification, with pluronic treated samples having the highest concentration. Both αCT1 (26.08 ± 3.50pg/mL) and microencapsulated αCT1 (46.40 ± 15.23pg/mL) treated corneas showed values lower than those seen in both controls, with both being significantly different compared to pluronic treated. By day 3, αCT1 treated samples again showed a spike while the other three treatments results varied in comparison to confocal quantification analysis. Day 5 analysis saw no significant changes in the results of αCT1 and microencapsulated αCT1 treated samples in comparison to the controls, but overall these two active treatments were found to once again be lower at this time than both control groups.

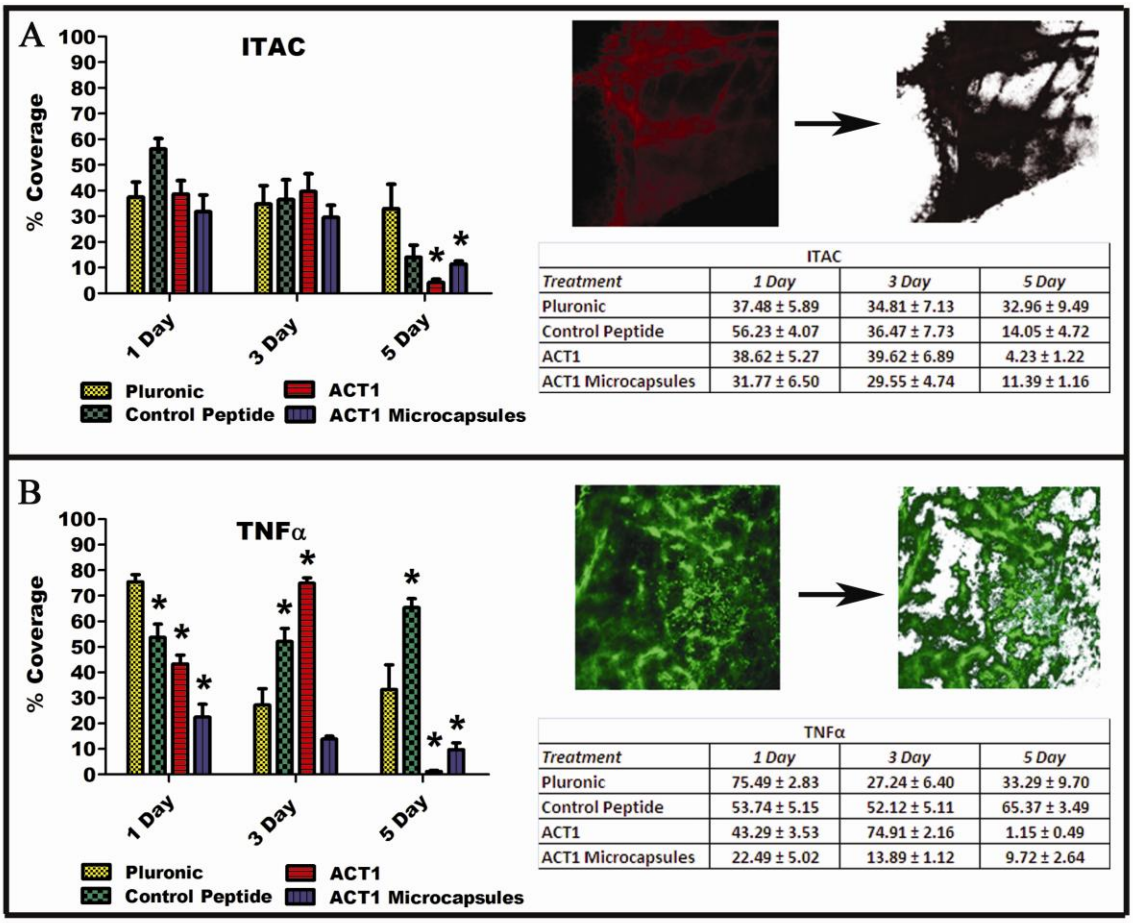

ITAC			
Treatment	*1 Day*	*3 Day*	*5 Day*
Pluronic	37.48 ± 5.89	34.81 ± 7.13	32.96 ± 9.49
Control Peptide	56.23 ± 4.07	36.47 ± 7.73	14.05 ± 4.72
ACT1	38.62 ± 5.27	39.62 ± 6.89	4.23 ± 1.22
ACT1 Microcapsules	31.77 ± 6.50	29.55 ± 4.74	11.39 ± 1.16

TNFα			
Treatment	*1 Day*	*3 Day*	*5 Day*
Pluronic	75.49 ± 2.83	27.24 ± 6.40	33.29 ± 9.70
Control Peptide	53.74 ± 5.15	52.12 ± 5.11	65.37 ± 3.49
ACT1	43.29 ± 3.53	74.91 ± 2.16	1.15 ± 0.49
ACT1 Microcapsules	22.49 ± 5.02	13.89 ± 1.12	9.72 ± 2.64

Figure 4.3 Confocal inflammation quantification over the first five days after wounding using antibodies for (A) ITAC and (B) TNFα. Within each box are the graphical, numerical, and image representations for each marker.

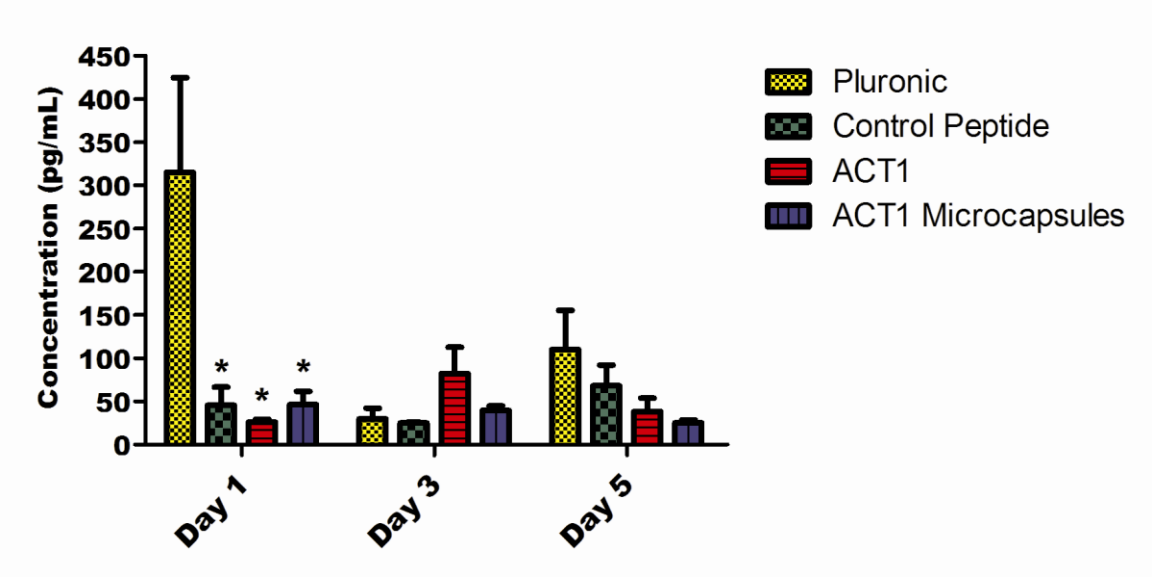

Figure 4.4 Elisa analysis of TNFα concentration in 1, 3, and 5 day corneal protein samples.

Table 4.5 Summary of TNFα Elisa results for 1, 3, and 5 day diabetic cornea samples. Results are the average concentration of TNFα in pg/mL ± SEM.

	Pluronic Treated	**Control Peptide**	**αCT1 Treated**	**αCT1 Microcapsule Treated**
Day 1	315.15 ± 109.70	45.51 ± 20.90	26.08 ± 3.50	46.40 ± 15.23
Day 3	29.80 ± 12.43	24.94 ± 0.94	82.21 ± 30.42	39.58 ± 5.39
Day 5	110.01 ± 45.47	68.16 ± 23.89	38.61 ± 15.33	25.14 ± 3.47

4.4.3 Examination of the EMT Pathway in Diabetic Wound Healing by RT-PCR and Western Blotting

Examination of both wound closure and inflammation data indicated a noticeable effect on corneal wound healing with both αCT1 treatments. As a result RT-PCR and western blotting was performed on a set of genes selected from the EMT pathway and related genes known to be insulin sensitive, as a means of investigating possible reasons for the therapeutic results. Figure 4.5 summarizes the results of the RT-PCR analysis of the five genes of interest. A consistent up regulation of Esr1, Krt8, TGFβ2, and GLUT4 at days 1, 3 and 14 is seen, while Krt19 was down regulated at days 1 and 3. Significance, determined by a pair wise fixed random reallocation test, was found for only αCT1 microcapsule treatments at day 1 in Krt8, TGFβ2, and GLUT4. At day 3 significant up regulation was found in both αCT1 and microencapsulated αCT1 treated samples with TGFβ2 and significance in Krt8 for αCT1 only. By day 14 all genes were up regulated, with TGFβ2 and Esr1 significant in αCT1 treated samples. All genes that were control peptide treated showed strong expression relative to both αCT1 and microencapsulated αCT1 groups at day 14.

Figures 4.6 and 4.7 represent the results of densitometry analysis of western blots from 1, 3, and 14 day samples for the same genes evaluated by RT-PCR. All results are presented as fold change differences vs pluronic treated samples. GAPDH was used as the internal control antibody for normalization. In all time points and treatments no values were found to be statistically significant fold changes in protein expression, however similar patterns of regulation matched the results found in RT-PCR quantification. Data from all three time points indicated similar up regulation of TGFβ2,

Krt8, and GLUT4 for αCT1 and microencapsulated αCT1 samples, as seen in the RT-PCR data. TGFβ2 was again up regulated through all three time points with values between ~1.2-1.4 fold different than pluronic treated, except at day 3 in control treated samples. Krt8 was inconsistently up regulated with biphasic results in the RT-PCR data, but significant up regulation was shown in microencapsulated αCT1 treated samples at 1 day and αCT1 treated samples at 3 days. Densitometry measurements at 1 and 3 days showed Krt8 up regulated in αCT1 (1 day- 1.37, 3 days-1.30 fold up regulated) and microencapsulated αCT1 treated (1 day- 1.43, 3 days- 1.89 fold up regulated) samples compared to both pluronic and control peptide treated. Similar to the RT-PCR results, Esr1 showed consistent up regulation in the western data, with particularly higher results in day 14 samples treated with αCT1 (1.74 fold) and microencapsulated αCT1 (1.70 fold) treatements. Krt19 western analysis indicated down regulation at 1 day for all three treatments, similar to the RT-PCR results. This deviated at days 3 and 14 with up regulation in the western analysis while the RT-PCR data showed down regulation at 3 days and up regulation at 14 days for all treatments. GLUT4 analysis remained the same in both western and RT-PCR analysis pattern, where all treatments were up regulated throughout the three time points.

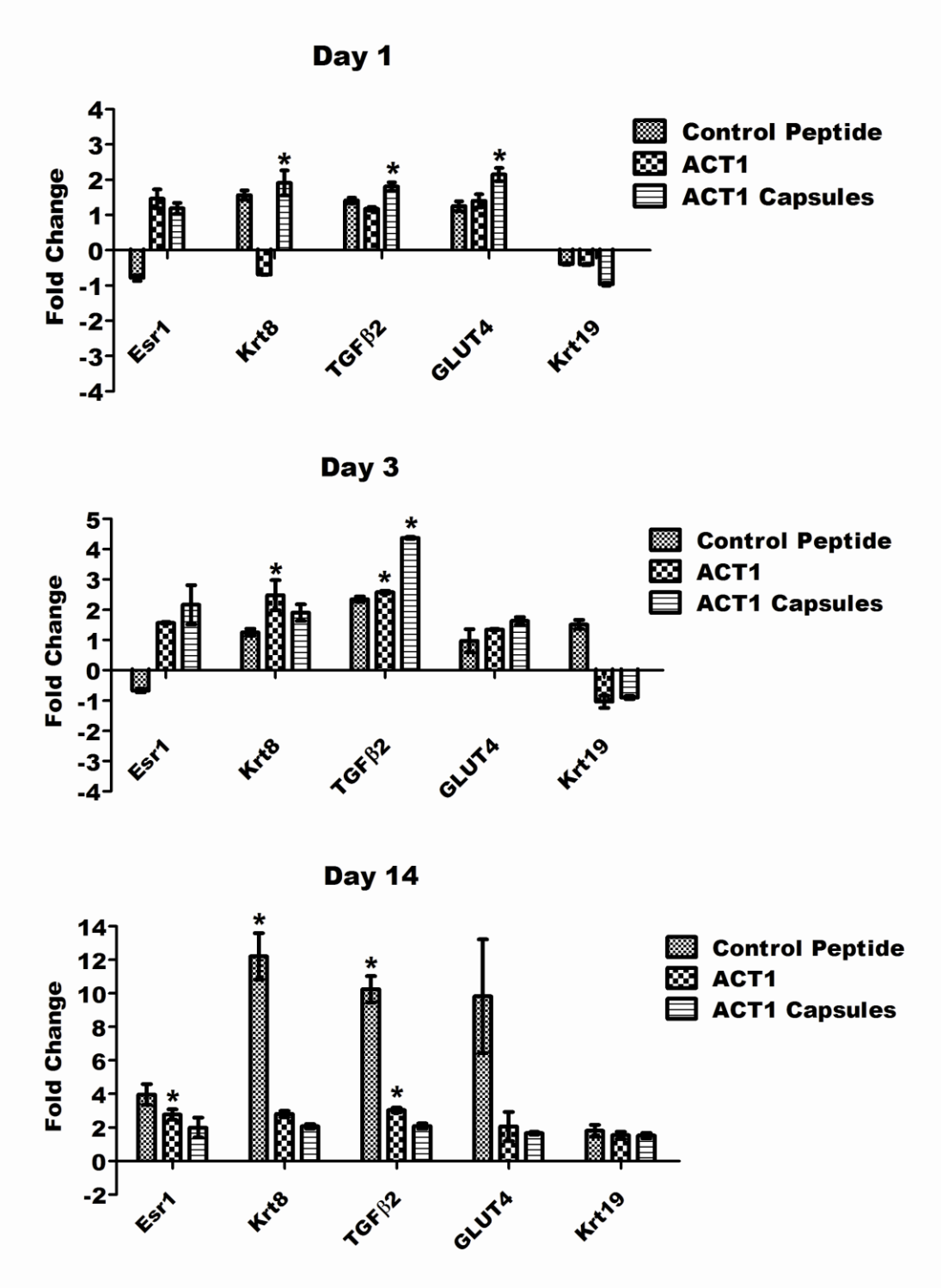

Figure 4.5 RT-PCR examination of EMT and insulin sensitive genes in 1, 3, and 14 day diabetic corneas. ARBP used as a reference gene with pluronic treated samples serving as baseline controls.

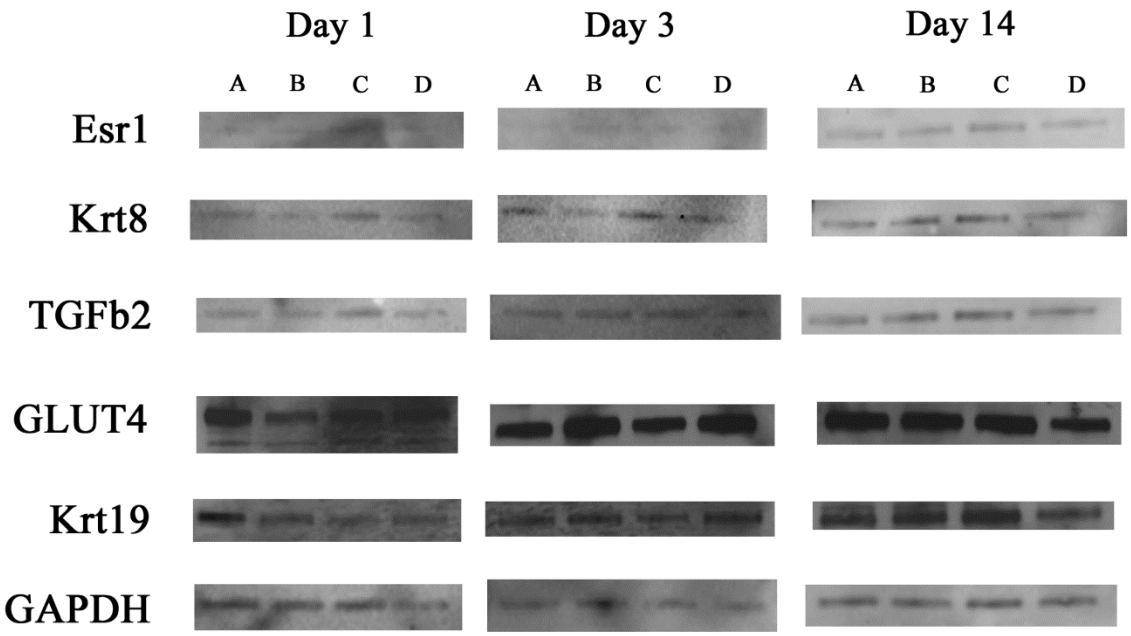

Figure 4.6 Western blot examination of EMT and insulin sensitive genes in 1, 3, and 14 day diabetic corneas. (**A**) Pluronic treated (**B**) Control Peptide treated (**C**) αCT1 treated (**D**) αCT1 microcapsule treated. GAPDH was used to normalize all samples.

A

Day 1	Control Peptide	αCT1	αCT1 Capsules
Esr1	1.25	0.91	1.02
TGFβ2	1.34	1.33	1.39
Krt8	0.89	1.37	1.43
Krt19	0.95	0.83	0.91
GLUT4	1.44	1.39	1.90

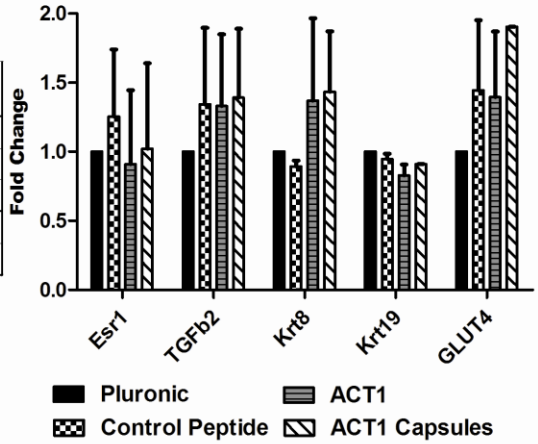

B

Day 3	Control Peptide	αCT1	αCT1 Capsules
Esr1	1.28	1.14	1.12
TGFβ2	0.81	1.20	1.19
Krt8	0.86	1.30	1.89
Krt19	0.83	1.23	1.80
GLUT4	0.81	1.19	1.87

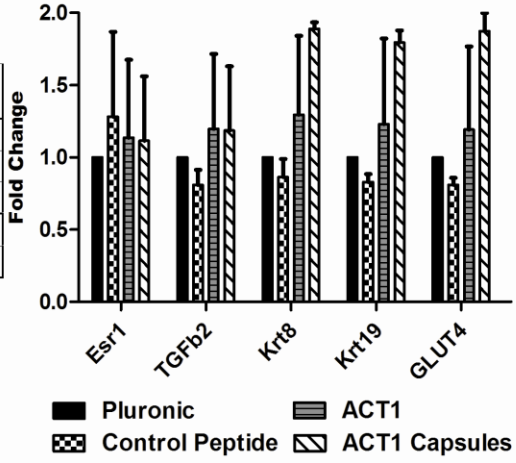

C

Day 14	Control Peptide	αCT1	αCT1 Capsules
Esr1	1.32	1.74	1.70
TGFβ2	1.25	1.29	1.72
Krt8	1.85	1.57	1.52
Krt19	1.84	1.71	1.33
GLUT4	0.93	1.78	1.72

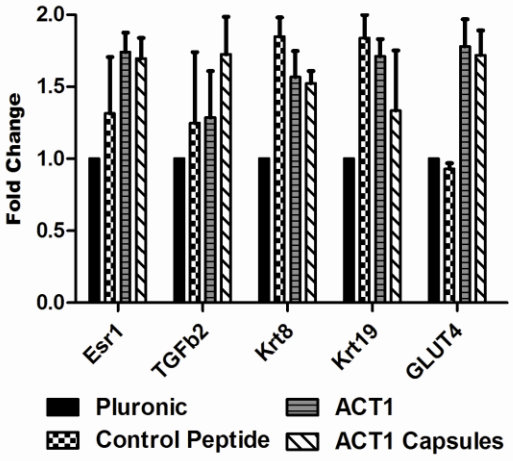

Figure 4.7 Western blot densitometric analysis of EMT and insulin sensitive genes in (**A**) 1 day (**B**) 3 day and (**C**) 14 day diabetic corneas. Average results for each time point are shown to the right of respective graphs. GAPDH was used to normalize all sample results.

4.5 Discussion

Corneal wound healing was found to approach complete closure in all four treatment groups by the 5 day time point, with pluronic gel treated samples averaging ~90% closure, αCT1 ~99%, and αCT1 microcapsule 100%. Statistical analysis using two way ANOVA to compare the percent differences in closure at each time point showed significant differences at days 1 and 3 for both αCT1 (20.83% and 13.41% faster than pluronic treated) and αCT1 microcapsule (24.67% and 23.96% faster than pluronic treated) treatment groups. Additional statistical analysis using the Kaplan-Meier method with analysis by the Mantel-Cox test, comparing survival distributions of two samples, also indicated significant differences in the wound healing curves of each of the two αCT1 treatments. The Kaplan-Meier method is typically used to estimate survival over time in cases such as cancer treatments in large groups of patients, while also accounting for difficulties and changes from patient to patient. This method is used to generate survival curves based on designation of alive/dead of each patient, followed by analysis of statistical differences in their patterns. Here this method was modified to replace alive/dead with open/closed in relation to corneal wound state. Doing so, we were able to analyze the probability of these curves occurring in larger studies. Overall these results indicated application of the αCT1 peptide enhances wound closure in a corneal injury model. Additional therapeutic effects in the form of increased wound healing rate (3.84% at 24hrs vs αCT1 alone) were shown to occur with the addition of controlled release A-PLO microcapsules containing αCT1. These results match the wound healing patterns previously seen in non-diabetic corneal wound closure. Comparing the differences in closure between αCT1 and microencapsulated αCT1 at each of the three

measured points, 1, 3, and 5 days, there was a consistently faster rate of closure in microencapsulated samples (3.84%, 3.17%, and 0.56% respectively). This led us to conclude A-PLO microencapsulated αCT1 provides a definite advantage in therapeutic treatment over direct αCT1 treatment.

Investigation of the mechanisms of αCT1 action to create enhanced wound healing speed was examined by looking at inflammatory levels over time and gene analysis from the EMT pathway. The results of the Western blotting and RT-PCR data indicated a relationship among genes that were up regulated significantly with αCT1 treatments in comparison to control treatments. Each of these genes are known to play either a direct or indirect role in inflammatory regulation. From the RT-PCR and western analysis, Krt8 and TGFβ2 were consistently up regulated for both αCT1 and microencapsulated αCT1 treatments at the three time points. Interestingly TGFβ2 was the only gene up regulated throughout all points. This cytokine directly limits the inflammatory response, promotes accumulation and proliferation of fibroblasts, and controls deposition of ECM for proper tissue repair (Carrington et al 2006). Specifically, Huh et al 2009 found TGFβ2 was highly expressed during chick corneal wound repair. Their data suggest TGFβ2 activates keratocytes to transform into fibroblasts, a known action of wound healing in the cornea. These fibroblasts are then reverted back to keratocytes as the wound closes. Keratins are tissue specific proteins typically associated with the cytoskeleton of epithelial cells. The estrogen receptor pathway is directly related to insulin sensitivity, type I diabetes, and the EMT process. Krt19 is thought to be down regulated in EMT (Aomatsu et al 2011) and related to the estrogen receptor pathway along with Esr1. Both Krt8 and Krt19 have been shown to be present in the limbal

epithelial cells of the cornea and are normal markers in healthy cells (Fu et al 2001, Merjava et al 2009 and 2011, Pai et al 2010). The Esr1 gene, or ERα, is important in protection against and reduction of inflammation, as well as glucose tolerance (Ribas et al 2009, Ricchiuti et al 2009). Glucose transporter 4, or GLUT4, in vivo levels are altered by the inflammatory activation of stress kinases (Simar et al 2012). This action is impaired in diabetes and obesity.

Both αCT1 treatment groups saw a significant decrease in inflammation by day 5 as the wounds approached complete closure. Specifically looking at the day 1 TNFα confocal results, we saw identical highest to lowest order between inflammation level and day 1 wound closure. During this rapid wound closure period, pluronic treated samples were shown to exhibit the most inflammation and the least change in wound closure. This was followed in order by control peptide treated, αCT1 treated, and αCT1 microcapsule treated, observing a direct coupling of inflammation levels to wound healing rate. A deviation in this exact pattern was found at day 3, with a spike in αCT1 levels for ITAC and TNFα. Overall when comparing the results at all three points for ITAC, TNFα and Elisa TNFα there was a pattern of lowered inflammation with αCT1 and microencapsulated αCT1 treatments compared to control groups, which corresponded to the rate at which corneal wound closure occurs.

We saw a mode of action where αCT1 stimulates multiple proteins responsible for inhibition of inflammation. Combined with our inflammatory data investigating markers for ITAC and TNFα, αCT1 is thought to increase wound healing rates by creating a complex reduction in inflammation that is significantly different than control treatments. This reduced inflammatory response may allow a more rapid induction of epithelial

migration and proliferation. Additional investigation of this reaction to αCT1 is required to make definitive statements, with a complex response to the peptide likely.

4.6 Conclusions

Treatment of diabetic corneal wound injuries with αCT1 peptide increased wound closure speed significantly compared to control groups. The addition of a polymeric αCT1 A-PLO microcapsule system further increased the wound healing speed over αCT1 alone. A possible mechanism of αCT1 action was suggested, based on inflammatory and RT-PCR investigation of key EMT genes, indicating the activation of anti-inflammatory cytokines and proteins. Suppression of inflammation may lead to a more rapid proliferation and migration response to wound closure in the cornea.

CHAPTER 5: SUMMARY AND FUTURE WORK

Summary

Microencapsulation of αCT1 by the electrospray method was shown to increase corneal wound healing speed compared to αCT1 directly applied in a pluronic gel solution in both diabetic and non-diabetic rat models. In the non-diabetic study, microencapsulated αCT1 led to wound closure 18% faster than αCT1 alone at 24hrs and 1.99% faster at 72hrs. Results from the diabetic study indicated a 3.84% increase at 24hrs, 3.17% increase at 72hrs, and 0.56% increase at 120hrs. Comparing the results, the decreased wound healing function of the diabetic rats impeded the ability of αCT1 to duplicate the drastic results seen in the non-diabetic model. While in both cases αCT1 significantly increased wound healing rates beyond the results seen in both control groups, we hypothesized the impaired inflammatory function of the diabetic rats coupled with our conclusions on the αCT1 mechanism of therapeutic action involving inflammatory suppression, directly led to the difference in wound closure results seen between the two corneal wound closure studies from chapters 3 and 4. Furthermore, our microencapsulation method provided a reproducible and biocompatible device to deliver αCT1 in a controlled manner. Limitations in this method come from the difficulties in microencapsulating a small peptide such as the one tested here. In these studies use of two polymer coatings, three pH values of gelling solution, and variations in alginate concentration and peptide loading ratio led to the synthesis of the microcapsules created here. A benefit and impediment to drug delivery system design is the vast number of

factors and parameters that can be adjusted, which in turn alter the physical, chemical, biological reactivity, and release characteristics of the microcapsules. As a result, we feel a compatible and functional design was obtained and applied to these wound models with significant results achieved.

This work proposed a unique synthesis of a drug delivery system for the αCT1 peptide. Additionally two distinct, yet connected, models of wound healing in the rat cornea detailed the analysis of the effects of therapeutic application of αCT1 in vivo. Furthermore, we provided data summarizing the effects of the application of this drug in two delivery methods, with and without the presence of a disease state, and analysis through multiple microscopic, biological, and statistical methods. Focus on both the inflammatory and EMT pathway genetic regulation led to a proposed method of αCT1 action. As a result, we feel this work provides a unique perspective in both the potential of αCT1 moving forward as a wound healing agent and the methods to which αCT1 functions in vivo.

Future Work

A complete and comprehensive analysis of the αCT1 peptide mode of in vivo action in wound closure is ongoing. Presented here is a promising start to evaluating the mechanism of αCT1 action by evaluation of the EMT pathway and inflammatory regulation. Studies focusing specifically on the mode of action with a broad range of EMT genes should be pursued. The EMT pathway itself is a complex relationship of interconnected pathways, which should be analyzed in more detail in order to determine the definite relationship that is occurring. The results presented here, coupled with previously published data, indicate a significant therapeutic potential with no visible

negative biological side effects. Additional animal models should be used to fully evaluate the potential of αCT1 in order to find the best transition from bench top to bedside application. At this time, potential wound model and disease states being investigated include diabetic ulcers, topical skin burn models, and type II diabetic knockout models. Continued research into further enhancement of the microcapsule design could also lead to significant increases in release time, which in turn could lead to greater wound closure speeds in future wound models.

References

Ai Z., Fischer A., Spray D.C, Brown A.M. and Fishman G.I. (2000). "Wnt-1 regulation of connexin43 in cardiac myocytes." Journal of Clinical Investigation **105**(2): 161-171.

Akarte A. S., Srinivasan B.P. and Gandhi S. (2012). "Vildagliptin selectively ameliorates GLP-1, GLUT4, SREBP-1c mRNA levels and stimulates β-Cell proliferation resulting in improved glucose homeostasis in rats with streptozotocin-induced diabetes." Journal of Diabetes and Its Complications **26**: 266-274.

Aomatsu K., Arao T., Abe K., Kodama A., Sugioka K., Matsumoto K., Kudo K., Kimura H., Fujita Y., Hayashi H., Nagai T., Shimomura Y. and Nishio K. (2012). "Slug is upregulated during wound healing and regulates cellular phenotypes in corneal eptihelial cells." Investigative Ophthalmology and Visual Science **53**(2): 751-756.

Aomatsu K., Arao T., Sugioka K., Matsumoto K., Tamura D., Kudo K., Kaneda H., Tanaka K., Fujita Y., Shimomura Y. and Nishio K. (2011). "TGF-beta Induces Sustained Upregulation of SNAI1 and SNAI2 through Smad and Non-Smad Pathways in a Human Corneal Epithelial Cell Line." Investigative Ophthalmology and Visual Science **52**(5): 2437-2443.

Arghya, P., ST. Dominique and Satya P. (2010). "Investigation on PEG integrated alginate-chitoan microcapsules for myocardial therapy using marrow stem cells genetically modified by recombinant baculovirus." Cardiovascular Engineering and Technology **1**(2): 154-164.

Arora S., Kumar Ojha S. and Vohora D. (2009). "Characterisation of Streptozotocin Induced Diabetes Mellitus in Swiss Albino Mice." Global Journal of Pharmacology **3**(2): 81-84.

Balasubramaniyan V., Dhar D.K., Warner A.E., Li W.V., Amiri A.F., Bright B., Mookerjee R.P., Davies N.A., Becker D.L. and Jalan R. (2013). "Importance of Connexin-43 based gap junction in cirrhosis and acute on chronic liver failure." Journal of Hepatology **Ahead of Print**.

Barker R., Price R. and Gourdie R.G. (2002). "Increased association of ZO-1 with connexin43 during remodeling of cardiac gap junctions." Circulation Research **90**: 317-324.

Barry F., Boynton R., Murphy M. and Zaia J. (2002). "The SH-3 and SH-4 antibodies recognize distinct epitopes on CD73 from Human Mesenchymal Stem Cells." Biochemical and Biophysical Research Communications **289**(2): 519-524.

Battal, M., Y. Hata, K. Matsuka, O. Ito, H. Matsuda, Y Yoshida and Kawazoe T. (1996). "Reduction of progressive burn injury by a stable prostaglandin I2 analogue, beraprost sodium (procyclin): an experimental study in rats." Burns **22**(7): 531-538.

Bender, J., H. Friedman, V. Giurgiutiu, C. Watson, M. Fitzmaurice and Yost M. (2006). "The use of biomedical sensors to monitor capsule formation around soft tissue implants." Annals of Plastic Surgery **56**(1): 72-77.

Bennett M. and Zukin R. (2004). "Electrical coupling and neuronal synchronization in the mammalian brain." Neuron **41**: 495-511.

Brembeck FH, Schwarz-Romond T, Bakkers J, Wilhelm S, Hammerschmidt M and Birchmeier W. (2004). "Essential role of BCL9-2 in the switch between beta-catenin's adhesive and transcriptional functions." Genes and Development **18**(18): 2225-2230.

Calafiore R., Basta G., Luca G., Boselli C., Bufalari A., Bufalari A., Cassarani M.P., Giustozzi G.M. and Brunetti P. (1999). "Transplantation of Pancreatic Islets Contained in Minimal Volume Microcapsules in Diabetic High Mammalians." Annals of the New York Academy of Sciences **875**: 219-232.

Carrington L., Albon J., Anderson I., Kamma C. and Boulton M. (2006). "Differential Regulation of Key Stages in Early Corneal Wound Healing by TGF-beta Isoforms and Their Inhibitors." Investigative Ophthalmology and Visual Science **47**(5): 1886-1894.

Casper, C.L., N. Yamaguchi, K.L. Kiick and Rabolt J.F. (2005). "Functionalizing electrospun fibers with biologically relevant macromolecules." Biomacromolecules **6:** 1998-2007.

Cavanagh P.R., Lipsky B. A., Bradbury A. W. and Botek G. (2005). "Treatment for diabetic foot ulcers." The Lancet **366**: 1725-1735.

Chakraborty, S., I. Liao, A. Adler and Leong K. (2009). "Electrohydrodynamics: a facile technique to fabricate drug delivery systems." Advanced Drug Delivery Reviews **61**: 1043-1054.

Champion, J. and Mitragotri S. (2006). "Role of target geometry in phagocytosis." Proceedings of the National Academic Society of the USA **103**(13): 4930-4934.

Chapman H. (2010). "Epithelial-mesenchymal interactions in pulmonary fibrosis." Annual Review of Physiology **16**(8): 600-612.

Chew, S., J. Wen, E. Yim and Leong K. (2005). "Sustained release of proteins from electrospun biodegradable fibers." Biomacromolecules **6**: 2017-2024.

Chew, S., Y. Wen, Y. Dzenis and Leong K. (2006). "The role of electrospinning in the emerging field of nanomedicine." Current Pharmaceutical Design **12**(36): 4751-4770.

Choi, J., K. Leong and Yoo H. (2008). "In vivo wound healing of diabetic ulcers using electrospun nanofibers immobilized with human epidermal growth factor (EGF)." Biomaterials **29**: 587-596.

Chu YS, Thomas WA, Eder O, Pincet F, Perez E, Thiery JP and Dufour S. (2004). "Force measurements in E-cadherin-mediated cell doublets reveal rapid adhesion strengthened by actin cytoskeleton remodeling through Rac and Cdc42." Journal of Cell Biology **167**(6): 1183-1194.

Daia C., Wanga B. and Zhaoa H. (2005). "Microencapsulation peptide and protein drugs delivery system." Colloids and Surfaces **41**: 117-120.

Dalhaimer, P., AJ. Engler, R. Parthasarathy and Discher D. (2004). "Targeted worm micelles." Biomacromolecules **5**(5): 1714-1719.

Dashevsky, A. (1998). "Protein loss by the microencapsulation of an enzyme (lactase) in alginate beads." International journal of Pharmaceutics **161**: 1-5.

Dbouk H., Mroue R., El-Sabban M. and Talhouk R. (2009). "Connexins: a myriad of functions extending beyond assembly of gap junction channels." Cell Communication and Signaling **7**(4): 1-17.

Derubeis A. and Cancedda R. (2004). "Bone marrow stromal cells (BMSCs) in bone engineering: limitations and recent advances." Annals of Biomedical Engineering **32**(1): 160-165.

Discher D. (2009). "Growth factors, matrices, and forces combine and control stem cells." Science **324**: 1673-1677.

Draget, K., K. Ostgaard and Smidsrod O. (1989). "Alginate-based solid media for plant tissue culture." Applied Microbiology and Biotechnology **31**(1): 79-83.

Dua H.S., Miri A. and Said D.G. (2010). "Contemporary limbal stem cell transplantation—a review." Clinical Experimental Ophthalmology **38**: 104-117.

Dupps J, Wilson S. (2006). "Biomechanics and wound healing in the cornea." Experimental Eye Research **83**: 709-720.

Duffy H., Delmar M. and Spray D. (2002). "Formation of the gap junction nexus: binding partners for connexins." Journal of Physiology **96**: 243-249.

Enayati M., Ahmad Z., Stride E. and Edirisinghe M. (2009). "Preparation of polymeric carriers for drug delivery with different shape and size using an electric jet." Current Pharmaceutical Biotechnology **10**: 600-608.

Enayati, M., Ming-Wei. Chang, F. Bragman, M. Edirisinghe and Stride E. (2011). "Electrohydrodynamic preparation of particles, capsules, and bubbles for biomedical engineering applications." Colloids and Surfaces A: Physiochemical and Engineering Aspects **382**: 154-164.

Engler C., Chakravarti S., Doyle J., Eberhart C., Meng H., Stark W., Kelliher C. and Jun A. (2010). "Transforming Growth Factor-beta Signaling Pathway Activation in Keratoconus." American Journal of Ophthalmology **151**(5): 752-759.

Evers L., Bhavsar D. and Mailander P. (2010). "The biology of burn injury." Experimental Dermatology **19**: 777-783.

Friedenstein A.J. (1976). "Precursor cells of mechanocytes." International Review of Cytology **47**: 327-359.

Fu X., Sun X., Li X. and Sheng Z. (2001). "Dedifferentiation of epidermal cells to stem cells in vivo." The Lancet **358**: 1067-1068.

Fukuda M. and Sasaki H. (2012). "Quantitative evaluation of corneal epithelial injury caused by n-heptanol using a corneal resistance measuring device in vivo." Clinical Ophthalmology **6**: 585-593.

Gaetea C., Tsapisa N., Silvaa L., Bourgauxa C. and Fattala E. (2008). "Morphology, structure and supramolecular organization of hybrid 1,2-dipalmitoyl-sn-glycero-3-phosphatidylcholine–hyaluronic acid microparticles prepared by spray drying." European Journal of Pharmaceutical Science **34**(1): 12-21.

Geletu M., Trotman-Grant A. and Raptis L. (2012). "Mind the gap; regulation of gap junctional, intercellular communication by the SRC oncogene product and its effectors." Anticancer Research **32**(10): 4245-4250.

Ghatnekar G., O'Quinn M., Jourdan L.J., Gurjarpadhy A., Draughn R. and Gourdie R.G. (2009). "Connexin43 carboxyl-terminal peptides reduce scar progenitor and

promote regenerative healing following skin wounding." Regenerative Medicine **4**(2): 205-223.

Giurgiutiu, V., Friedman H., Bender J., Borg T., Yost M., Newcomb W., Black A., Bost J. and Stewart C. (2004). "Electromechanical impedance sensor for in vivo monitoring the body reaction to implants." Journal of Investigative Surgery **17**(5): 257-270.

Gombotz, W. and Wee S.F. (1998). "Protein release from alginate matrices." Advanced Drug Delivery Reviews **31**: 267-285.

Goodwin R., Nesbitt T., Price R., Wells C., Yost M. and Potts J. (2005). "Three-dimensional model system of valvulogenesis." Developmental Dynamics **233**: 122-2005.

Gray, C.J. and Dowsett J. (1988). "Retention of Insulin in Alginate Gel Beads." Biotechnology and Bioengineering **31**: 607-612.

Grochot-Przeczek A., Lach R., Mis J., Skrzypek K., Gozdecka M., Sroczynska P., Dubiel M., Rutkowski A., Kozakowska M., Zagorska A., Walczynski J., Was H., Kotlinowski J., Drukala J., Kurowski K., Kieda C., Herault Y., Dulak J. and Jozkowicz A. (2009). "Heme Oxygenase-1 Accelerates Cutaneous Wound Healing in Mice." PLoS one **4**(6): 1-16.

Grove J., Bruscia E. and Krause D. (2004). "Plasticity of bone marrow-derived stem cells." Stem Cells and Development: 487-500.

Grupcheva C., Laux W., Rupenthal I., McGhee J., McGhee C. and Green C. (2012). "Improved Corneal Wound Healing through Modulation of Gap Junction Communication Using Connexin43-Specific Antisense Oligodeoxynucleotides." Investigative Ophthalmology and Visual Science **53**(3): 1130-1138.

Gu F., Amsden B. and Neufeld R. (2004). "Sustained delivery of vascular endothelial growth factor with alginate beads." Journal of Controlled Release **96**: 463-472.

Guarino M., Tosoni A. and Nebuloni M. (2009). "Direct contribution of epithelium to organ fibrosis: epithelial-menenchymal transition." Human Pathology **40**: 1365-1376.

Hernandez R., Orive G., Murua A. and Pedraz J. (2010). "Microcapsules and microcarriers for in situ cell delivery." Advanced Drug Delivery Reviews **62**: 711-730.

Herve J.C., Bourmeyster N. and Sarrouilhe D. (2004). "Diversity in protein-protein interactions of connexins: emerging roles." Biochimica et Biophysica Acta **1662**: 22-41.

Hilborn, J¨ons and Bjursten L.M. (2007). "A new and evolving paradigm for biocompatibility." Journal of Tissue Engineering and Regenerative Medicine **1**(2): 110-119.

Hildebrand, G. and Tack J. (2000). "Microencapsulation of peptides and proteins." International journal of Pharmaceutics **196**: 173-176.

Hori K., Sotozono C., Hamuro J., Yamasaki K., Kimura Y., Ozeki M., Tabata Y. and Kinoshita S. (2007). "Controlled-release of epidermal growth factor from cationized gelatin hydrogel enhances corneal epithelial wound healing." Journal of Controlled Release **118**: 169-176.

Huh M., Chang Y. and Jung J. (2009). "Temporal and spatial distribution of TGF-ß isoforms and signaling intermediates in corneal regenerative wound repair." Histology and Histopathology **24**: 1405-1416.

Hunter A., Barker R., Zhu C. and Gourdie R.G. (2005). "Zonula occludens-1 alters connexin43 gap junction size and organization by influencing channel accretion." Molecular Biology of the Cell **16**: 5686-5698.

Hwang, Y.K., U. Jeong and Cho E.C. (2008). "Production of uniform-sized polymer core-shell microcapsules by coaxial electrospraying." Langmuir **24**: 2446-2451.

Jaworek A. and Krupa A. (1999). "Classification of the modes of EHD spraying." Journal of Aerosol Science **30**(7): 975.

Jaworek A. and Krupa A. (1999). "Jet and drop formation in electrohydrodynamic spraying of liquids: a systematic approach." Experiments in Fluids **27**(1): 43-52.

Jin, H., DA. Heller and Stano M.S. (2008). "Single-particle tracking of endocytosis and exocytosis of single-walled carbon nanotubes in NIH-3T3 cells." Nano Letters **8**(6): 1577-1585.

Kalluri, R. and Neilson E. (2003). "Epithelial-mesenchymal transition and its implications for fibrosis." The Journal of Clinical Investigation **112**(12): 1776-1784.

Kam, NW., Z. Liu and Dai H. (2006). "Carbon nanotubes as intracellular transporters for proteins and DNA: an investigation of the uptake mechanism and pathway." Angewandte Chemie **45**(4): 591-595.

Karamichos D., Hutcheon A.E.K and Zieske J.D (2011). "Transforming growth factor beta 3 regulates assembly of a non fibrotic matrix in a 3D corneal model." Journal of Tissue Engineering and Regenerative Medicine **5**(8): 228-238.

Katti, D.S., K. Robinson, F. Ko and Laurencin C. (2004). "Bioresorbable nanofiber-based systems for wound healing and drug delivery: optimization of fabrication parameters." Journal of Biomedical Material Research B **70B**: 286-296.

Kawakita T., Espana E., Higa K., Kato N., Li W. and Tseng S. (2012). "Activation of Smad-Mediated TGF-b Signaling Triggers Epithelial–Mesenchymal Transitions in Murine Cloned Corneal Progenitor Cells." Journal of Cellular Physiology **228**: 225-234.

Kemp K., Hows J. and Donaldson C. (2005). "Bone marrow-derived mesenchymal stem cells." Leukemia and Lymphoma **46**(11): 1531-1544.

Kneser U., Schaefer D.J., Polykandroitis E. and Horch R.E. (2006). "Tissue engineering of bone: the reconstructive surgeon's point of view." Jounal of Cellular and Molecular Medicine **10**(1): 7-19.

Kojima T., Kokai Y., Chiba H., Yamamoto M., Mochizuki Y. and Sawada N. (2001). "Cx32 but not Cx26 is associated with tight junctions in primary cultures of rat hepatocytes." Experimental Cell Research **263**(2): 193-201.

Kong B., Michalski C.W, Hong X., Valkovskaya N., Rieder S., Abiatari I., Streit S., Erkan M., Esposito I., Friess H. and Kleeff J. (2010). "AZGP1 is a tumor suppressor in pancreatic cancer inducing mesenchymal-to-epithelial transdifferentiation by inhibiting TGF-β-mediated ERK signaling." Oncogene **29:** 5146-5158.

Kowalczyk AP, Bornslaeger EA, Norvell SM, Palka HL and Green KJ. (1999). "Desmosomes: intercellular adhesive junctions specialized for attachment of intermediate filaments." International Review of Cytology **185**: 237-302.

Laing JG, Manley-Markowski RN, Civitelli R Koval M and Steinberg T.H. (2001). "Connexin45 interacts with zonula occludens-1 in osteoblastic cells." Cell Communication and Adhesion **8**(4): 209-212.

Langer, G. and Yamate G. (1969). "Encapsulation of liquid and solid aerosol particles to form dry powders." Colloid Interface Science **29**: 450-455.

Lee J., Dedhar S., Kalluri R. and Thompson E. (2006). "The epithelial-mesenchymal transition: new insights in signaling, development and disease." The Journal of Cell Biology **172**(7): 973-981.

Lee J., Ko M. and Kay E. (2012). "Endothelial mesenchymal transformation mediated by IL-1b-induced FGF-2 in corneal endothelial cells." Experimental Eye Research **95**: 35-39.

Lee K. and Mooney D. (2012). "Alginate: Properties and biomedical applications." Progress in Polymer Science **37**: 106-126.

Lee Y.H., Chang J.J., Chien C.T., Yang M.C. and Chien H.F. (2012). "Antioxidant Sol-Gel Improves CutaneousWound Healing in Streptozotocin-Induced Diabetic Rats." Experimental Diabetes Research **2012**: 1-11.

Lim J and Thiery J.P. (2012). "Epithelial-mesenchymal transitions: insights from development." Development(139): 3471-3486.

Lin, J., W. Yu, X. Liu, H. Xie, W. Wang and Ma X. (2008). "In vitro and in vivo characterization of alginate-chitosan-alginate artificial microcapsules for therapeutic oral delivery of live bacterial cells." Journal of Bioscience and Bioengineering **105**(6): 660-665.

Lu H., Lu Q., Zheng Y. and Li Q. (2012). "Notch signaling promotes the corneal epithelium wound healing." Molecular Vision **18**: 403-411.

Lucas T., Siu E., Esteves C., Monteiro H., Oliveira C., Porto C. and Lazari M. (2008). "17Beta-Estradiol Induces the Translocation of the Estrogen Receptors ESR1 and ESR2 to the Cell Membrane, MAPK3/1 Phosphorylation and Proliferation of Cultured Immature Rat Sertoli Cells." Biology of Reproduction **78**: 101-114.

Ma A., Zhao B., Boulton M. and Albon J. (2010). "A role for notch signaling in corneal wound healing." Wound Repair and Regeneration **19**: 98-106.

Martin D., Cox N., Hathcock T., Neimeyer G. and Baker H. (2002). "Isolation and characterization of multipotential mesenchymal stem cells from feline bone marrow." Experimental Hematology **30**: 879-886.

Martin P. (1997). "Wound healing-aiming for perfect skin regeneration." Science **276**: 75-81.

Mbanaso E.N. and Roscoe D.H. (1982). "Alginate: an alternative to agar in plant protoblast culture." Plant Science Letters **25**(1): 61-66.

Mercade-Prieto R., Nguyen B., Allen R., York D., Preece J., Goodwin T. and Zhang Z. (2011). "Determination of the elastic properties of single microcapsules using micromanipulation and finite element modeling." Chemical Engineering Science **66**: 2042-2049.

Merjava S., Brejchova K., Vernon A., Daniels J. and Jirsova K. (2011). "Cytokeratin 8 Is Expressed in Human Corneoconjunctival Epithelium, Particularly in Limbal Epithelial Cells." Investigative Ophthalmology and Visual Science **52**(2): 787-794.

Merjava S., Neuwirth A., Mandys V. and Jirsova K. (2009). "Cytokeratins 8 and 18 in adult human corneal endothelium." Experimental Eye Research **89**: 426-431.

Mirza A, Foster L, Valentine H, Welch I, West CM and Pritchard S. (2012). "Investigation of the epithelial to mesenchymal transition markers S100A4, vimentin and Snail1 in gastroesophageal junction tumors." Diseases of the Esophagus **Ahead of Print**.

Moore K., Amos J., Davis J., Gourdie R.G. and Potts J. (2013). "Characterization of polymeric microcapsules containing a low molecular weight peptide for controlled release." Microscopy and Microanalysis **19**(1): 213-226.

Muro S., Garnacho C. and Champion J. (2008). "Control of endothelial targeting and intracellular delivery of therapeutic enzymes by modulating the size and shape of ICAM-1 targeted carriers." Molecular Therapy **16**(8): 1450-1458.

Murphy J.A. (1980). "Non-coating techniques to render biological specimens conductive." Scanning Electron Microscopy: **1**: 209-220.

Netto MV, Mohan RR, Ambrósio R Jr, Hutcheon AE, Zieske JD and Wilson SE. (2005). "Wound healing in the cornea: a review of refractive surgery complications and new prospects for therapy." Cornea **24**(5): 509-522.

Norris R., Moreno-Rodriguez R., Sugi Y., Hoffman S., Amos J., Hart M., Potts J., Goodwin R. and Markwald R. (2008). "Periostin regulates atrioventricular valve maturation." Developmental Biology **316**: 200-213.

Ondeykal J.G., Herath K., Jayasuriya H., Polishook J., Bills G., Dombrowski A., Mojena M., Koch G., DiSalvo J., DeMartino J., Nanakorn W., Morenberg C., Balick M., Stevenson D., Slattery M. and Singh S.B. (2005). "Discovery of structurally diverse natural product antagonists of chemokine receptor CXCR3." Molecular Diversity **9**: 123-129.

O'Quinn M., Palatinus J., Harris B., Hewett K. and Gourdie R.G. (2011). "A peptide mimetic of the connexin43 carboxyl terminus reduces gap junction remodeling and induced arrhythmia following ventricular injury." Circulation Research **108**: 704-715.

Orive G., Tam S., Pedraz J. and Halle J. (2006). "Biocompatibility of alginate poly-L-lysine microcapsules for cell therapy." Biomaterials **27**: 3691-3700.

Ormonde S., Chou C., Goold L., Petsoglou C., Al-Taie R., Sherwin T., McGhee C. and Green C. (2012). "Regulation of Connexin43 Gap Junction Protein Triggers Vascular Recovery and Healing in Human Ocular Persistent Epithelial Defect Wounds." Journal of Membrane Biology **245**: 381-388.

Oviedo-Orta E. and Evans W. (2004). "Gap junctions and connexin-mediated communication in the immune system." Biochimica et Biophysica Acta **1662**: 102-112.

Pai V. and Glasgow B. (2010). "MUC16 as a Sensitive and Specific Marker for Epithelial Downgrowth." Arch Ophthalmol. **128**(11): 1407-1412.

Paine M., Alexander M. and Stark J. (2007). "Nozzle and liquid effects on the spray modes in nanoelectrospray." Journal of Colloid and Interface Science **305**(1): 111-123.

Paul A., Shum-Tim D. and Prakash S. (2010). "Investigation on PEG integrated alginate-chitosan microcapsules for myocardial therapy using marrow stem cells genetically modified by recombinant baculovirus." Cardiovascular Engineering and Technology **1**(2): 154-164.

Pham, Q., Sharma U. and Mikos A. (2006). "Electrospinning of polymeric nanofibers for tissue engineering applications: a review." Tissue Engineering **12**(5): 1197-1211.

Pradhan L., Andersen N., Nabzdyk C., LoGerfo F. and Veves A. (2007). "Wound-healing Abnormalities in Diabetes and New Therapeutic Interventions." US Endocrinology **1**: 68-72.

Radisky D. (2005). "Epithelial-mesenchymal transition." Journal of Cell Science **118**(19): 4325-4326.

Rao V., Prescott E., Shelke N., Trivedi R., Thomas P., Struble C., Gadek T., O'Neill C. and Kompella U. (2010). "Delivery of SAR 1118 to the Retina via Ophthalmic Drops and its Effectiveness in a Rat Streptozotocin (STZ) Model of Diabetic Retinopathy (DR)." Investigative Ophthalmology and Visual Science **51**(10): 5198-5204.

Regas FC. and Ehrlich H.P. (1992). "Elucidating the vascular response to burns by a new rat model." Journal of Trauma **32**: 556-563.

Rémond M., Iaffaldano G., O'Quinn M., Mezentseva N., Garcia V., Harris B., Gourdie R.G., Eisenberg C. and Eisenberg L. (2011). "GATA6 reporter gene reveals myocardial phenotypic heterogeneity that is related to variations in gap junction coupling." American Journal of Physiology- Heart and Circulatory Physiology **301**: 1952-1964.

Rhett J.M, Jourdan J. and Gourdie R.G. (2011). "Connexin 43 connnexon to gap junction transition is regulated by zonula occludins-1." Molecular Biology of the Cell **22**: 1516-1528.

Rhett J.M, Ongstad E., Jourdan J. and Gourdie R.G. (2012). "Cx43 Associates with Nav1.5 in the Cardiomyocyte Perinexus." Journal of Membrane Biology **245**: 411-422.

Rhett J.M. , Ghatnekar G.S., Palatinus J.A., O'Quinn M., Yost M. and Gourdie R.G. (2008). "Novel therapies for scar reduction and regenerative healing of skin wounds." Trends in Biotechnology **26**(4): 173-180.

Rho K., Jeong L., Lee G., Seo B., Park Y., Hong S., Roh S., Cho J., Park W. and Min B. (2006). "Electrospinning of collagen nanofibers: effects on the behavior of normal human keratinocytes and early stage wound healing." Biomaterials **27**: 1452-1461.

Ribas V., Nguyen M.T.A., Henstridge D.C., Nguyen A., Beaven S., Watt M. and Hevener A. (2009). "Impaired oxidative metabolism and inflammation are associated with insulin resistance in ER alpha-deficient mice." American Journal of Physiology- Endocrinology and Phsiology **298**: 304-319.

Ricchiuti V., Lian C., Oestreicher E., Tran L., Stone J., Yao T., Seely E., Williams G. and Adler G. (2009). "Estradiol increases angiotensin II type 1 receptor in hearts of ovariectomized rats." Journal of Endocrinology **200**: 75-84.

Rosi´nski S., Lewi´nska D., W´ojcik M., Orivec G., Pedraz J.L. and Wery´nski A. (2005). "Mass transfer characteristics of poly-lysine, poly-ornithine and poly-methylene-co-guanidine membrane coated alginate microcapsules." Journal of Membrane Science **254**: 249-257.

Rowley-Conway, G. (2010). "Infection prevention and treatment in patients with major burn injuries." Nursing Standard **7**: 51-58.

Rutledge, G. and Fridrikh S. (2007). "Formation of fibers by electrospinning." Advanced Drug Delivery Reviews **59**: 1384-1391.

Schultz G., Clark W. and Rotatori D.S. (1991). "EGF and TGF-α in wound healing and repair." Journal of Cellular Biochemistry **45**(4): 346-352.

Segretain, D. and Falk M. (2004). "Regulation of connexin biosynthesis, assembly, gap junction formation, and removal." Biochimica et Biophysica Acta **1662**: 3-21.

Shi L., Chang Y., Yang Y., Zhang Y., Fu-Shin X. Yu and Wu X. (2012). "Activation of JNK Signaling Mediates Connective Tissue Growth Factor Expression and Scar Formation in Corneal Wound Healing." PLoS one **7**(2): 1-9.

Shimmura S., Miyashita H., Konomi K., Shinozaki N., Taguchi T. , Kobayashi H., Shimazaki J., Tanaka J. and Tsubota K. (2005). "Transplantation of corneal

endothelium with Descemet's membrane using a hyroxyethyl methacrylate polymer as a carrier." British Journal of Ophthalmology **89**: 134-137.

Simar D., Jacques A. and Caillaud C. (2012). "Heat shock proteins induction reduces stress kinases activation, potentially improving insulin signalling in monocytes from obese subjects." Cell Stress and Chaperones **17**: 615-621.

Simone E., Dziubia T. and Muzykantov V. (2008). "Polymeric carriers: role of geometry in drug delivery." Expert Opinion Drug Delivery **5**(12): 1283-1300.

Singer A., McClain S., Taira B., Romanov A., Rooney J. and Zimmerman T. (2009). "Validation of a porcine comb burn model." American Journal of Emergency Medicine **27**: 285-288.

Singh U. P., Singh S., Taub D.D. and Lillard Jr. J.W. (2003). "Inhibition of IFN-γ-Inducible Protein-10 Abrogates Colitis in IL-$10^{-/-}$ Mice." Journal of Immunology **171**: 1401-1406.

Soder B., Propst J., Brooks T., Goodwin R., Friedman H., Yost M. and Gordie R.G. (2009). "The connexin43 carboxyl-terminal peptide ACT1 modulates the biological response to silicone implants." Journal of the American Society of Plastic Surgeons **123**(5): 1440-1451.

Soetikno V., Saria F., Sukumarana V., Lakshmanana A., Harimaa M., Suzukic K., Kawachid H. and Watanabea K. (2011). "Curcumin decreases renal triglyceride accumulation through AMPK–SREBP signaling pathway in streptozotocin-induced type 1 diabetic rats." Journal of Nutritional Biochemistry: 1-7.

Sweetnam D., Holmes A., Tennant K., Zamani A., Walle M., Jones P., Wong C. and Brown C. E. (2012). "Diabetes Impairs Cortical Plasticity and Functional Recovery Following Ischemic Stroke." The Journal of Neuroscience **32**(15): 5132-5143.

Takka, S. and Gurel A. (2010). "Evaluation of chitosan/alginate beads using experimental design: formulation and in vitro characterization." American Association of Pharmaceutical Scientists **11**(1): 460-466.

Tam S.K., Bilodeau S., Dusseault J., Langlois G., Hallé J.P. and Yahia L.H. (2011). "Biocompatibility and physicochemical characteristics of alginate–polycation microcapsules." Acta Biomaterialia **7**: 1683-1692.

Toyofuku T., Yabuki M., Otsu K., Kuzuya T., Hori M. and Tada M. (1998). "Direct association of the gap junction protein connexin-43 with ZO-1 in cardiac myocytes." Journal of Biological Chemistry **273**(21): 12725-12731.

Trinkaus-Randall V. and Nugent M. (1998). "Biological response to a synthetic cornea." Journal of Controlled Release **53**: 205-214.

Tsuchida S., Arai Y., Kishida T., Takahashi K., Honjo K., Terauchi R., Inoue H., Oda R., Mazda O. and Kubo T. (2012). "Silencing the Expression of Connexin 43 Decreases Inflammation and Joint Destruction in Experimental Arthritis." Journal for Orthopedic Research **Ahead of Print**: 1-6.

Valarmathi M., Davis J., Yost M., Goodwin R. and Potts J. (2009). "A three-dimensional model of vasculogenesis." Biomaterials **30**: 1098-1112.

Valarmathi M., Yost M., Goodwin R. and Potts J. (2008). "A three-dimensional tubular scaffold that modulates the osteogenic and vasculogenic differentiation of rat bone marrow stromal cells." Tissue Engineering **14**(4): 491-504.

Vandenberg G.W., Drolet C., Scott S.L. and de la Nou¨e J. (2001). "Factors affecting protein release from alginate–chitosan coacervate microcapsules during production and gastric/intestinal simulation." Journal of Controlled Release **77**: 297-307.

Vinkin M., Decrock E., Leybaert L., Bultynck G., Himpens B., Vanhaecke T. and Rogeirs V. (2011). "Non-channel functions of connexins in cell growth and cell death." Biochimica et Biophysica Acta **1818**(8): 2002-2008.

Vogelmann R, Nguyen-Tat MD, Giehl K, Adler G, Wedlich D and Menke A. (2005). "TGFbeta-induced downregulation of E-cadherin-based cell-cell adhesion depends on PI3-kinase and PTEN." Journal of Cell Science **118**(20): 4901-4912.

Wan K., Chan V. and Dillard D. (2002). "Constitutive equation for elastic indentation of a thin-walled bio-mimetic microcapsule by an atomic force microscope tip." Colloids and Surfaces B: Biointerfaces **27**: 241-248.

Wang T., Zhou X., Yu Y., Dai J., Qu X., Le Q. and Chu R. (2011). "Expression of Smad7 inhibits fibrogenic responses of keratocytes to transforming growth factor β2." Chinese Medicine **124**(13): 1988-1993.

Weiss W. (2001). "Cadherin structure: a revealing zipper." Structure **3**(5): 425-427.

Wilson S., Mohan R., Mohan R., Ambro´sio Jr R., Hong J. and Lee J. (2001). "The Corneal Wound Healing Response: Cytokine-mediated Interaction of the Epithelium, Stroma, and Inflammatory Cells." Progress in Retinal and Eye Research **20**(5): 625-637.

Wright B., Cave R., Cook J., Khutoryanskiy V., Mi S., Chen B., Leyland M. and Connon C. (2012). "Enhanced viability of corneal epithelial cells for efficient

transport/storage using a structurally modified calcium alginate hydrogel." Regenerative Medicine **7**(3): 295-307.

Wu Y., MacKay J.A., McDaniel J.R., Chilkoti A. and Clark R.L. (2009). "Fabrication of elastin-like polypeptide nanoparticles for drug delivery by electrospraying." Biomacromolecules **10**(1): 19-24.

Xu Y. and Hanna M.A. (2007). "Electrosprayed bovine serum albumin-loaded tripolyphosphate cross-linked chitosan capsules: synthesis and characterization." Journal of Microencapsulation **24**(143-151): 143-151.

Xu Y., Skotak M. and Hanna M.A. (2006). "Electrospray encapsulation of water-soluble protein with polylactide: effects of formulations and process on morphology and particle size." Microencapsulation **23**: 69-78.

Yang L., Chan T., Demare J., Iwashina T., Ghahary A., Scott P. and Tredget E. (2001). "Healing of burn wounds in transgenic mice overexpressing transgenic growth factor beta-1 in the epidermis." American Journal of Pathology **159:** 2147-2157.

Yang Y.Y., Chunga T. and Ng N.P. (2001). "Morphology, drug distribution, and in vitro release profiles of biodegradable polymeric microspheres containing protein fabricated by double-emulsion solvent extraction/evaporation method." Biomaterials **22**(3): 231-341.

Yao L., Li Z., Su W., Li Y., Lin M., Zhang W., Liu Y., Wan Q. and Liang D. (2012). "Role of Mesenchymal Stem Cells on Cornea Wound Healing Induced by Acute Alkali Burn." PLoS one **7**(2): e30842.

Ye H. Q., Maeda M., Yu F. S. and Azar D.T. (2000). "Differential expression of MT1-MMP (MMP-14) and collagenase III (MMP-13) genes in normal and wounded rat corneas." Investigative Ophthalmology and Visual Science **41**: 2894–2899.

Zieske J.D., Guimaraes S.R. and Hutcheon A.E.K (2001). "Kinetics of keratocyte proliferation in response to epithelial debridement." Experimental Eye Research **72**: 33-40.

Zhang, W. and He X. (2009). "Encapsulation of Living Cells in Small (~100micrometer) Alginate Microcapsules by Electrostatic Spraying: A Parametric Study." Journal of Biomechanical Engineering **131**: 1-6.

Zhang W., Li B-G., Zhang C., Xie X.H. and Tang T.T. (2008). "Biocompatibility and membrane strength of C3H10T1/2 cell-loaded alginate-based microcapsules." Cryotherapy **10**(1): 90-97.

Zhang W., Yang G., Zhang A., Xu L. and He X. (2010). "Preferential vitrification of water in small alginate microcapsules significantly augments cell cryopreservation by vitrification." Biomed Microdevices **12**: 89-96.

Zhao Y., Shimizu T., Nishihira J., Koyama Y., Kushibiki T., Honda A., Watanabe H., Abe R., Tabata Y. and Shimizu H. (2005). "Tissue regeneration using macrophage migration inhibitory factor-impregnated gelatin microbeads in cutaneous wounds" American Journal of Pathology **167**(6): 1519-1529.

Zhou C., Nitschke A., Xiong W., Zhang Q., Tang Y., Bloch M., Elliott S., Zhu Y., Bazzone L., Yu D., Weldon C., Schiff R., McLachlan J., Beckman B., Wiese T., Nephew K., Shan B., Burow M. and Wang G. (2008). "Proteomic analysis of tumor necrosis factor-alpha resistant human breast cancer cells reveals a MEK5/Erk5-mediated epithelial-mesenchymal transition phenotype." Breast Cancer Research **10**(6): R105.

Zwaginga JJ. and Doevendans P. (2003). "Stem cell-derived angiogenic/vasculogenic cells: possible therapies for tissue repair and tissue engineering." Clinical and Experimental Pharmacology and Physiology **30**: 900-908.

APPENDIX A.1: RELEASE STUDY EXAMINING DIFFERENCES IN THE RATIO OF αCT1 TO ALGINATE

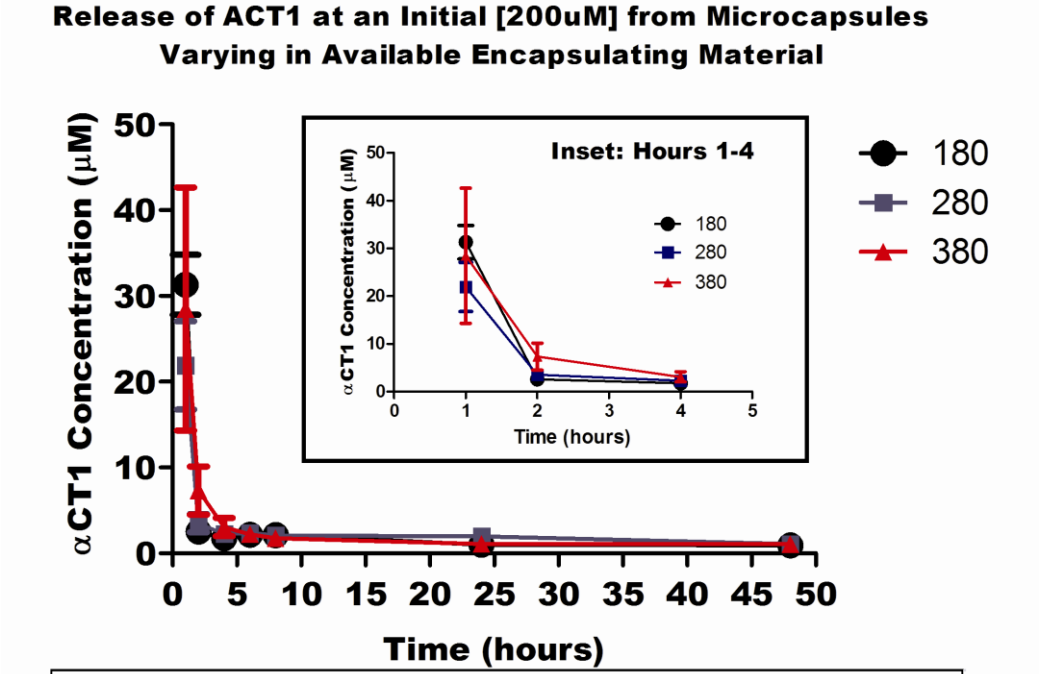

Average Peptide Concentration (uM) + Standard Error			
Time (Hours)	180 ul	280 ul	380 ul
1	31.31 ± 3.49	21.93 ± 5.15	28.48 ± 14.18
2	2.57 ± 0.09	3.53 ± 1.07	7.34 ± 2.80
4	1.79 ± 0.41	2.27 ± 0.13	3.07 ± 1.06
6	2.18 ± 0.04	2.39 ± 0.06	2.24 ± 0.08
8	2.16 ± 0.12	2.12 ± 0.21	1.75 ± 0.34
24	1.04 ± 0.02	1.99 ± 0.92	1.12 ± 0.07
48	0.93 ± 0.01	1.11 ± 0.12	1.06 ± 0.04

Appendix A.2: CORNEAL WOUND CLOSURE SUMMARY OF PERCENT DIFFERENCES BETWEEN TIME POINTS FOR EACH TREATMENT